ABSTRACT

GENERALIZED DISCRETE FOURIER TRANSFORM WITH NON-LINEAR PHASE: THEORY AND DESIGN

by
Handan Agirman-Tosun

Constant modulus transforms like discrete Fourier transform (DFT), Walsh transform, and Gold codes have been successfully used over several decades in various engineering applications, including discrete multi-tone (DMT), orthogonal frequency division multiplexing (OFDM) and code division multiple access (CDMA) communications systems. Among these popular transforms, DFT is a linear phase transform and widely used in multicarrier communications due to its performance and fast algorithms. In this thesis, a theoretical framework for Generalized DFT (GDFT) with nonlinear phase exploiting the phase space is developed. It is shown that GDFT offers sizable correlation improvements over DFT, Walsh, and Gold codes. Brute force search algorithm is employed to obtain orthogonal GDFT code sets with improved correlations. Design examples and simulation results on several channel types presented in the thesis show that the proposed GDFT codes, with better auto and cross-correlation properties than DFT, lead to better bit-error-rate performance in all multi-carrier and multi-user communications scenarios investigated. It is also highlighted how known constant modulus code families such as Walsh, Walsh-like and other codes are special solutions of the GDFT framework. In addition to theoretical framework, practical design methods with computationally efficient implementations of GDFT as enhancements to DFT are presented in the thesis. The main advantage of the proposed method is its ability to

design a wide selection of constant modulus orthogonal code sets based on the desired performance metrics mimicking the engineering specs of interest.

Orthogonal Frequency Division Multiplexing (OFDM) is a leading candidate to be adopted for high speed 4G wireless communications standards due to its high spectral efficiency, strong resistance to multipath fading and ease of implementation with Fast Fourier Transform (FFT) algorithms. However, the main disadvantage of an OFDM based communications technique is of its high PAPR at the RF stage of a transmitter. PAPR dominates the power (battery) efficiency of the radio transceiver. Among the PAPR reduction methods proposed in the literature, Selected Mapping (SLM) method has been successfully used in OFDM communications. In this thesis, an SLM method employing GDFT with closed form phase functions rather than fixed DFT for PAPR reduction is introduced. The performance improvements of GDFT based SLM PAPR reduction for various OFDM communications scenarios including the WiMAX standard based system are evaluated by simulations. Moreover, an efficient implementation of GDFT based SLM method reducing computational cost of multiple transform operations is forwarded. Performance simulation results show that power efficiency of non-linear RF amplifier in an OFDM system employing proposed method significantly improved.

GENERALIZED DISCRETE FOURIER TRANSFORM WITH NON-LINEAR PHASE: THEORY AND DESIGN

by
Handan Agirman-Tosun

A Dissertation
Submitted to the Faculty of
New Jersey Institute of Technology
in Partial Fulfillment of the Requirements for the Degree of
Doctor of Philosophy in Electrical Engineering

Department of Electrical and Computer Engineering

January 2010

APPROVAL PAGE

GENERALIZED DISCRETE FOURIER TRANSFORM WITH NON-LINEAR PHASE: THEORY AND DESIGN

Handan Agirman-Tosun

12/8/09

Dr. Ali N. Akansu, Dissertation Advisor — Date
Professor of Electrical and Computer Engineering, NJIT

12/08/09

Dr. Yeheskel Bar-Ness, Committee Member — Date
Distinguished Professor of Electrical and Computer Engineering, NJIT

12/08/09

Dr. Elza Erkip, Committee Member — Date
Associate Professor of Electrical and Computer Engineering, Polytechnic, NYU

12/08/09

Dr. Richard A. Haddad, Committee Member — Date
Professor of Electrical and Computer Engineering, NJIT

12/08/09

Dr. Alexander M. Haimovich, Committee Member — Date
Professor of Electrical and Computer Engineering, NJIT

December 8, 2009

Dr. Edip Niver, Committee Member — Date
Professor of Electrical and Computer Engineering, NJIT

12/08/09

Dr. Osvaldo Simeone, Committee Member — Date
Assistant Professor of Electrical and Computer Engineering, NJIT

BIOGRAPHICAL SKETCH

Author: Handan Agirman-Tosun

Degree: Doctor of Philosophy

Date: January 2010

Undergraduate and Graduate Education:

- Doctor of Philosophy in Electrical Engineering,
  New Jersey Institute of Technology, Newark, NJ, 2010
- Master of Science in Electrical Engineering,
  Middle East Technical University, Ankara, Turkey, 2005
- Bachelor of Science in Electrical Engineering,
  Hacettepe University, Ankara, Turkey, 2002

Major: Electrical Engineering

Presentations and Publications:

A.N. Akansu and H. Agirman-Tosun, "Generalized Discrete Fourier Transform with Nonlinear Phase," submitted to IEEE Trans. on Signal Processing.

H. Agirman-Tosun and A. N. Akansu, "An Efficient Selective Mapping Using Generalized DFT for PAPR Reduction in OFDM Communications," submitted to IEEE Trans. on Communications.

A.N. Akansu and H. Agirman-Tosun, "Generalized Discrete Fourier Transform: Theory and Design Methods," Proc. IEEE Sarnoff Symposium, March 2009.

A.N. Akansu and H. Agirman-Tosun, "Improved Correlation of Generalized Discrete Fourier Transform with Nonlinear Phase for OFDM and CDMA Communications," Proc. EUSIPCO European Signal Processing Conference, Aug. 2009.

H. Agirman-Tosun and A.N. Akansu, "Continuous Phase Modulation for Multi-Level Spreading Codes in CDMA Communications," Proc. Sarnoff Symposium, pp. 1-5, April 2008.

H. Agirman-Tosun and A.N. Akansu, "BER Performance of DS-CDMA Communications for Continuous Phase Modulation and Various Binary Code Families," Annual Conference on Information Sciences and Systems Proceedings, pp. 330-334, March 2008.

H. Agirman-Tosun and A.N. Akansu, "Generalized DFT Based SLM for PAPR Reduction in OFDM Communications," submitted to IEEE, ICASSP, 2010.

A.N. Akansu and H. Agirman-Tosun, "Generalized Discrete Fourier Transform with Optimum Correlations," submitted to IEEE, ICASSP, 2010.

Sevgili annem
Gülten Ağırman,
sevgili babam
Atila Ağırman
ve
biricik eşim
Dursun Çağrı Tosun'a

To my beloved mother
Gülten Ağırman,
my beloved father,
Atila Ağırman
and,
my one and only husband
Dursun Çağrı Tosun

ACKNOWLEDGMENT

First of all, I would like to express my sincere gratitude to my advisor, Prof. Ali. N. Akansu for all his support, encouragement and his guidance throughout my doctoral studies. He taught me how to see the whole picture in every aspect of life and how to handle problems in the most efficient way. His enthusiasm has always inspired me.

I would like to thank Prof. Richard A. Haddad of the Electrical and Computer Engineering of NJIT for his trust in me for this work. I have learned from him how to grow peaceful inside and enjoy life even while doing the most difficult work. My special thanks are due to Prof. Yeheskel Bar-Ness, Prof. Alexander M. Haimovich, Prof. Edip Niver and Asst. Prof. Osvaldo Simeone of the ECE Department of NJIT and Assoc. Prof. Elza Erkip of the ECE Department of the Polytechnic Institute of NYU for their helpful suggestions and their invaluable time that they spent for being members of my dissertation committee. Also, I would like to thank Dr. John A. Egan of the Humanities Department of NJIT for his helps in writing my thesis.

I am very grateful to Prof. Nirwan Ansari and the staff of the ECE department, especially Tanita S. Turner, Anthony Lambiase, Barbara Feltz and Jacinta Y. Williams for their help in solving many administrative problems I met during my years at NJIT.

I would like to thank my lab partners and colleages Radharani Poluri, Mustafa Ugur Torun and Nikhil Modi for their encouragement, psychological support and trust in me. I am very fortunate that I met them. Thank you a lot for your valuable friendship.

The last and the most, I would like to thank my parents and my husband for their love, endless support and patience during my research. Without their psychological support, this dissertation would not be completed.

TABLE OF CONTENTS

TABLE OF CONTENTS
(Continued)

TABLE OF CONTENTS
(Continued)

LIST OF TABLES

LIST OF FIGURES

LIST OF FIGURES
(Continued)

Figure **Page**

LIST OF FIGURES
(Continued)

Figure **Page**

LIST OF FIGURES
(Continued)

Figure **Page**

LIST OF FIGURES
(Continued)

Figure **Page**

LIST OF FIGURES
(Continued)

Figure **Page**

CHAPTER 1

INTRODUCTION

1.1 Motivation

A Block Transform is used to decompose a correlated input signal into decorrelated transform coefficients. Some examples of block transform families are Discrete Cosine Transform (DCT), Discrete Sine Transform (DST), Karhunen and Loeve Transforms (KLT). Among these transforms, KLT does not only decorrelate the input signal but also pack the signal energy into less transform domain coefficients compared to the others. However, KLT is signal-dependent: it requires the knowledge of statistical properties of the input signal. On the other hand, DCT, DST and DFT are fixed transforms meaning that they are signal independent. Among these fixed transforms, DFT finds several applications in digital signal processing and communications due to its perfect spectral resolution and easy implementation.

All block transforms mentioned above are orthogonal: the basis functions are orthogonal to each other. In communications, special examples of applications using orthogonal function sets are Time Division Multiple Access (TDMA), Frequency Division Multiple Access (FDMA), Code Division Multiple Access (CDMA) and Orthogonal Frequency Division Multiplexing (OFDM). Among them, TDMA employs time-localized orthogonal function sets where the basis functions are all-pass like in frequency-domain. Conversely, in FDMA, functions are frequency localized in frequency-domain and widely spread in time-domain. In CDMA, function sets are not only spread in the time-domain, but also in the frequency-domain. In these multiple access schemes, function sets are designed to be orthogonal either in frequency-, time- or

code-domain. Orthogonality in time is required to reduce interference (Intersymbol Interference, ISI) in between different subsymbols transmitted on the same carrier as in TDMA communications. On the other hand, orthogonality in frequency ensures no interference (Intercarrier Interference, ICI) between different carriers or subchannels as in OFDM and FDMA systems. In CDMA applications, orthogonality is in code domain to mitigate multi-user interference (MUI). For the synchronous communications case, orthogonality is enough to ensure no interference in all these applications. With any imperfection in synchronization, or in general, in asynchronous cases, orthogonality is not enough to mitigate interference: correlation properties of function sets play a crucial role.

Design of orthogonal function sets with desirable properties has been under study for several decades. DCT, DST, DFT, Oppermann, Frank-Zadoff and Chu sequences are some examples of function set families with closed form expressions, for all available sizes. However, designs in the literature show that several function sets are obtained through optimization tools since there exist no closed form expressions for these sets. In these designs, optimized function sets are presented in look-up tables for limited sizes and the system employing any of these is expected to save the look-up table in memory. Moreover, for systems with multi-size function sets, complexity increases with number of the sets used.

OFDM is proposed for 4G communications systems due to its spectral efficiency, strong resistance to multipath fading, and ease of implementation with the Fast Fourier Transform (FFT) algorithm. However, the main drawback of an OFDM system is its high peak-to-average ratio (PAPR). The signals with high peak values cause in-band and

out-of-band interferences when passed through non-linear power amplifiers. Of several methods proposed in the literature, Selective Mapping (SLM) is shown to be powerful for PAPR reduction. In this method, several OFDM frames corresponding to the same information are generated using multiple phase vectors, and the one with minimum PAPR is sent through the channel along with the side information. One drawback of this method is the absence of a closed form expression for phase generation; it assumes availability of look-up tables of phase vectors at the transmitter and receiver ends. Moreover, in this method, multiple inverse transforms are performed in the transmitter, which results in very complex design for the transmitters.

Discrete Fourier Transform (DFT) has become the most popular orthogonal transform since the introduction of its efficient implementation, namely FFT. DFT bases are orthogonal, show linear-phase dependence, and are localized in frequency, making them a perfect match for frequency-localized applications such as OFDM. Beyond orthogonality, DFT bases provide very low cross-correlations for all sizes. Orthogonality and low cross-correlation properties of DFT bases are the underlying inspiration of this dissertation. The linear phase property of this set is waived to form the proposed framework, which is named the Generalized Discrete Fourier Transform with Non-linear Phase. Theoretical analysis of the proposed framework and efficient design methods for its implementation are treated in this dissertation. The proposed framework is employed in the generation of orthogonal functions sets with desirable correlation properties. These orthogonal codes are later employed in a DS/CDMA system in AWGN and Rayleigh channel. Moreover, the proposed framework with its closed form phase generating function is employed in SLM to reduce peak power fluctuations without additional

transmitter complexity. Throughout this thesis, unless otherwise stated, the abbreviation "*GDFT*" refers to "*Generalized Discrete Fourier Transform with Non-linear Phase*".

1.2 State of The Art

The orthogonal function sets widely used in the Digital Signal Processing area include the bases of DFT, DCT, DST, Discrete Walsh-Hadamard Transform (WHT) and KLT. DFT has been employed for spectral analysis whereas DCT, DST, KLT and WHT are traditionally used for signal compaction applications. WHT is also used as spreading codes for CDMA communications, especially for Direct Sequence CDMA (DS/CDMA) communications. The basics of these orthogonal transforms including their comparisons in terms of fast computation algorithms and Eigen analyses are well discussed in [1-12].

There has been a flurry of research activities on spreading sequences with desirable correlation properties in the literature. Binary spreading codes like Walsh [11] and Gold sequences [13] were introduced first and successfully used in early CDMA technologies. Ideally speaking, all spreading codes used in a DS/CDMA communications system should have pseudo-noise properties. One of the binary spreading code families satisfying this criterion is binary maximal length shift-register or m-sequences. Later, different code families produced from m-sequences were introduced, e.g. Gold, Gold-like, Kasami and others [13-15].

Among various binary spreading families, Gold codes have been successfully used for asynchronous communications in DS/CDMA systems due to their low cross-correlation features. Most popular binary spreading sequences however, including Gold codes, are limited with respect to their code lengths and dimensions. As an example,

Walsh sequences are defined for the lengths of power of two [11]. Similarly, Gold codes offer sequence lengths of 2^m-1 for certain m values [13, 16].

All of the above-mentioned spreading codes are binary-valued and have limited correlation improvements due to the limitation on amplitudes and phases of samples in the code sequence. One possible improvement in cross-correlation properties is achieved by designing spreading codes with non-binary real chip values as proposed in the literature [17-20]. However, these codes when employed in systems with non-linear high power amplifiers, cause performance degradation decreasing the efficiency of the amplifier. Therefore, multi-valued spreading codes are not preferred in CDMA communications.

More recently, research has focused on constant amplitude function sets due to efficiency limitations of non-linear power amplifiers employed in transceivers. Hence, complex roots of unity are widely proposed as function sets by many authors. All elements of such a set are placed on the unit circle of the complex plane. Some examples are Frank-Zadoff, Chu and Oppermann complex codes [21-24]. Oppermann has shown that Frank-Zadoff and Chu Sequences are the special cases of his family of sequences [23, 25]. Although Oppermann codes have a wide-range of correlations properties, they are limited in size. For the case where the length of code set, N, is a prime number, the size of the Oppermann code set is maximum and equal to N-1. For other values of N, the set size is always smaller than N-1.

In the literature, various techniques have been proposed to reduce PAPR in OFDM based systems. These include partial transmit sequences (PTS) [26, 27], SLM [28, 29], Coding [30], Active Constellation Extension (ACE)[31], clipping and filtering

[32, 33], Tone Injection (TI) or Tone Reservation (TR) [34] and Interleaving [35]. All of these techniques have their advantages and disadvantages in terms of performance distortion, average power increase or date rate reduction. Clipping does not require power increase, however causes signal distortion introducing out-of-band interference. Although it is distortionless, Coding technique requires choosing low PAPR codes but they still have the largest Hamming distances in their signaling space. ACE, TI and TR methods are distortionless but require higher average power and thus are not power-efficient methods. SLM, PTS and Interleaving techniques are distortionless, do not require average power increase to reduce PAPR, which makes them favorable for OFDM systems. Among these methods, Interleaving and SLM techniques are very similar in their working principles; both require sending side information to the receiver. In SLM, the side information is the index of the corresponding phase vector used in transmitter for PAPR reduction and it is the permutation index in Interleaving. In [36], Baxley and Zhou concluded that although PTS requires much less inverse transform operations in the transmitter, SLM technique has better quantified PAPR reduction per unit of complexity metric.

1.3 Dissertation Overview

Excluding KLT, most of the block transforms are fixed: independent of the input signal. Real block transforms are widely used in signal analysis applications and the complex block transform DFT, is very popular in signal processing and communications. However, all popular fixed transforms are either real or linear phase with even or odd symmetry between their basis functions. In this thesis, the phase is relaxed to form non-linear phase real or complex orthogonal basis sets. Examples of these basis sets and their

performance comparisons along with the competing basis sets are given for several applications including CDMA and OFDM systems .

In Chapter 2, time and frequency representations of function sets are introduced. The orthogonality property, auto- and cross-correlations and also, the spreads of functions in any set are defined in terms of time and frequency representations of the functions. The Uncertainty Principle defining the limit of time and frequency spread of a function is given for the continuous- and discrete- time case.

In Chapter 3, several real and complex orthogonal function sets employed in signal processing and communications are explained. Real Bases of DCT, DST and WHT are discussed in terms of time- and frequency-domain representations. Complex bases of DFT and Oppermann function sets are explained in detail and basic limitations of Oppermann sets are discussed.

In Chapter 4, the proposed framework, Generalized Discrete Fourier Transform with Non-linear Phase is explained in detail. Theoretical analysis of the framework is explained in the context of roots of unity analysis. Efficient design methods for generating GDFT matrix out of DFT matrix are discussed in detail.

In Chapter 5, the GDFT framework is employed in the generation of complex orthogonal function sets with various auto- and cross-correlation properties. In order to compare GDFT function sets, several performance metrics are defined in terms of Aperiodic Correlation Function (ACF). Optimum complex orthogonal function sets based on the considered performance metrics are listed and compared with the common function sets listed in the literature including DFT, WHT and Oppermann function sets.

Theoretical analysis of multi-user detection in DS/CDMA systems on an AWGN and a multi-path Rayleigh channel is presented in Chapter 6. The proposed framework is employed in the design of complex orthogonal spreading codes suitable for DS/CDMA systems. These orthogonal code sets are obtained through optimization on several correlation metrics. Then, the proposed GDFT sets are compared with the popular spreading code sets in terms of bit-error-rate performance on an AWGN and a multi-path channel for synchronous and asynchronous communications. Critical dependence of detection performance on the correlation metrics of the sets is discussed.

Basics of OFDM communications are discussed in Chapter 7. The main drawback of OFDM systems, peak power fluctuation, and its effect on system performance are explained in detail. In order to reduce these peak power fluctuations, two GDFT-based methods, *Phase Optimized GDFT* and *Efficient GDFT* based SLM methods, are proposed. The proposed methods are employed in an OFDM system with non-linear Rapp amplifier and the improvement in the efficiency of the amplifier is quantified. Improvements in BER and in spectra of an OFDM system employing these proposed PAPR reduction methods are also presented.

Conclusions and future research are presented in Chapter 8.

CHAPTER 2

TIME-FREQUENCY REPRESENTATION OF SIGNALS

2.1 Introduction

Discrete-time signals are traditionally represented in time and frequency domains. If $\phi(n)$ denotes the discrete-time signal in time, the frequency domain representation $\Phi(e^{j\omega})$ is defined by Discrete-time Fourier Transform (DTFT) as [37, 38],

$$\Phi(e^{j\omega}) = \sum_{n=-\infty}^{+\infty} \phi(n) e^{-j\omega n} \tag{2.1}$$

According to *Parseval Theorem*, the total energy of a function or signal in time is equal to the total energy in frequency domain [37, 38],

$$\begin{aligned} E_\phi &= \sum_{n=-\infty}^{+\infty} \phi(n)\phi^*(n) = \sum_{n=-\infty}^{+\infty} |\phi(n)|^2 \\ &= \frac{1}{2\pi} \int_{-\pi}^{\pi} \Phi(e^{j\omega})\Phi^*(e^{j\omega}) d\omega = \frac{1}{2\pi} \int_{-\pi}^{\pi} |\Phi(e^{j\omega})|^2 d\omega \end{aligned} \tag{2.2}$$

From *Parseval Theorem*, one can conclude that both time and frequency domain representations show how the energy of the signal is distributed in time and frequency, respectively. In other words, a signal or a function is simply the shape of the energy E_ϕ in time or frequency domain. As an example, in Figure 2.1, eight numbers of unit energy and orthogonal discrete-time functions are shown in time and frequency domains.

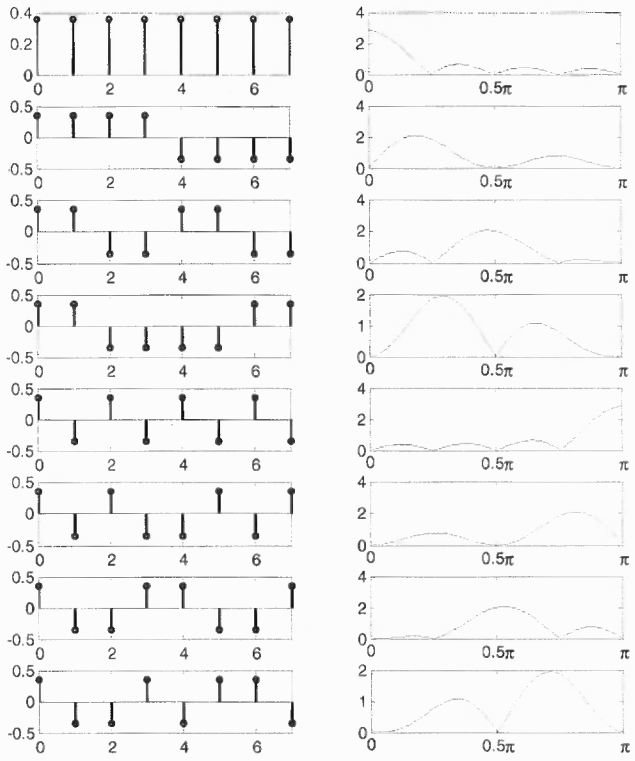

Figure 2.1 Time and frequency domain representations of size-8 WHT bases.

These functions are used in Code Division Multiple Access systems as spreading codes and called discrete Walsh-Hadamard codes. Note that all these functions have the same unit energy in both time and frequency. This figure shows how unit energy can be represented in many forms both in time and frequency. These types of orthogonal function sets are commonly used in signal analysis applications and in multi-carrier and multi-user communications. As an example, the function or basis set corresponds to rows of unitary DFT matrix in OFDM communications and to rows in a discrete Walsh-Hadamard matrix in DS/CDMA communications. In this section, correlation properties

and time and frequency spreads of any function set will be discussed in terms of time and frequency domain representations.

Consider a function or basis set similar to one given in Figure 2.1 as $\{\phi_k(n)\}$, $k=0,1,...,N-1$. Let $\phi_k(n) \rightarrow \Phi_k(e^{j\omega})$ and $\phi_l(n) \rightarrow \Phi_l(e^{j\omega})$ denote the DTFT pairs satisfying the equations

$$\begin{aligned}
\Phi_k(e^{j\omega}) &= \sum_{n=-\infty}^{+\infty} \phi_k(n) e^{-j\omega n} \\
\phi_k(n) &= \frac{1}{2\pi} \int_{-\pi}^{\pi} \Phi_k(e^{j\omega}) e^{j\omega n} d\omega \\
\Phi_l(e^{j\omega}) &= \sum_{n=-\infty}^{+\infty} \phi_l(n) e^{-j\omega n} \\
\phi_l(n) &= \frac{1}{2\pi} \int_{-\pi}^{\pi} \Phi_l(e^{j\omega}) e^{j\omega n} d\omega
\end{aligned} \tag{2.3}$$

The auto-correlation function of k^{th} function is given by time and frequency domain representation as,

$$\begin{aligned}
R_{\phi_k\phi_k}(m) &= \sum_{n=-\infty}^{+\infty} \phi_k(n)\phi_k^*(n-m) \\
&= \frac{1}{2\pi} \int_{-\pi}^{\pi} \Phi_k(e^{j\omega})\Phi_k^*(e^{j\omega}) e^{j\omega m} d\omega = \frac{1}{2\pi} \int_{-\pi}^{\pi} \left|\Phi_k(e^{j\omega})\right|^2 e^{j\omega m} d\omega
\end{aligned} \tag{2.4}$$

From (2.4), one can conclude that $R_{\phi_k\phi_k}(m)$ is the inverse DTFT of the magnitude square of $\Phi_k(e^{j\omega})$. Similarly, the cross-correlation function of k^{th} and l^{th} functions is given by the time and the frequency domain representations as

$$R_{\phi_k\phi_l}(m) = \sum_{n=-\infty}^{+\infty} \phi_k(n)\phi_l^*(n-m) = \frac{1}{2\pi} \int_{-\pi}^{\pi} \Phi_k(e^{j\omega})\Phi_l^*(e^{j\omega}) e^{j\omega m} d\omega. \tag{2.5}$$

Orthogonality of the functions $\phi_k(n)$ and $\phi_l(n)$ simply assures the following,

$$\sum_{n=-\infty}^{+\infty} \phi_k(n)\phi_l^*(n) = \frac{1}{2\pi}\int_{-\pi}^{\pi} \Phi_k(e^{j\omega})\Phi_l^*(e^{j\omega})d\omega = \delta(k-l) \qquad (2.6)$$

The ideal function set with respect to correlation properties, is characterized by the ideal auto-correlation function,

$$R_{\phi_k\phi_k}^{ideal}(m) = \delta(m) = \begin{Bmatrix} 1 & m=0 \\ 0 & m\neq 0 \end{Bmatrix} \quad k = 0,1,\ldots,N-1 \qquad (2.7)$$

and the ideal cross-correlation function requires sinc functions and is given as

$$R_{\phi_k\phi_l}^{ideal}(m) = 0 \quad \text{for } k \neq l, 0 \leq k,l \leq N-1 \qquad (2.8)$$

Any imperfection in auto-correlation and cross-correlation functions results in Inter-carrier Interference (ICI), Inter-symbol Interference (ISI) and Multiple-user Interference (MUI) in multi-user and multi-carrier communications. Therefore, depending on the application, the correlation properties of the functions should be considered in the design of the set.

In multiple-access communications and signal analysis applications, not only the correlations between functions but also the time and frequency localizations of the functions are crucial. For example in FDMA systems, the functions in the set are required to be precisely frequency localized since each user is assigned a frequency band. Thus, the functions in the set are required to be maximally narrow in frequency domain in order to serve the maximum number of users in a limited frequency band. Similarly, in CDMA communications, the basis functions or user spreading codes are required to be maximally spread both in time and frequency. Oppositely, signal analysis applications where the basic objective is to extract local features of a signal in both time- and frequency-domains, require a function set whose spread is simultaneously narrow in both

domains [39]. However, the Uncertainty Principle defines the limits of the spreads in time and frequency domain as explained in the next section.

2.2 Uncertainty Principle

2.2.1 Uncertainty in Continuous-time

Let $\phi(t) \leftrightarrow \Phi(\Omega)$ denotes the continuous-time Fourier transform pair satisfying the relations

$$\begin{aligned} \Phi(\Omega) &= \int_{-\infty}^{+\infty} \phi(t) e^{-j\Omega t} dt \\ \phi(t) &= \frac{1}{2\pi} \int_{-\infty}^{+\infty} \Phi(\Omega) e^{j\Omega t} d\Omega \end{aligned} \tag{2.9}$$

Uncertainty Principle for the continuous time case, asserts that [39]

$$\sigma_T \sigma_\Omega \geq \frac{1}{2} \tag{2.10}$$

where σ_T and σ_Ω are, respectively, the RMS spreads of $\phi(t)$ and $\Phi(\Omega)$ around the center values. That is,

$$\begin{aligned} \sigma_T^2 &= \frac{\int_{-\infty}^{+\infty} (t-\bar{t})^2 |\phi(t)|^2 dt}{E}, \\ \sigma_\Omega^2 &= \frac{\int_{-\infty}^{+\infty} (\Omega-\bar{\Omega})^2 |\Phi(\Omega)|^2 dt}{E}, \end{aligned} \tag{2.11}$$

where E is the total energy in the signal and given as,

$$E = \int_{-\infty}^{+\infty} |\phi(t)|^2 dt = \int_{-\infty}^{+\infty} |\Phi(\Omega)|^2 df \tag{2.12}$$

and $\bar{t}$ and $\bar{\Omega}$ refer to the center of the time and frequency signals as

$$\bar{t} = \frac{\int_{-\infty}^{+\infty} t|\phi(t)|^2 dt}{E}$$
$$\bar{\Omega} = \frac{\frac{1}{2\pi}\int_{-\infty}^{+\infty} \Omega|\Phi(\Omega)|^2 d\Omega}{E} \tag{2.13}$$

2.2.2 Uncertainty in Discrete-time

The discrete-time version of the Uncertainty Principle is as follows; $\phi(n) \leftrightarrow \Phi(e^{i\omega})$ is the DTFT pair satisfying the equations [37, 38],

$$\Phi(e^{j\omega}) = \sum_{n=-\infty}^{+\infty} \phi(n)e^{-j\omega n}$$
$$\phi(n) = \frac{1}{2\pi}\int_{-\pi}^{\pi} \Phi(e^{j\omega})e^{j\omega n} d\omega \tag{2.14}$$

Time and frequency centers of discrete-time signals are calculated as

$$\bar{n} = \frac{\sum_{n=-\infty}^{+\infty} n|\phi(n)|^2}{E}$$
$$\bar{\omega} = \frac{\frac{1}{2\pi}\int_{-\pi}^{\pi} \omega|\Phi(e^{j\omega})|^2}{E} \tag{2.15}$$

where, E is the total energy of the signal,

$$E = \sum_{n=-\infty}^{+\infty} |\phi(n)|^2 = \frac{1}{2\pi}\int_{-\pi}^{\pi} |\Phi(e^{j\omega})|^2 d\omega \tag{2.16}$$

The spreads of the function $\phi(n)$ in time and frequency are

$$\sigma_n^2 = \frac{\sum_{n=-\infty}^{+\infty} (n-\bar{n})^2 |\phi(n)|^2}{E}$$
$$\sigma_\omega^2 = \frac{\frac{1}{2\pi}\int_{-\pi}^{\pi} (\omega-\bar{\omega})^2 |\Phi(e^{j\omega})|^2 d\omega}{E} \tag{2.17}$$

Time-frequency tile of discrete-time function with the corresponding time and frequency spreads is displayed in Figure 2.2.

For the case of $\bar{\omega}=0, \bar{n}=0$, it is shown that the time-frequency product or resolution cell $\sigma_\omega \sigma_n$ is given as [39]

$$\sigma_\omega \sigma_n \geq \frac{|1-\mu|}{2}$$
$$\mu \square \frac{\left|\Phi(e^{j\omega})_{\omega=\pi}\right|^2}{E} = \frac{|\Phi(-1)|^2}{E} \tag{2.18}$$

In the continuous-time case, the lower limit of the resolution cell is simply ½. If the frequency response of the discrete-time signal has a zero at the frequency π, ($\left|\Phi(e^{j\omega})_{\omega=\pi}\right|=0$), the uncertainty limit for the discrete-time case becomes ½ as it is in the continuous-time case. However, $\left|\Phi(e^{j\omega})_{\omega=\pi}\right|$ need not be zero in the discrete-time case.

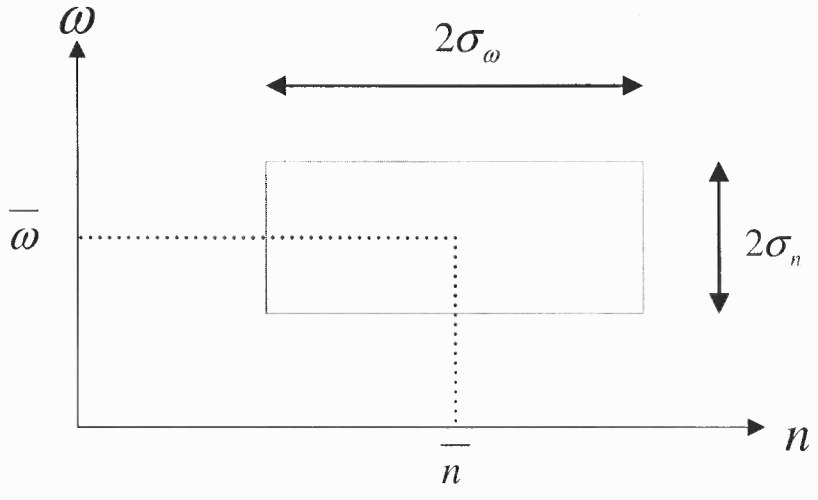

Figure 2.2 Time-frequency tile of a discrete-time function.

CHAPTER 3

ORTHOGONAL BLOCK TRANSFORMS

3.1 Introduction

A block transform in signal analysis applications, is widely used to decorrelate an input signal. In these applications, the correlated input signal is represented as a linear combination of the basis functions of the block transform. Each basis function contributes to the composite signal as much the corresponding uncorrelated transform coefficient. Among the various orthogonal transforms, KLT is optimum compared to all other transforms; it perfectly decorrelates the input signal as well as packing the signal energy into less possible transform domain coefficients. However, it is signal dependent. On the other hand, DCT, DST, WHT and DFT are signal independent orthogonal transforms and all the basis functions in the transform matrix or set are linear-phase.

In communications, orthogonal function sets are employed in multi-user communications. Each user is assigned a different function from a set. The functions in the set are orthogonal either in time, frequency or code domain. All the users' signals are summed and the composite signal is sent to the channel. This transmitted signal can be represented as a linear combination of orthogonal functions of the set used in the application.

Assume that a function set $\{\phi_k(n)\}$, $k = 0,1,...,N-1$ satisfies the orthonormality condition of

$$\sum_{n=0}^{N-1} \phi_k(n)\phi_l^*(n) = \delta(k-l) = \begin{Bmatrix} 1 & k=l \\ 0 & otherwise \end{Bmatrix} \tag{3.1}$$

If Equation (3.1) is satisfied, any nontrivial discrete-time signal $x(n)$ can be represented as a linear-combination of the functions in this set as

$$x(n) = \sum_{k=0}^{N-1} \theta_k \phi_k(n) \quad 0 \le n \le N-1 \tag{3.2}$$

and the transform domain coefficients are defined as

$$\theta_k = \sum_{n=0}^{N-1} x(n) \phi_k^*(n) \quad 0 \le k \le N-1 \tag{3.3}$$

The functions in the set $\{\phi_k(n)\}$, $k = 0,1,...,N-1$ form an orthonormal basis set. Since the transform is orthonormal, the total energy in the time domain is equal to the total energy in the transform domain.

DCT, DST, WHT and DFT are the most popular examples of block transforms used in digital signal processing. The orthogonal functions of DCT, DST and WHT are real-valued whereas those of DFT are complex-valued. Other than these block transforms, Oppermann proposed an orthogonal function set family with a wide range of correlation properties [25]. In this chapter, all these function sets will be briefly explained to form the basic theoretical background of the main interest of this thesis, Generalized Discrete Fourier Transform with Non-linear Phase.

3.2 Real Orthogonal Transforms

3.2.1 Discrete Cosine Transform

DCT is widely used in image processing and signal compaction applications. For highly correlated input signals, it closely approximates the optimum transform, KLT. This orthogonal set is defined as [39]

$$\phi_k(n) = \frac{1}{c_k}\cos\frac{(2n+1)k\pi}{2N}, \quad 0 \le n,k \le N-1$$
$$c_k = \begin{cases} \sqrt{N} & k=0 \\ \sqrt{N/2} & k \neq 0 \end{cases} \tag{3.4}$$

and in matrix notation,

$$A_{DCT} = [\phi_k(n)], \quad A_{DCT}^{-1} = A_{DCT}^{T} \tag{3.5}$$

DCT is Fourier related transform with only real entries. DCT transform can be considered as twice the length DFT of real valued signals with even symmetry. There are eight listed DCT's in the literature [1, 8]. The one in Equation (3.4) is the most commonly used one in signal processing. Transform bases of this type of DCT in time and frequency domains for $N=8$ is given in Figure 3.1.

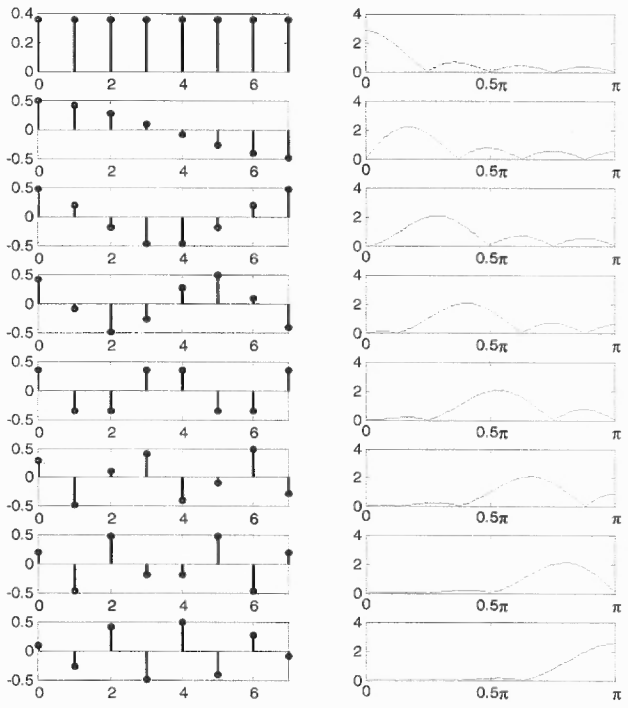

Figure 3.1 DCT transform bases in time and frequency domains for $N=8$.

3.2.2 Discrete Sine Transform

DST is also used in signal analysis and this family is defined as [40]

$$\phi_k(n) = \sqrt{\frac{2}{N+1}} \sin \frac{(n+1)(k+1)\pi}{(N+1)}, \quad 0 \le k,n \le N-1 \tag{3.6}$$

Similar to DCT, there are eight different DST's in the literature and the one in Equation (3.6) is the most common one. DST corresponds to twice the length DFT of real signals with odd symmetry. Similarly, bases of DST as defined by Equation (3.6) in time and frequency domains are given in Figure 3.2.

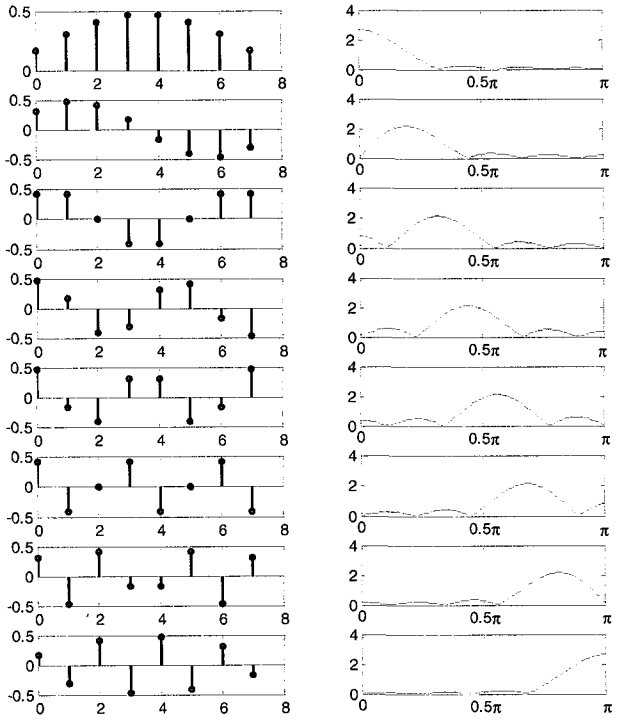

Figure 3.2 DST transform bases in time and frequency domains for $N=8$.

3.2.3 Discrete Walsh-Hadamard Transform

The discrete-time Walsh function set is generated from the analog Walsh functions. It is a complete set of N orthogonal sequences defined on $[0, N-1]$. The samples of each discrete sequence are +1 or -1 valued. The sequences of the set are defined as [39]

$$\begin{aligned} &\phi_0(n) = 1, \quad 0 \le n \le N-1 \\ &\phi_1(n) = \begin{Bmatrix} 1 & 0 \le n \le N/2-1 \\ -1 & N/2 \le n \le N-1 \end{Bmatrix} \\ &\phi_k(n) = \phi([\frac{k}{2}], 2n)\phi(k-2[\frac{k}{2}], n), \quad k = 2,3,\ldots,N\text{-}1 \end{aligned} \tag{3.7}$$

By simple shuffling of the rows of the discrete Walsh matrix, Hadamard matrices are formed. These matrices of order $N = 2^p$ are defined recursively as,

$$\begin{aligned} H_1 &= \frac{1}{\sqrt{2}}\begin{bmatrix} 1 & 1 \\ 1 & -1 \end{bmatrix} \\ H_{2N} &= \frac{1}{\sqrt{2}}\begin{bmatrix} H_N & H_N \\ H_N & -H_N \end{bmatrix} = H_1 \otimes H_N \end{aligned} \tag{3.8}$$

where $\otimes$ represents the Kronecker product. Figure 3.3 displays the WHT bases generated by Equation (3.7). Hadamard matrices are very popular in signal processing and also in communications due to the simple generation of higher size codes by a Kronecker product operation.

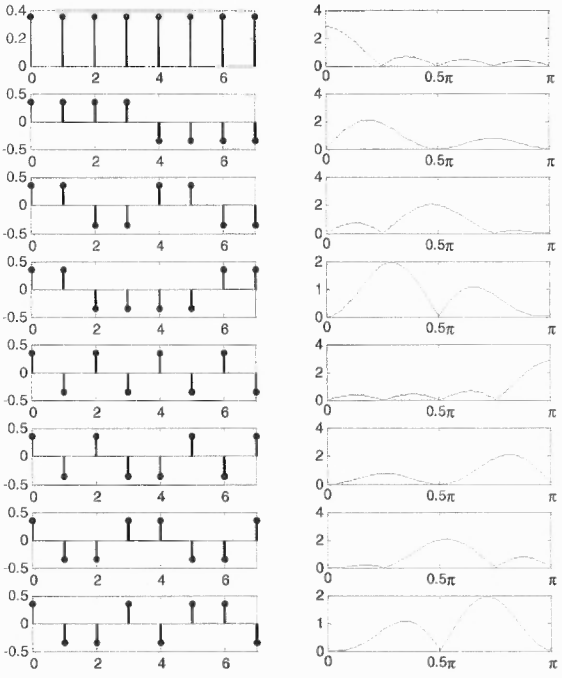

Figure 3.3 WHT transform bases in time and frequency domains for $N=8$.

All the transform bases mentioned so far have even or odd symmetry in the time domain, therefore they are all linear-phase in the frequency domain.

3.2.4 Non-Linear Phase Walsh-like Code Sets

Discrete-time Walsh codes or basis functions are widely used for downlink communications in CDMA communications due to their orthogonality and ease of implementation. These codes are linear-phase in frequency. In other words, they are either even or odd symmetric in time. Most recently, orthogonal non-linear phase Walsh-like code sets are proposed where the linear phase property of Walsh sets is waived to form orthogonal code sets suitable for both uplink and downlink in CDMA communications. These codes are shown to outperform Walsh code sets in asynchronous

or uplink communication in CDMA communications [41, 42]. One of the size-8 Walsh-like codes in the time and the frequency domain are displayed in Figure 3.4

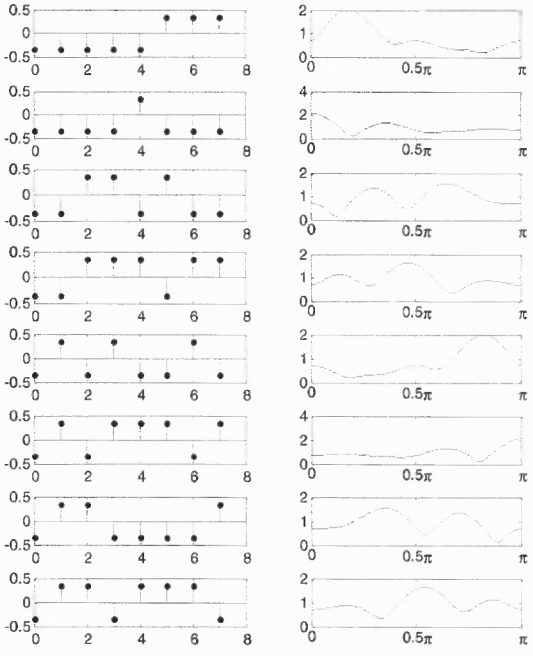

Figure 3.4 Walsh-like transform bases in time and frequency domains for $N=8$.

3.3 Complex Orthogonal Transforms

3.3.1 Discrete Fourier Transform

The DFT is the most popular orthogonal transform in spectral analysis due to its perfect spectral resolution and ease of implementation through FFT. The set of the orthogonal complex functions is defined as

$$\phi_k(n) = e^{j\frac{2\pi}{N}kn} \quad 0 \le k \le N-1, \;\; 0 \le n \le N-1 \tag{3.9}$$

The real and imaginary parts of each function in the set preserve the even and odd symmetry, therefore the functions in DFT set are linear-phase in frequency.

The DFT bases in the time and the frequency domains are given in Figure 3.5.

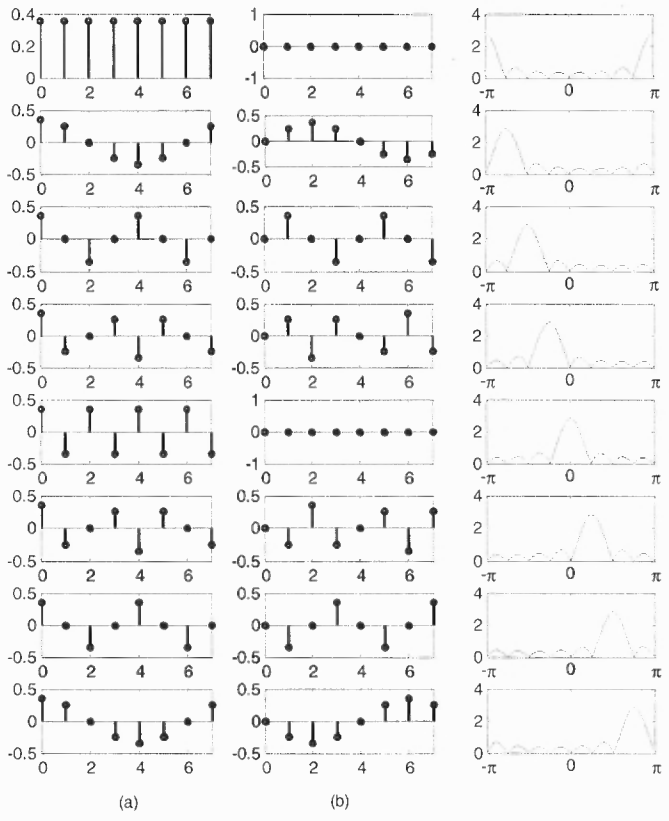

Figure 3.5 DFT transform bases a) real parts b) imaginary parts in time and frequency domains for *N=8*.

Each basis function of DFT corresponds to each row of the unitary DFT matrix as,

$$A_{DFT} = \frac{1}{\sqrt{N}}[e^{j\frac{2\pi}{N}kn}]$$
$$\phi_k(n) = \frac{1}{\sqrt{N}} e^{j\frac{2\pi}{N}kn} \quad k = 0,1,\ldots N-1, n = 0,1,\ldots N-1 \tag{3.10}$$

These basis functions are linear phase in both time and frequency and orthogonal to each other, satisfying the equation,

$$\sum_{n=1-N}^{N-1} \phi_k(n)\phi_l^*(n) = \frac{1}{2\pi}\int_{-\pi}^{\pi} \Phi_k(e^{j\omega})\Phi_l^*(e^{j\omega})d\omega = \delta(k-l) \qquad (3.11)$$

The phase function of k^{th} basis for N size DFT set can be defined as

$$\theta_k(n) = kn \quad k = 0,1,...,N-1, \quad n = 0,1,...,N-1. \qquad (3.12)$$

In order to emphasize the linearity of these functions in time, the constant $2\pi / N$ is omitted in Equation (3.10). The phase function of each basis function for N=8 is displayed in Figure 3.6. As can be seen from the figure, it is obvious that the phase functions of DFT bases are linear.

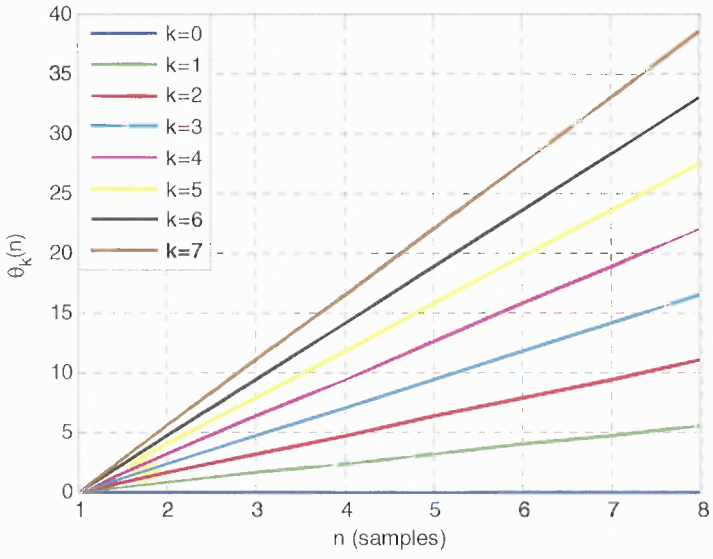

Figure 3.6 Phase functions of DFT bases in time for N=8.

The amplitude spectrum of each basis in the frequency domain is given in Figure 3.7.

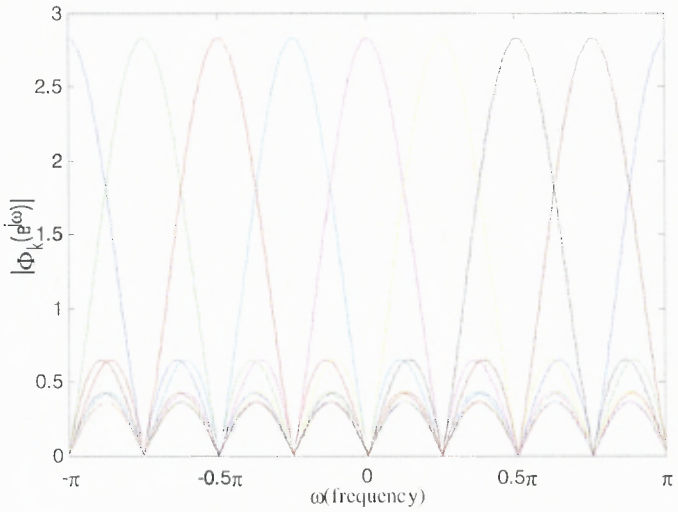

Figure 3.7 Amplitude Spectrum of DFT bases in frequency for $N=8$.

It is well known that the basis vectors of the unitary DFT are the eigenvectors of a *circulant* matrix, satisfying the equation [43]

$$A_{DFT}^{*T} R_{xx} A_{DFT} = \Lambda \tag{3.13}$$

where R_{xx} is a circulant matrix in the form of

$$R_{xx} = \begin{bmatrix} r_0 & r_{N-1} & \cdots & r_1 \\ r_1 & r_0 & \cdots & r_2 \\ \vdots & \vdots & \vdots & \vdots \\ r_{N-1} & r_{N-2} & \cdots & r_0 \end{bmatrix}$$

and Λ is a diagonal matrix and each diagonal element represents the strength of the corresponding eigenvector or frequency band,

$$\Lambda = diag\{\lambda_0, \lambda_1, \ldots \lambda_{N-1}\} \tag{3.14}$$

Moreover, if the circulant matrix represents a covariance of a real signal, the eigenvalues corresponds to variances of the signal at the corresponding frequency band. As a conclusion, the unitary DFT matrix diagonalizes any circulant matrix and completely decorrelates any signal whose covariance matrix has the circulant property.

3.3.2 Oppermann Function Set

Oppermann proposed a new family of constant modulus complex function sets and also showed that the well-known Frank-Zadoff and Chu Sequences are the special cases of his family [23].

The Oppermann function family is defined as [23]

$$A_{OPP}(k,i) = (-1)^{ki} \exp\left(\frac{j\pi(k^m i^p + i^n)}{N}\right) \qquad (3.15)$$
$$i = 1, 2, ..., N$$

where k is an integer in the range $[1, N)$ and relatively prime to N. In order to generate the maximum number of sequences in a set, N has to be chosen as a prime number [23, 25]. The number of sequences in this case is equal to $N-1$. In [25], it was proven that Oppermann codes are orthogonal only for the case of $p=1$ and m is any positive nonzero integer. Also, Oppermann proved that for the case of $p=1$, all the functions in a set have the same auto-correlation magnitudes [23]. The auto-correlation functions of each sequence differ only in phase. Figure 3.8 displays the Oppermann function set for $N=7$ and $\{m, p, n\} = \{1, 1, 2.98\}$ in time and frequency domains.

As mentioned in Section 3.2.3, Walsh-Hadamard function set is linear phase in frequency, with even or odd symmetry in time. A Walsh-like function set is generated, waiving the requirement of the linear-phase property of Walsh-Hadamard basis functions.

Similarly, the DFT function set is linear-phase in time as the phase function of each basis $\theta_k(n)$ is a linear function of the time index, *n,* and linear-phase in frequency due to the symmetry properties of real and imaginary parts of each basis in time. The approach of designing the non-linear phase Walsh-like function sets is followed in this dissertation. In the next chapter, the theoretical background of the proposed method will be introduced where DFT and Oppermann sets are defined in the proposed framework.

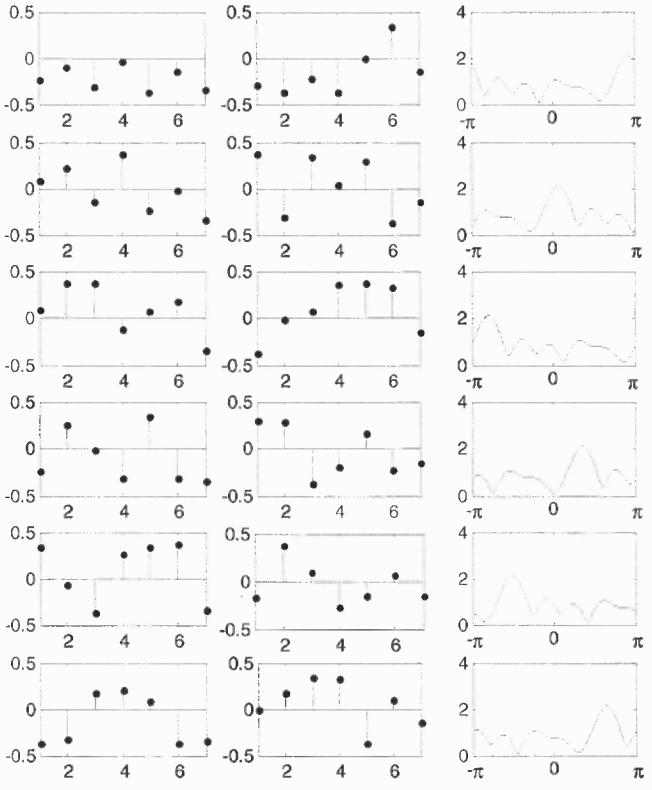

Figure 3.8 Orthogonal Oppermann function set for *N*=7 and $\{m, p, n\} = \{1, 1, 2.98\}$ [23, 24].

CHAPTER 4

GENERALIZED DISCRETE FOURIER TRANSFORM WITH NON-LINEAR PHASE

4.1 Introduction

Generalized Discrete Fourier Transform with Non-linear Phase provides a unified framework, where the linear phase DFT is extended to non-linear phase DFT. The theoretical analysis of GDFT framework will be given in this chapter starting from the well-known roots of unity concept. In the following chapters, several applications where GDFT framework is employed to improve system performance will be discussed.

4.2 Theory of DFT and GDFT

An N^{th} root of unity is a complex number satisfying the equation

$$z^N = 1 \quad N = 0,1,2,... \tag{4.1}$$

If z holds (4.1) but $z^m \neq 1 ; 0 < m < N-1$, then z is defined as a primitive N^{th} root of unity. As an example, $z_1 = e^{j\frac{2\pi}{4}}$ and $z_2 = e^{j\frac{3\pi}{2}}$ are the two primitive N^{th} roots of unity for $N=4$. The complex number $z_1 = e^{j(2\pi/N)}$ is the primitive N^{th} root of unity with the smallest positive argument. There are N distinct N^{th} roots of unity for any primitive and expressed as

$$z_k = (z_p)^k \quad k = 1,2,3, \ ... \ , N \quad \forall p \tag{4.2}$$

All *primitive N^{th} roots of unity* satisfy the unique summation property of a geometric series expressed as follows [44, 45]

$$\sum_{n=0}^{N-1}(z_p)^n = \frac{(z_p)^N - 1}{z_p - 1} = \begin{Bmatrix} 1, N = 1 \\ 0, N > 1 \end{Bmatrix} \quad \forall p \tag{4.3}$$

Now, define a periodic, constant modulus, complex sequence $\{e_r(n)\}$ as the r^{th} *power* of the first *primitive* N^{th} *root of unity* z_1 raised to the n^{th} *power* as

$$\begin{aligned} &e_r(n) \square (z_1^r)^n = e^{j(2\pi r/N)n} \\ &n = 0,1,2,\ldots,N-1 \text{ and } r = 0,1,2,\ldots,N-1 \end{aligned} \tag{4.4}$$

This complex sequence over a finite discrete-time interval in a geometric series is expressed according to Equation (4.3) as follows

$$\begin{aligned} &\frac{1}{N}\sum_{n=0}^{N-1} e_r(n) = \frac{1}{N}\sum_{n=0}^{N-1}(z_1^r)^n = \frac{1}{N}\sum_{n=0}^{N-1} e^{j(2\pi r/N)n} \\ &= \begin{Bmatrix} 1, & r = mN \\ 0, & r \neq mN \\ & m = \text{integer} \end{Bmatrix} \end{aligned} \tag{4.5}$$

This mathematical property is utilized for the factorization of Equation (4.5) into two orthogonal constant modulus functions where one defines the discrete Fourier transform (DFT) set $\{e_k(n)\}$ satisfying the orthonormality condition

$$\begin{aligned} &< e_k(n), e_l^*(n) >= \frac{1}{N}\sum_{n=0}^{N-1} e_k(n) e_l^*(n) = \frac{1}{N}\sum_{n=0}^{N-1} e^{j(2\pi/N)(k-l)n} \\ &= \begin{Bmatrix} 1, & k-l = r = mN \\ 0, & k-l = r \neq mN \\ & m,n = \text{integer} \end{Bmatrix} \end{aligned} \tag{4.6}$$

The notation (*) represents the complex conjugate of a function. One might rewrite the first primitive N^{th} root of unity as $z_1 = e^{j\omega_0}$ where $\omega_0 = 2\pi/N$, and it is called *the fundamental frequency* defined in radians.

Equation (4.5) can be generalized by introducing a product function in the phase defined as $\varphi_{kl}(n) = \varphi_k(n) - \varphi_l(n) = r$ and expressing a constant amplitude orthogonal set as follows,

$$\frac{1}{N}\sum_{n=0}^{N-1} e^{j(2\pi/N)rn} = \frac{1}{N}\sum_{n=0}^{N-1} e^{j(2\pi/N)\varphi(n)n} = \frac{1}{N}\sum_{n=0}^{N-1} e_k(n)e_l^*(n)$$

$$= \frac{1}{N}\sum_{n=0}^{N-1} e^{j(2\pi/N)[\varphi_k(n)-\varphi_l(n)]n} = \begin{cases} 1, & \varphi(n)=\varphi_k(n)-\varphi_l(n)=r=mN \\ 0, & \varphi(n)=\varphi_k(n)-\varphi_l(n)=r\neq mN \\ & m,n=\text{integer} \end{cases} \tag{4.7}$$

Hence, the basis functions of the new orthogonal set are defined as

$$e_k(n) \square e^{j(2\pi/N)\varphi_k(n)n} \quad k,n = 0,1,\ldots,N-1 \tag{4.8}$$

This orthogonal function set is called as the Generalized Discrete Fourier Transform with Non-Linear Phase. It is noted that infinitely many sets with constant amplitude and nonlinear phase functions are available.

As an example, one might define the discrete time *rational function* $\varphi_k(n)$ in Equation (4.8) as the ratio of two polynomials,

$$\varphi_k(n) = \frac{N_k(n)}{D_k(n)} = \frac{\sum_{j=1}^{N} a_{kj} n^{b_{kj}}}{\sum_{j=1}^{M} c_{kj} n^{d_{kj}}} \quad N \le M;\ k = 0,1,\ldots,N-1. \tag{4.9}$$

Assume that the denominator polynomial $D_k(n)=1$ in Equation (4.9), then *the order N* numerator polynomial in *n* is defined as follows

$$\varphi_k(n) = N_k(n) = \sum_{j=1}^{N} a_{kj} n^{b_{kj}} = a_{k1}n^{b_{k1}} + a_{k2}n^{b_{k2}} + a_{k3}n^{b_{k3}} + \ldots + a_{kN}n^{b_{kN}}. \tag{4.10}$$

In general, the polynomial coefficients $\{a_{kj}\}$ and $\{c_{kj}\}$ are complex, the powers $\{b_{kj}\}$ and $\{d_{kj}\}$ are real numbers. The following remarks link the proposed GDFT framework to the other known transforms and show its potential impact on a multicarrier communications system.

Remark 1: DFT is a special solution of GDFT where $\varphi_k(n) = a_{k1} = k$, $a_{k2} = a_{k3} = ... = a_{kN} = 0$ and $b_{k1} = b_{k2} = ... = b_{kN} = 0$ in Equation (4.9) and Equation (4.10) for all k. Note that having constant valued $\{\varphi_k(n)\}$ functions for all k makes DFT a linear-phase transform.

Remark 2: In general, n and k parameters do not have to be integer numbers and might be real as long as they satisfy the orthogonality conditions of Equation (4.7). Since there are N orthogonal functions in the set, one needs to have N distinct and real k values. In that case, the real k values are mapped into k integer numbers from *0* to *N-1* and used as the indices of the basis functions in a set.

Remark 3: There are infinitely many possible GDFT sets available in the phase space with constant power where one can design the optimal basis for the desired figure of merit. If the application considered requires a function set with minimized auto- and cross-correlation properties and does not mind about the non-linear phase, naturally, DFT is not the optimal solution for this specs. Therefore, one can exploit this fact to design various GDFT's where CDMA and OFDM performances in a multicarrier communications system might be improved over the existing solutions like Walsh transform and DFT.

Remark 4: Since DFT is a special solution of GDFT, it offers only one set to be used in a multicarrier communications system. Therefore, the carrier level (physical layer) security is quite vulnerable against a potential intrusion to the system. In contrast, the proposed GDFT provides many possible carrier sets of the same and various lengths with comparable or better correlation performance than DFT. The availability of rich library of orthogonal constant amplitude transforms with good performance allows us to design

adaptive systems where basis assignments as well as code allocations are made dynamically and intelligently to exploit the current channel conditions in order to deliver better communications performance and improved physical layer security.

4.3 GDFT Design

Consider the DFT matrix of size-N as

$$A_{DFT} = [A_{DFT}(k,n)] = [e^{j(2\pi/N)kn}] \quad k,n = 0,1,2,...,N-1 \tag{4.11}$$

GDFT can be defined as the generalization to DFT based on the performance metrics related to the application under consideration. Hence, GDFT matrix is expressed as a product of two orthogonal matrices as follows

$$\begin{aligned} A_{GDFT} &= A_{DFT}G \\ A_{GDFT}A_{GDFT}^{-1} &= I \\ A_{GDFT}^{-1} &= A_{GDFT}^{*T} \quad GG^{*T} = I \end{aligned} \tag{4.12}$$

where the notation $(^{*T})$ indicates that conjugate and transpose operations applied to the matrix and I is the *identity matrix.*

Note that G is the complex orthogonal generalization matrix yielding A_{GDFT} in Equation (4.12) with the desired time and frequency domain features. Figure 4.1 summarizes several G matrix families that are useful to design A_{GDFT} out of A_{DFT} matrix.

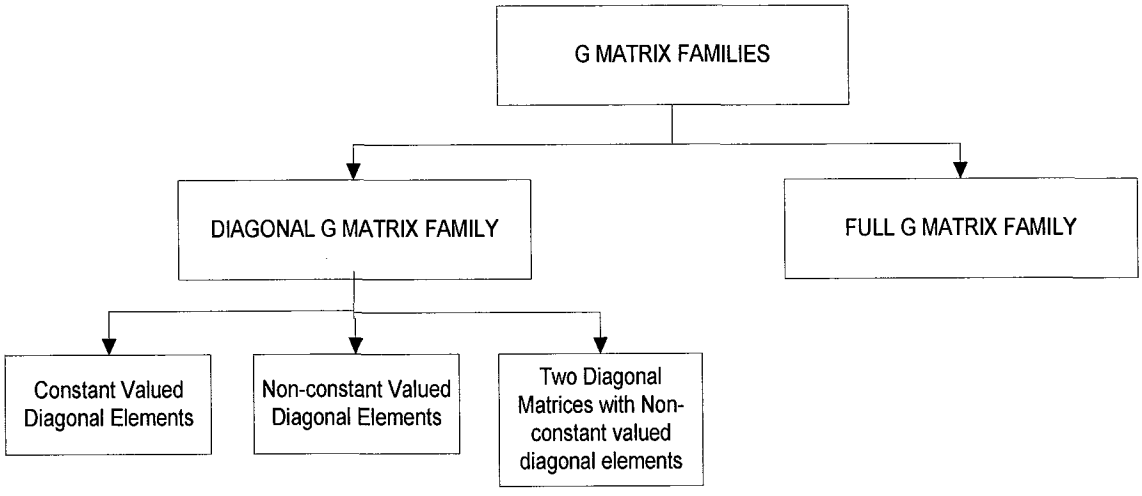

Figure 4.1 *G* Matrix Families used for generating GDFT matrices out of DFT matrix.

4.3.1 Diagonal *G* Matrix Family

The diagonal elements of G matrix must be constant amplitude for orthonormality of GDFT basis functions in Equation (4.12) and one might define it in the following three forms.

Constant Valued Diagonal Elements: The elements of this diagonal matrix are the same constant amplitude complex number as expressed in

$$G(k,n)=\begin{cases} e^{j\theta}, & k=n \\ 0, & k\neq n \\ & k,n=0,1,...N \end{cases} \tag{4.13}$$

This type of G matrix generates θ radians per cycle phase shifted version of A_{DFT} matrix as A_{GDFT}. Moreover, the linear phase property of A_{DFT} is still preserved in this case.

Non-Constant Diagonal Elements: With non-zero, non-constant and constant modulus diagonal elements, G matrix of this family is defined as

$$G(k,n)=\begin{Bmatrix} e^{j\theta_{kk}}, & k=n \\ 0, & k\neq n \\ & k,n=0,1,...,N \end{Bmatrix} \tag{4.14}$$

The rows (basis functions) of A_{GDFT} in Equation (4.12) are obtained as the element by element products of A_{DFT} rows with the elements of diagonal G matrix in this scenario. It is observed that each sample of a basis function in A_{DFT} is phase shifted independently of the other samples. Therefore, the resulting basis function set is entirely different than DFT function set. On the other hand, elements of each column in A_{DFT} matrix are phase shifted in the same amount.

Non-Constant Two Diagonal Matrices G_1 and G_2: A_{GDFT} matrix is redefined in such a way that phase shaping of its basis functions will be even more flexible as shown in the following matrix equation

$$\begin{aligned} A_{GDFT} &= G_1 A_{DFT} G_2 \\ A_{GDFT} A_{GDFT}^{*T} &= I \\ G_1 G_1^{*T} &= I \text{ and } G_2 G_2^{*T} = I \end{aligned} \tag{4.15}$$

where

$$G_1(k,n)=\begin{Bmatrix} e^{j\theta_{kk}} & k=n \\ 0 & k\neq n \\ & k,n=0,1,\ldots,N-1 \end{Bmatrix} \tag{4.16}$$

and

$$G_2(k,n)=\begin{Bmatrix} e^{j\gamma_{nn}} & n=k \\ 0 & n\neq k \\ & n,k=0,1,\ldots,N-1 \end{Bmatrix} \tag{4.17}$$

Note that the kernel generating A_{GDFT} matrix for this case is expressed as follows

$$\{e_k(n)\} \square e^{j[(2\pi/N)kn+\theta_{kk}+\gamma_{nn}]} \quad k,n=0,1,\ldots,N-1 \quad (4.18)$$

This design method allows uniquely modifying the phase of the $(k,n)^{th}$ element of the A_{DFT} matrix as the $(k,n)^{th}$ element of the A_{GDFT} matrix.

4.3.2 Full *G* Matrix Family

The elements of the orthogonal G matrix in Equation (4.12) might or might not be constant amplitude in this case and defined as

$$G(k,n)=\left[\begin{matrix} g_{k,n}e^{j\theta_{k,n}} \\ k,n=0,1,\ldots N \end{matrix}\right] \quad (4.19)$$

where $g_{k,n}$ and $\theta_{k,n}$ are the amplitude and phase values, respectively, for the $(k,n)^{th}$ element of the matrix.

The overall computational cost of A_{GDFT} implementation is the combined implementation cost of A_{DFT} and G matrices. Since DFT has its efficient fast algorithms, FFT, the complexity of G matrix dictates the required additional computational resources to implement GDFT. Therefore, this point needs to be considered in applications when one generalizes DFT into GDFT.

Remark 5: It is shown that popular orthogonal Walsh transforms and recently proposed Walsh-like transforms are special solutions of GDFT.

$$\begin{aligned} A_{WALSH} &= A_{GDFT} = A_{DFT}G_{WALSH} \\ A_{WALSH-LIKE} &= A_{GDFT} = A_{DFT}G_{WALSH-LIKE} \end{aligned} \quad (4.20)$$

As an example, G_{WALSH} matrix for $N=4$ and $G_{WALSH-LIKE}$ for $N=8$ are shown to be as follows,

$$G_{WALSH} = \begin{bmatrix} 1 & 0 & 0 & 0 \\ 0 & 0 & 0.71e^{j\pi 0.25} & 0.71e^{-j\pi 0.25} \\ 0 & 1 & 0 & 0 \\ 0 & 0 & 0.71e^{-j\pi 0.25} & 0.71e^{j\pi 0.25} \end{bmatrix}$$

$$G_{WALSH-LIKE} = \begin{bmatrix} e^{i\pi} & 0 & 0 & 0 & 0 & 0 & 0 & 0 \\ 0 & 0.65e^{-i0.63\pi} & 0 & 0.65e^{i0.87\pi} & 0 & 0.27e^{-i0.13\pi} & 0 & 0.27e^{-i0.63\pi} \\ 0 & 0 & 0.71e^{-i0.75\pi} & 0 & 0 & 0 & 0.71e^{-i0.25o} & 0 \\ 0 & 0.27e^{-i0.87\pi} & 0 & 0.27e^{-i0.37\pi} & 0 & 0.65e^{-i0.37\pi} & 0 & 0.65e^{i0.13\pi} \\ 0 & 0 & 0 & 0 & e^{-i\pi} & 0 & 0 & 0 \\ 0 & 0.27e^{i0.87\pi} & 0 & 0.27e^{i0.37\pi} & 0 & 0.65e^{i0.37\pi} & 0 & 0.65e^{-i0.13\pi} \\ 0 & 0 & 0.71e^{i0.75\pi} & 0 & 0 & 0 & 0.71e^{i0.25\pi} & 0 \\ 0 & 0.65e^{i0.63\pi} & 0 & 0.65e^{-i0.87\pi} & 0 & 0.27e^{i0.13\pi} & 0 & 0.27e^{i0.63\pi} \end{bmatrix}$$

Similarly, DST, DCT and other known block transforms can also be expressed within the GDFT framework with their unique G matrices.

Remark 6: It is shown below that the orthogonal Oppermann codes are also special solutions to the proposed GDFT framework. The Oppermann codes are defined as [23]

$$A_{OPP}(k,i) = (-1)^{ki} \exp\left(\frac{j\pi(k^m i^p + i^n)}{N}\right) \qquad (4.21)$$
$$i = 1,2,\ldots..,N$$

where k is an integer in the range $[1,N)$ and relatively prime to N. Note that if one defines the parameters of Equation (4.10) for this case as $a_{kj} = 0 \;\; j = 3,4,\ldots,N$, $b_{kj} = 0 \;\; j = 3,4,\ldots,N$ and

$$a_{k1} = \frac{k^m + kN}{2}$$
$$b_{k1} = 0; \quad a_{k2} = \frac{1}{2}; \quad b_{k2} = n-1 \qquad (4.22)$$

The maximum number of the functions in a set, *N-1*, is obtained when *N* is chosen as a prime number. In order to generate the complete Oppermann set using Equation (4.22), the sequence with the index $k=0$ is included in the set. In this case, G_{OPP} for the Oppermann set of *N*=7 with the parameters $\{N,m,p,n\}=\{7,1,1,2.98\}$ is shown to be as follows,

$$G_{OPP}=\begin{bmatrix} 0 & 0 & 0 & 0 & 0 & 0 & e^{-j\pi 0.87} \\ 0 & 0 & 0 & 0 & e^{-j\pi} & 0 & 0 \\ 0 & 0 & e^{-j\pi 0.8} & 0 & 0 & 0 & 0 \\ e^{-j\pi 0.71} & 0 & 0 & 0 & 0 & 0 & 0 \\ 0 & 0 & 0 & 0 & 0 & e^{j\pi 0.63} & 0 \\ 0 & 0 & 0 & e^{-j\pi 0.54} & 0 & 0 & 0 \\ 0 & e^{-j\pi 0.59} & 0 & 0 & 0 & 0 & 0 \end{bmatrix}$$

Note that, the first row in the function set generated with G_{OPP} will be ignored if one needs to generate the Oppermann codes using G_{OPP}. With some shuffling on this matrix, one can easily show that this G_{OPP} matrix is a member of diagonal *G* matrix family.

Remark 7: The term Generalized DFT was also used by other authors in the literature for their methods reported in [46-49] where the time and frequency index *n* and *k* in Equation (4.11) is simply replaced with *n+a* and *k+b for* some real *a* and *b*, respectively. Thus, the function set in their design is simply the shifted version of the DFT set with linear-phase property. Therefore, GDFT is the superset of their technique.

CHAPTER 5

CORRELATIONS OF GENERALIZED DFT

5.1 Introduction

Theoretically speaking, there are infinitely many orthonormal function sets due to the sake of Gram-Schmidt algorithm. All these function sets differ in the time and frequency spreads and also the correlation properties of the basis functions. In signal analysis applications, mostly the time and frequency domain spreads are crucial and the function sets are designed on these metrics. If the application requires a function set optimum on correlation properties such as CDMA systems, the set is optimized on several correlation-based metrics.

There are several different types of correlation functions defined in the literature to characterize function sets such as even correlation, periodic correlation etc. All the metrics used in this study depend on *aperiodic correlation functions (ACF)* of code sets. In Equation (5.1), the metric $d_{k,l}(m)$ is defined as the ACF between two complex sequences, namely $e_k(n)$ and $e_l(n)$ [50],

$$d_{k,l}(m)=\begin{cases} \dfrac{1}{N}\displaystyle\sum_{n=0}^{N-1-m} e_k(n)e_l^*(n+m), & 0<m\le N-1 \\ \dfrac{1}{N}\displaystyle\sum_{n=0}^{N-1+m} e_k(n-m)e_l^*(n), & 1-N<m\le 0 \\ 0 \quad , & |m|\ge N \end{cases} \tag{5.1}$$

5.2 Performance Metrics

The following correlation metrics are used for optimal GDFT design and performance comparisons of various function sets. The considered function set is defined as $\{e_k(n)\}$; k=0,1,2,...,M-1, n=0,1,..N–1 where N is the length of each function or basis and M defines the set size.

Maximum Value of Out of Phase Auto-correlation (d_{am}): d_{am} is the maximum value of M autocorrelation sequences for the entire set obtained from Equation (5.1) and given as

$$d_{am} = \max_{\substack{0 \le k < M \\ 1 \le m < N}} \left\{ \left| d_{k,k}(m) \right| \right\} \tag{5.2}$$

Maximum Value of Cross-correlation (d_{cm}): d_{cm} is the maximum value of all possible cross-correlation sequences in a function set also calculated from Equation (5.1) and is expressed as

$$d_{cm} = \max_{\substack{0 \le k,l < M \; k \ne l \\ 0 \le m < N}} \left\{ \left| d_{k,l}(m) \right| \right\} \tag{5.3}$$

Maximum Value of Auto- and Cross-Correlation Sequences ($d_{\max}$): The maximum correlation value $d_{\max}$ of a set of sequences is calculated as

$$d_{\max} = \max\{d_{am}, d_{cm}\} \tag{5.4}$$

Mean Square Value of Auto-correlation Sequences, (R_{AC}), and Cross-correlation Sequences, (R_{CC}): The quantitative measures given above are important to highlight the worst case scenarios in general. In contrast, the average performance counts more in some applications. Therefore, the mean square values of cross-correlation sequences are

taken into account as another performance metric. Furthermore, the average of mean square auto-correlation sequences for each function in the set, R_{AC}, and the average of mean square cross-correlation sequences for all function pairs in the set, R_{CC}, are introduced as follows [50],

$$R_{AC} = \frac{1}{M} \sum_{k=0}^{M-1} \sum_{\substack{m=1-N \\ m \neq 0}}^{N-1} \left| d_{k,k}(m) \right|^2 \tag{5.5}$$

$$R_{CC} = \frac{1}{M(M-1)} \sum_{k=0}^{M-1} \sum_{\substack{l=0 \\ l \neq k}}^{M-1} \sum_{m=1-N}^{N-1} \left| d_{k,l}(m) \right|^2 \tag{5.6}$$

The merit factor (F): The merit factor for the k^{th} code is the ratio of the energy in the main lobe of the autocorrelation function over the total energy in its side lobes and mathematically expressed as [51]

$$F_k = \frac{d_{k,k}(0)}{2\sum_{m=1}^{N-1} \left| d_{k,k}(m) \right|^2} \tag{5.7}$$

In the following sections, optimum GDFT sets based on the above metrics will be discussed. The cost function, $C_{N,M}$, for the optimization of GDFT sets with N-length M-sequences based on these metrics is defined as follows

$$C_{N,M} = \alpha \sum_{k=0}^{M-1} F_k - \beta d_{am} - \delta d_{cm} - \eta R_{AC} - \gamma R_{CC} \tag{5.8}$$

5.3 Bounds for Correlation Metrics

In the literature, several bounds are proposed for the metrics defined in the previous section. Sarwate showed the relationship between the peak auto-correlation d_{am} and the peak cross-correlation d_{cm} for complex valued codes as follows [52],

$$(2N-1)d_{cm}{}^2 + \frac{2(N-1)}{(M-1)} d_{am}{}^2 \geq 1 \tag{5.9}$$

which leads to the Welch bound for constant modulus complex sets, expressed as [53],

$$d_{\max} = \max\{d_{am}, d_{cm}\} = \sqrt{\frac{M-1}{M(2N-1)-1}} \tag{5.10}$$

In Table 5.1, the achievable Welch bounds for various length constant modulus complex sets are given.

Table 5.1 Welch Bounds for Various Code Lengths

M=N	$d_{\max}$
8	0.243
16	0.172
32	0.123
64	0.088

Natarajan, Das and Stevens showed that for any complex code sequency, the R_{AC} and the R_{CC} metrics are bounded by ,

$$R_{CC}(M-1) + R_{AC} \geq M-1 \tag{5.11}$$

where M defines the size of the set.

The maximum value of R_{AC} for a constant modulus complete set ($M = N$) is shown to be,

$$R_{AC,\max} = \frac{(N-1)(2N-1)}{3N} \tag{5.12}$$

The proof of Equation (5.12) is given in Appendix A. Inserting $R_{AC,\max}$ in Equation (5.11) leads to $R_{CC,\min}$ as,

$$R_{CC,\min} = \frac{N+1}{3N} \tag{5.13}$$

Table 5.2 $R_{AC,\min}$ and $R_{CC,\max}$ Values for Various Length Constant Modulus Basis Sets

N=M	$R_{AC,\max}$	$R_{CC,\min}$
8	4.375	0.375
16	9.688	0.354
32	20.344	0.344
64	41.672	0.339

In the literature, for any constant modulus code, the bound for d_{am} is given as [22, 54-57]

$$d_{am} \geq \frac{1}{N} \tag{5.14}$$

Moreover, any constant modulus complex sequence meeting the bound is called as polyphase Barker Code. Barker Codes are widely used in radar applications, where the detection performance directly relates to the auto-correlation property of the waveform employed in the system.

5.4 Phase Shaping Function and GDFT Design

In this section, the optimal design of function sets based on the performance metrics defined in the previous sections will be considered. In order to simplify the analysis and decrease the number of variables to optimize for each function set, the phase function $\{\varphi_k(n)\ n\}$ of Equation (4.8) is decomposed into two functions in the time variable, *n,* as follows

$$\begin{aligned}
&\hat{\varphi}_k(n) = \varphi_k(n)n = kn + \psi(n) \text{ for } k = 0,1,...,N-1 \text{ and } n = 1,...,N-1 \\
&\psi(n) = \hat{\varphi}_k(n) - kn = [\varphi_k(n) - k]n \text{ for } k = 0,1,...,N-1 \text{ and } n = 1,...,N-1 \\
&\psi(0) \in \mathbf{R} \quad \hat{\varphi}_k(0) = \psi(0)
\end{aligned} \tag{5.15}$$

Hence, the basis functions in this case, are defined as,

$$e_k(n) \triangleq e^{j\frac{2\pi}{N}(kn+\psi(n))} \qquad k,n = 0,1,\ldots,N-1 \tag{5.16}$$

The cross-correlation sequence of a *basis function pair (k,l)* from this set with length-*N* becomes,

$$\begin{aligned}
R_{\hat{\varphi}_k\hat{\varphi}_l}(m) &= \sum_{n=0}^{N-1} e^{j(\frac{2\pi}{N})\hat{\varphi}_k(n)}\ e^{-j(\frac{2\pi}{N})\hat{\varphi}_k(n+m)} \\
&= \sum_{n=0}^{N-1} e^{j(\frac{2\pi}{N})[-lm+(k-l)n+\psi(n)-\psi(n+m)]}
\end{aligned} \tag{5.17}$$

where $R_{\hat{\varphi}_k\hat{\varphi}_l}(m) = 0;\ \forall m$ for the ideal case, and $R_{\hat{\varphi}_k\hat{\varphi}_l}(0) = 0$ implies the orthogonality of the basis function pair. Similarly, the auto-correlation function of a basis function from this set is defined as

$$R_{\hat{\varphi}_k\hat{\varphi}_k}(m) = \sum_{n=0}^{N-1} e^{j(\frac{2\pi}{N})\hat{\varphi}_k(n)}\, e^{-j(\frac{2\pi}{N})\hat{\varphi}_k(n+m)}$$

$$= \sum_{n=0}^{N-1} e^{j(\frac{2\pi}{N})[-km+\psi(n)-\psi(n+m)]} \tag{5.18}$$

where $R_{\hat{\varphi}_k\hat{\varphi}_k}(m) = \delta(m)$ for the ideal case.

Remark 2: It is found out that the magnitude of auto-correlation functions of the individual codes in any GDFT set defined in the form of Equation (5.16) are the same.

Proof: The auto-correlation sequences of the basis $e^{j(\frac{2\pi}{N})\hat{\varphi}_k(n)}$ and $e^{j(\frac{2\pi}{N})\hat{\varphi}_l(n)}$ are given as,

$$R_{\hat{\varphi}_k\hat{\varphi}_k}(m) = \sum_{n=0}^{N-1} e^{j(\frac{2\pi}{N})\hat{\varphi}_k(n)}\, e^{-j(\frac{2\pi}{N})\hat{\varphi}_k(n+m)} = \sum_{n=0}^{N-1} e^{j(\frac{2\pi}{N})[-km+\psi(n)-\psi(n+m)]}$$

$$R_{\hat{\varphi}_l\hat{\varphi}_l}(m) = \sum_{n=0}^{N-1} e^{j(\frac{2\pi}{N})\hat{\varphi}_l(n)}\, e^{-j(\frac{2\pi}{N})\hat{\varphi}_l(n+m)} = \sum_{n=0}^{N-1} e^{j(\frac{2\pi}{N})[-lm+\psi(n)-\psi(n+m)]} \tag{5.19}$$

Magnitudes of this autocorrelation sequences are therefore,

$$\left|R_{\hat{\varphi}_k\hat{\varphi}_k}(m)\right| = \left|e^{-j(\frac{2\pi}{N}km)} \sum_{n=0}^{N-1} e^{j(\frac{2\pi}{N})[\psi(n)-\psi(n+m)]}\right| = \left|\sum_{n=0}^{N-1} e^{j(\frac{2\pi}{N})[\psi(n)-\psi(n+m)]}\right|$$

$$\left|R_{\hat{\varphi}_l\hat{\varphi}_l}(m)\right| = \left|e^{-j(\frac{2\pi}{N}lm)} \sum_{n=0}^{N-1} e^{j(\frac{2\pi}{N})[\psi(n)-\psi(n+m)]}\right| = \left|\sum_{n=0}^{N-1} e^{j(\frac{2\pi}{N})[\psi(n)-\psi(n+m)]}\right| \tag{5.20}$$

Therefore,

$$\left|R_{\hat{\varphi}_k\hat{\varphi}_k}(m)\right| = \left|R_{\hat{\varphi}_l\hat{\varphi}_l}(m)\right| = \left|\sum_{n=0}^{N-1} e^{j(\frac{2\pi}{N})[\psi(n)-\psi(n+m)]}\right| \tag{5.21}$$

The correlation sequences of a pair of basis functions are incorporated in the R_{AC} and R_{CC} metrics of Equation (5.5) and Equation (5.6), respectively in the following design example. The numerical optimization software tools Mathematica and MATLAB are used to obtain optimal phase shaping functions with respect to the metrics of Equation

(5.5) and Equation (5.6). In Figure 5.1 and Figure 5.2 the optimal phase shaping functions minimizing the correlation metrics R_{AC} and R_{CC} for the first two functions of the GDFT ($k = 0, l = 1$) with N=8 are displayed.

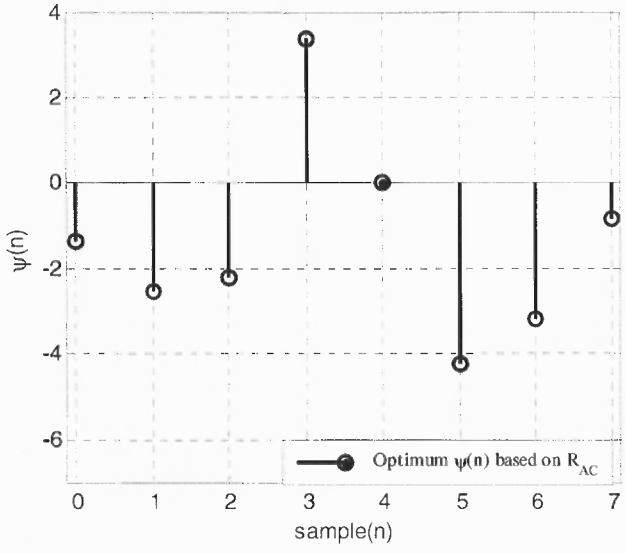

Figure 5.1 Optimal phase shaping functions minimizing the correlation metric R_{AC} for the first two functions of GDFT set with N=8.

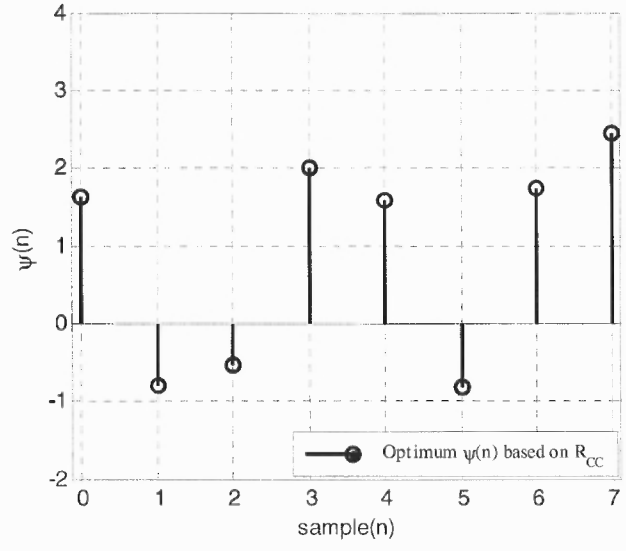

Figure 5.2 Optimal phase shaping functions minimizing the correlation metric R_{CC} for the first two functions of GDFT set with N=8.

The resulting R_{AC} and R_{CC} values for these optimal GDFT designs are tabulated in Table 5.3 along with their DFT counterparts for comparison purposes.

Table 5.3 R_{AC} and R_{CC} Values for the First Two Functions of Optimal GDFT Sets with $N=8$ Along with Their DFT Counterparts

Numerical Search Tool and Optimal Phase Shaping Function	OPTIMIZATION METRIC (N=8)	
	R_{AC}	R_{CC}
GDFT (Mathematica, *FindMinimum*)	**0.0877**	**0.4219**
$\psi(n)$	{ -1.37, -2.53, -2.21, 3.39, 0.0, -4.21, -3.19, -0.83 }	{ 1.637, -0.79, -0.54, 2.01, 1.59, -0.83, 1.73, 2.44}
GDFT (MATLAB, *fminsearch*)	0.086	0.4205
$\psi(n)$	{ -1.38, -2.56, -2.24, 3.42, 0.07, -4.27, -3.27, -0.80 }	{ 1.673, -0.87, -0.51, 2.02, 1.51, -0.86, 1.70, 2.46 }
DFT	**4.375**	**0.8536**

fminsearch of MATLAB finds the minimum value of a function of several variables. This function needs an initial value to start and is mostly preferred in unconstrained non-linear optimization processes. It uses Nelder-Mead Simplex Method [68] to find minimum values. *FindMinimum of* Mathematica is similar to *fminsearch* with the difference of the methods it uses in the optimization process. Several optimization methods are available with *FindMinimum* including Gauss-Newton, Nonlinear Conjugate Gradient, Principal Axes Methods. These methods are well discussed in [69, 70]. In the search process explained above, no method is specified in the optimization with *FindMinimum*. In that case, *FindMinimum* automatically assigns the method according to the specifications of the function to be minimized.

In the previous design example, only first two functions with the indices $k=0, l=1$ are considered. If the design is generalized to all the pairs in the set, the optimum pair based on R_{AC} and R_{CC} obtained is the basis functions with the indices $k=1$ and $l=5$. Note that for the DFT set, the optimum pair with respect to the optimization metric has the same indices. The corresponding R_{AC} and R_{CC} values for the GDFT and the DFT pair are listed in Table 5.4.

Table 5.4 R_{AC} and R_{CC} Values for the Functions with Indices $k=1$ and $l=5$ of Optimal GDFT Sets with $N=8$ Along with Their DFT Counterparts

Optimal Phase Shaping Function	OPTIMIZATION METRIC (N=8)	
	R_{AC}	R_{CC}
GDFT	**0.086**	**0.089**
$\psi(n)$	{ -1.38 -2.56 -2.24 3.42 0.07 -4.27 -3.27 -0.80 }	{ -3.12 -3.38 -3.2 -1.86 -1.27 0.06 0.25 -0.01 }
DFT	**4.375**	**0.125**

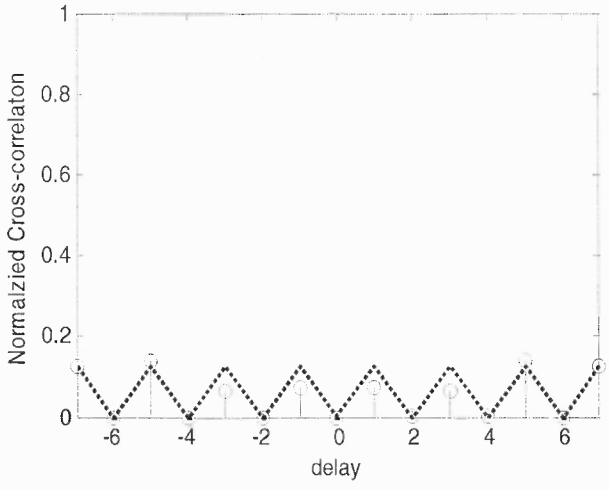

Figure 5.3 Normalized cross-correlation sequences of the functions with indices $k=1$, $l=5$ of optimal GDFT set based on R_{CC} along with DFT set for $N=8$.

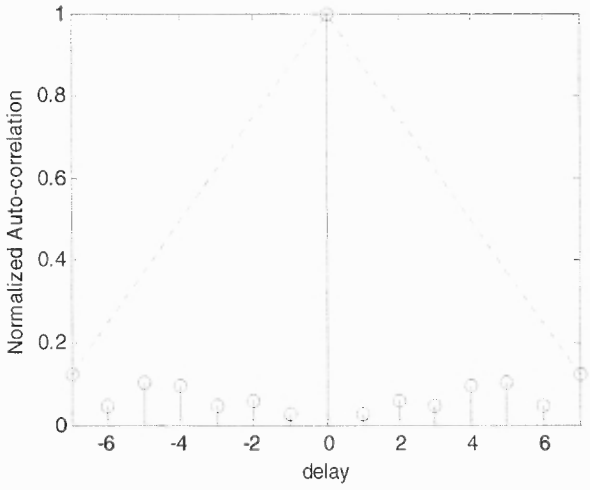

Figure 5.4 Normalized auto-correlation of the functions with indices $k=1$, $l=5$ of optimal GDFT set based on R_{AC} along with DFT set for *N=8*.

Remark 3: Oppermann showed that the minimum value of R_{CC} obtained between any pair taken from his family is equal to $\frac{1}{N}$ where N denotes the code length [25],. This minimum value is equal to 0.125 for *N=8*. From Table 5.4, it is observed that the minimum achievable R_{CC} with a GDFT pair for *N=8* is equal to 0.089 which is lower than the minimum achievable value with Oppermann family.

Note that the optimal design method explained in this section might be generalized for any performance metric and for any size GDFT. In chapter 6, an example of communications applications for the proposed GDFT framework will be presented, where the correlations dictate the system performance.

5.5 Optimal GDFT Design with Brute Force Search

In the previous section, the optimal pairs ($M=2$) in a GDFT set with respect to the performance metrics are discussed. In this section, the design will be extended to complete sets where $N = M$. As a simple example, only two terms in Equation (4.10) are used as

$$\begin{aligned} &\varphi_k(n) = a_{k1} n^{b_{k1}} + a_{k2} n^{b_{k2}} \\ &a_{k1}=k \\ &b_{k1}=0 \\ &\varphi_k(n) = k + a_{k2} n^{b_{k2}} \end{aligned} \tag{5.22}$$

Therefore, the basis functions of the set are defined according to Equation (4.8) as

$$\begin{aligned} &e_k(n) = e^{j(2\pi/N)\varphi_k(n)n} \\ &e_k(n)=e^{j(2\pi/N)(k+a_{k2}n^{b_{k2}})n} = e^{j(2\pi/N)[kn+a_{k2}n^{(b_{k2}+1)}]} \\ &e_k(n)=e^{j(2\pi/N)kn} e^{j(2\pi/N)[a_{k2}n^{(b_{k2}+1)}]} \quad k,n=0,1,\ldots,N-1 \end{aligned} \tag{5.23}$$

Note that the first exponential term of the last equation is the DFT kernel with linear phase while the second exponential term defines the G matrix and $\{e_k(n)\}$ are the row sequences of A_{GDFT} matrix that is defined in the following matrix form

$$A_{GDFT} = A_{DFT} G \tag{5.24}$$

In this form, by changing the values of real a_{k2} and b_{k2} coefficients, one might obtain many different GDFT sets with desirable auto- and cross-correlation properties and nonlinear phase functions.

The entire phase space is searched with various search grid resolutions using ff force search algorithm in order to find the optimum G matrices. In the previous section, several metrics have been defined for the evaluation of various code sets. This section displays the values of these metrics for optimal A_{GDFT} matrices obtained in the solutions space utilizing a brute-force search where the search grid resolution is defined by the binary valued $a_{k2} = a_2$ and $b_{k2} = b_2$ coefficients with the corresponding number of bits per coefficient. Table 5.5 tabulates the optimal values of the metric $d_{\max}$ along with other performance metrics for various search grid resolutions defined as $\Delta_{a_2,b_2} = N/2^b$ where b is the search grid resolution in bits per coefficient and $0 \le a_2, b_2 \le N-1$ for the code length of $N = 8$.

Table 5.5 Values of Various Metrics When Optimal Design is Based on the Performance Metric $d_{\max}$ for the Code Length of N=8

b ***(bits/c)***	d_{am}	d_{cm}	$d_{\max}$ ***(OPT)***	R_{AC}	R_{CC}	F
4	0.301	0.442	0.442	0.526	0.925	1.900
6	0.376	0.409	0.409	0.854	0.878	1.171
8	0.341	0.387	0.387	0.576	0.918	1.738
9	0.376	0.387	0.387	1.095	0.843	0.912

As can be seen from the table, there is no more improvement in $d_{\max}$ after 8-bit of resolution in the design. This is due to the limited structure of $\varphi_k(n)$ in Equation (5.22).

Similarly, Table 5.6 displays the correlation performance metrics for various known codes along with the optimal A_{GDFT} set obtained through a brute force search based on the design metric $d_{\max}$ for the length of $N=8$.

Table 5.6 Performance Metrics for Various Popular Code Families with the Length of $N=7$ *or* 8

Code	d_{am}	d_{cm}	$d_{\max}$	R_{AC}	R_{CC}	F
Walsh [8x8]	0.875	0.875	0.875	2.375	0.661	0.421
Walsh-like [8x8], [41]	0.625	0.625	0.625	0.875	0.875	1.143
DFT [8x8]	0.875	0.327	0.875	4.375	0.375	0.220
7/8 Gold	0.714	0.714	0.714	0.857	0.878	1.167
Oppermann Set,[25] ($opt\, d_{\max}$) (m=1, p=1, n=2.98, $N=7$)	0.425	0.419	0.425	1.278	0.787	0.783
A_{GDFT} [8x8] ($opt\, d_{\max}$)	0.376	0.387	0.387	1.095	0.843	0.912

Among all the codes compared, GDFT set gives the minimum $d_{\max}$ value. Comparing the $d_{\max}$ value of optimum size-8 GDFT set as given in Table 5.6 with the Welch bound for $N=M=8$ as given in Table 5.1 ,one can see that the achievable $d_{\max}$ value with GDFT is equal to 1.6 times the Welch bound. Also, it is observed that the DFT set yields the maximum value of R_{AC} or the minimum value of R_{CC} for this length when compared its R_{AC} and R_{CC} values with Table 5.2 for $N=8$.

In Figure 5.3, the variation of design metrics R_{AC}, R_{CC} and d_{cm} with the coefficient b_2 when $a_2 = 1$ is displayed. For this specific value of a_2, it was observed that R_{CC} is below one for any value of b_2. On the other hand, R_{AC} value changes between its maximum, 4.375, and 0.2136.

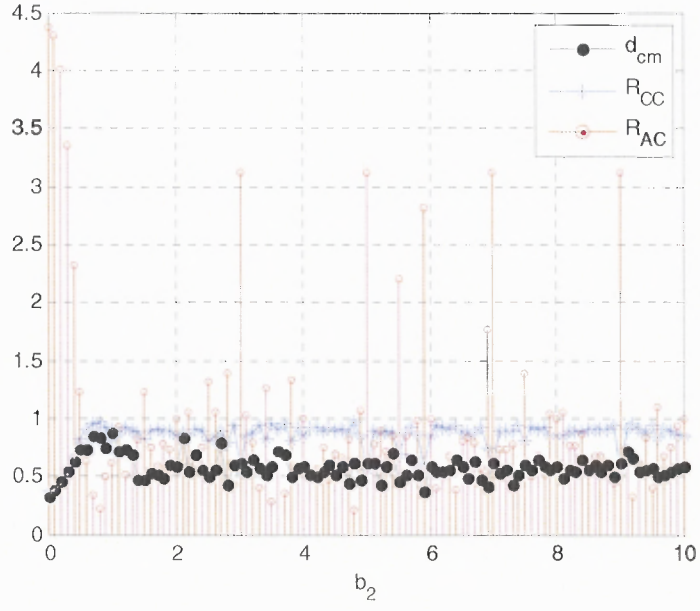

Figure 5.5 The variations of the design metrics R_{AC}, R_{CC} and d_{cm} as a function of the coefficient b_2 for $a_2 = 1$ and code length of N=8.

Figure 5.4 and Figure 5.5 display the inter-dependence of the auto- and cross-correlation metrics R_{AC} and R_{CC}, respectively, on both of the design parameters a_2 and b_2 defined in Equation (5.22). In a communications application, depending on the system type of either OFDM based or CDMA based, one might choose optimum values of a_2 and b_2 for the desired values of auto- and cross-correlation metrics, R_{AC} and R_{CC}, respectively. In OFDM systems, frequency localization is more important and the

optimization is emphasized on R_{CC} parameters whereas in a DS-CDMA system, for higher number of users, R_{AC} and R_{CC} both are equally significant. The low values of R_{AC} is desired to mitigate multi-path effect of the channel. In contrast, the low values of R_{CC} is required to minimize multi-user interference (MUI) that dictates the system's BER performance. However, these two parameters can not be minimized at the same time due to their mathematical relationship expressed as in Equation (5.11).

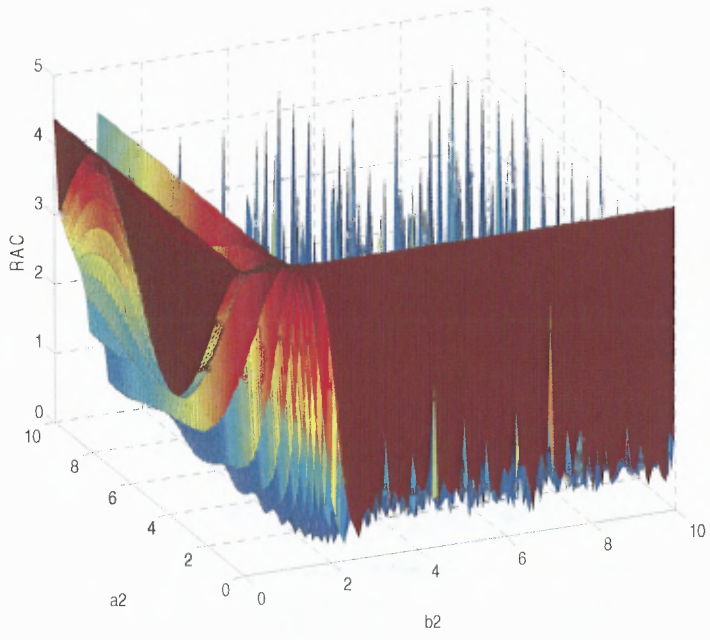

Figure 5.6 Variation of the auto-correlation metric R_{AC} as a function of the design parameters a_2 and b_2.

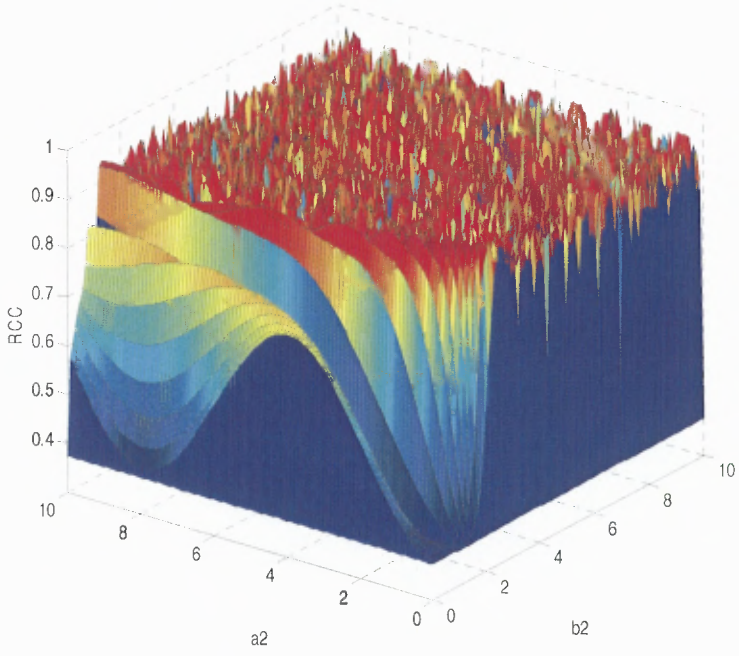

Figure 5.7 Variation of the cross-correlation metric R_{CC} as a function of the design parameters a_2 and b_2.

Note that the orthogonal DFT set corresponds to only one point in these figures. However the proposed method is able to generate infinitely many orthogonal sets with various correlation properties.

5.6 Closed Form Phase Shaping Function

In the previous design example, $\psi(n)$ function in Equation (5.15) was in the form of

$$\psi(n) = a_2 n^{(b_2+1)} \quad n = 0,1,...,N-1 \tag{5.25}$$

Now, no restriction is put on the form of $\psi(n)$ functions and all the available phase space, $[0, 2\pi]$, is searched based on the metrics defined in Section 5.2. The resolution of the search algorithm is defined by the number of bits representing each phase value. For

m number of bits, the phase resolution is given as $\Delta\theta = \frac{2\pi}{2^m}$. m is chosen as five in the search process. Later this brute force based optimal solutions are used to define a closed form expression for the *phase shaping function (PSF)*, $\psi(n)$, given in Equation (5.15) via curve-fitting. A signal processing software tool, namely *Table Curve 2D*, is used for curve-fitting operation. The fitted *PSF* to the phase of the optimal GDFT set obtained based on the minimization of the design metric d_{cm} for $N=8$ is expressed as

$$\psi(n) = a_1 \exp\left(-\left[\frac{n-b_1}{c_1}\right]^2\right) + a_2 \exp\left(-\left[\frac{n-b_2}{c_2}\right]^2\right) \qquad n = 0,1,.....,N\text{-}1 \tag{5.26}$$

This is a second degree Gaussian function defined with six defining parameters $\{a_1, b_1, c_1, a_2, b_2, c_2\}$. This PSF has shown to yield the minimum values of d_{cm} as well as R_{AC} obtained by the brute-force algorithm for all sizes. For d_{cm} optimized GDFT, the set of parameters is given as $\{a_1 = 1, b_1 = 1.75, c_1 = 3.75, a_2 = 1.75, b_2 = 6, c_2 = 0.5\}$. Similarly, for R_{AC} optimized GDFT set, these parameters are obtained as $\{a_1 = \text{-}1.13, b_1 = 5.03, c_1 = 0.18, a_2 = 6.35, b_2 = 1.83, c_2 = 1.3\}$. Note that all the sequences in the minimum R_{AC} set for $N=8$ satisfy the equality of Equation (5.14) and therefore they all are *polyphase Barker Codes*. Table 5.7 displays the correlation performance metrics for various known codes along with these optimal A_{GDFT} sets for the length of $N=7$ *or* 8.

Table 5.7 Performance Metrics for Various Popular Code Families Along with Optimum GDFT Sets on d_{cm} and R_{AC} for *N=7 or 8*

Code	d_{am}	d_{cm}	$d_{\max}$	R_{AC}	R_{CC}	F
Walsh [8x8]	0.875	0.875	0.875	2.375	0.661	0.421
Walsh-like [8x8], [41]	0.625	0.625	0.625	0.875	0.875	1.143
DFT [8x8]	0.875	0.327	0.875	4.375	0.375	0.220
7/8 Gold	0.714	0.714	0.714	0.857	0.878	1.167
7/6 Oppermann [24] $(opt\, d_{cm})\{m,n,p\} = \{1,1.025,7\}$	0.857	0.381	0.857	3.714	0.381	0.269
$^{A}GDFT$ [8x8] $(opt\, d_{cm})$	0.682	0.288	0.682	3.111	0.550	0.321
$^{A}GDFT$ [8x8] $(opt\, R_{AC})$	0.125	0.679	0.679	0.089	0.987	11.23

Figure 5.9 and Figure 5.11 display the closed form phase shaping functions, $\psi(n)$'s, defined by identifying the parameter set of Equation (5.26) for low-d_{cm} and low-R_{AC} GDFT design, respectively. Moreover, Figure 5.10 and 5.12 display the nonlinear phase functions of low-d_{cm} and low-R_{AC} GDFT sets generated by using $\psi(n)$ of Equation (5.26) along with linear phase functions of DFT where $\psi(n) = 0$ for *N=8*, in the time domain, respectively. It is shown that relaxing the linear phase property of DFT offers nonlinear phase GDFT solutions with various correlation properties.

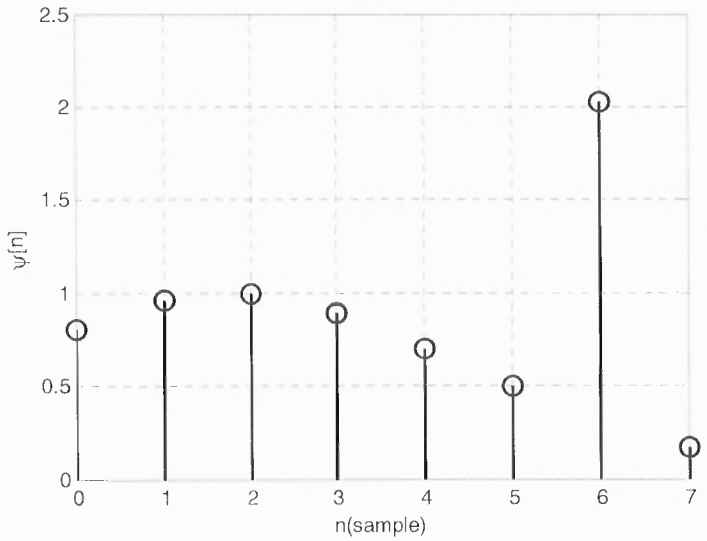

Figure 5.8 Closed form phase shaping function of Equation (5.26), $\psi(n)$, for optimal GDFT set based on d_{cm}, for $N = 8$.

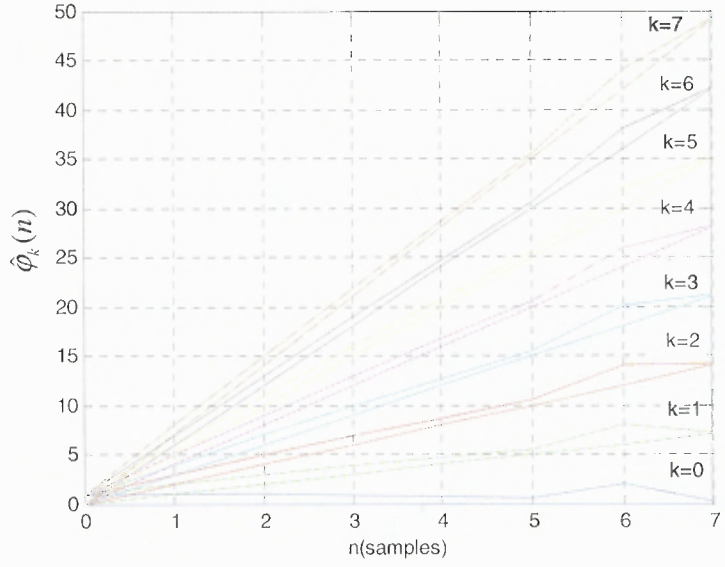

Figure 5.9 $\hat{\varphi}_k(n)$ for the linear phase DFT set along with $\hat{\varphi}_k(n)$ for optimal non-linear phase GDFT set based on d_{cm} for $N=8$.

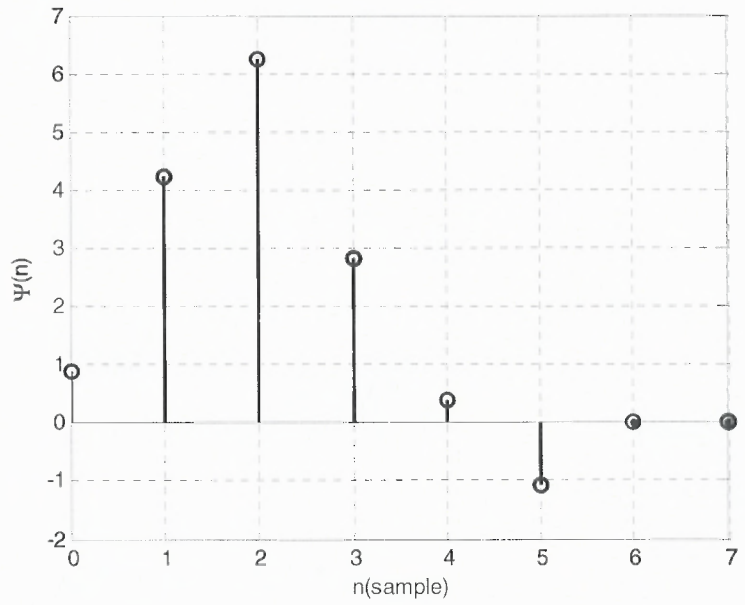

Figure 5.10 Closed form phase shaping function of Equation (5.26), $\psi(n)$, for optimal GDFT set based on R_{AC}, for $N=8$.

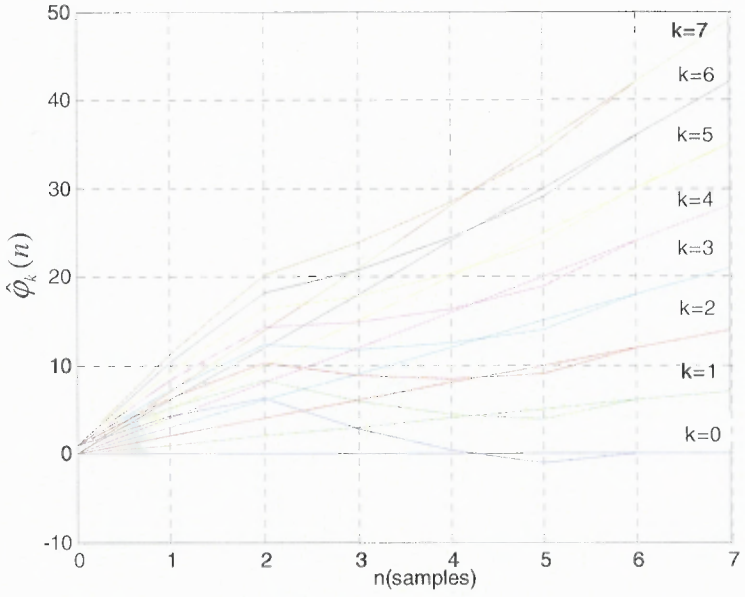

Figure 5.11 $\hat{\varphi}_k(n)$ for the linear phase DFT set along with $\hat{\varphi}_k(n)$ for optimal non-linear phase GDFT set on R_{AC} for $N=8$.

In Figure 5.13, phases of DFT functions (bases), including the constant $2\pi / N$ in Equation (3.12) are displayed. Similarly, in Figure 5.14, phases of GDFT bases optimized on d_{cm} are displayed. The shape of the phase function of the first basis in GDFT set simply becomes the *PSF* defined in Equation (5.26) for GDFT case whereas it is simply equal to zero for DFT case.

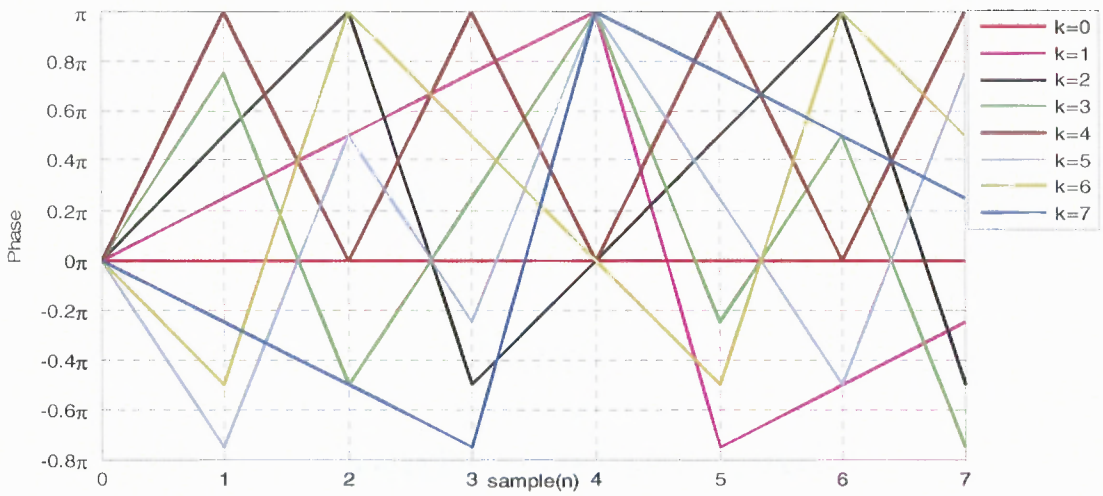

Figure 5.12 Phases of DFT bases in time for $N=8$.

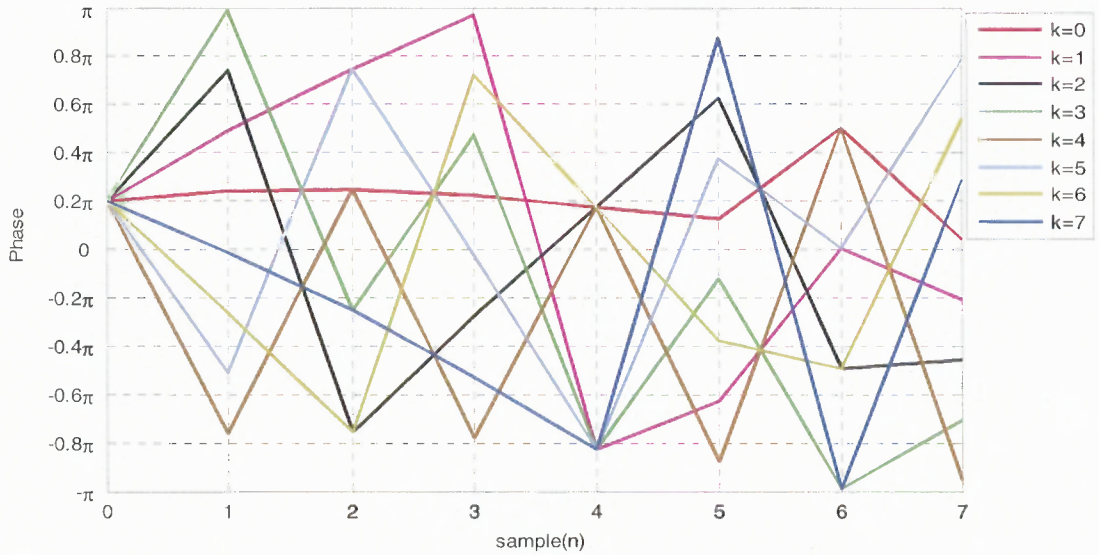

Figure 5.13 Phases of GDFT bases optimized on d_{cm} in time for $N=8$.

For comparison purposes, amplitude spectrums of DFT and GDFT functions optimized on d_{cm} and R_{AC} are displayed in Figure 5.15, Figure 5.16 and Figure 5.17, respectively. One important observation from these figures is that changing phase property of the basis from linear to non-linear reflected itself in amplitude change in frequency domain, which will be worked on in detail in the context of Hilbert Transform in the future.

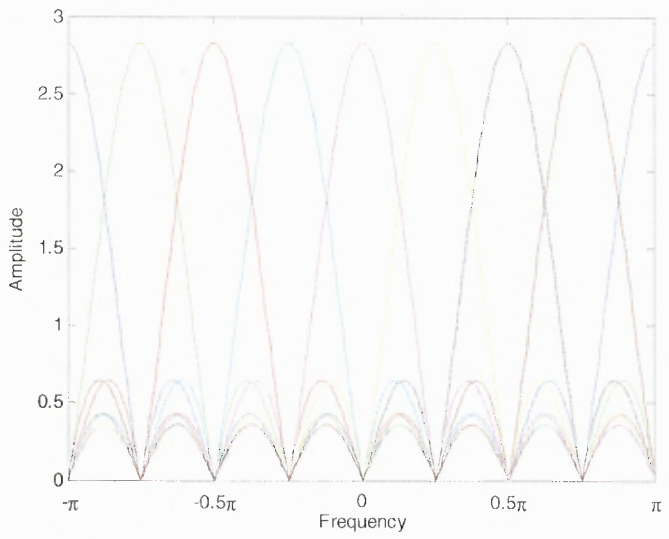

Figure 5.14 Amplitude spectrum of the linear phase functions of DFT set for *N=8*.

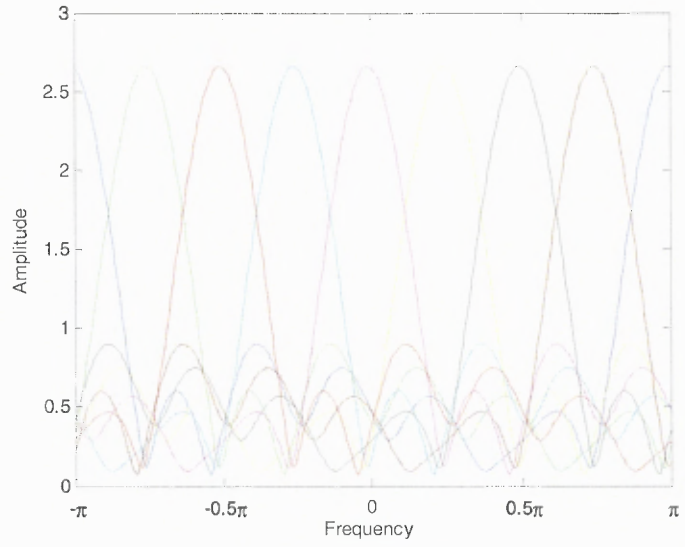

Figure 5.15 Amplitude spectrum of the non-linear phase functions of optimal GDFT set based on d_{cm} obtained using Equation (5.26) for $N=8$.

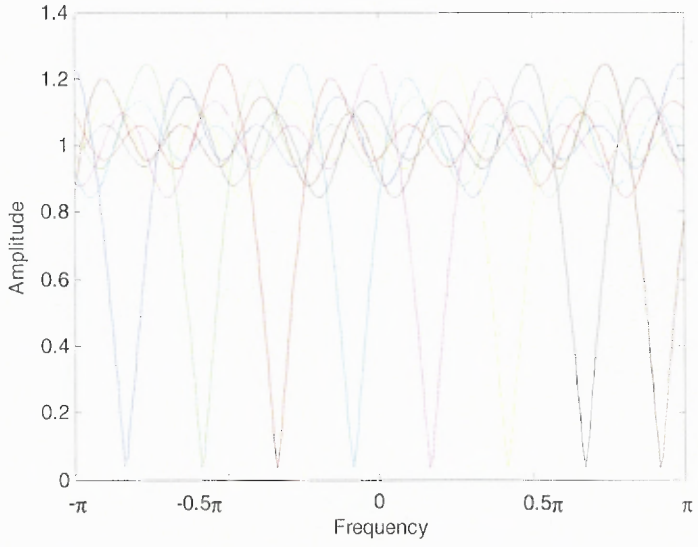

Figure 5.16 Amplitude spectrum of the non-linear phase functions of optimal GDFT set based on R_{AC} obtained using Equation (5.26) for $N=8$.

In order to emphasize the non-linear phase properties of GDFT sets, in Figure 5.15 and Figure 5.16, the phase spectrums of linear-phase DFT and GDFT set optimized on d_{cm} are displayed, respectively.

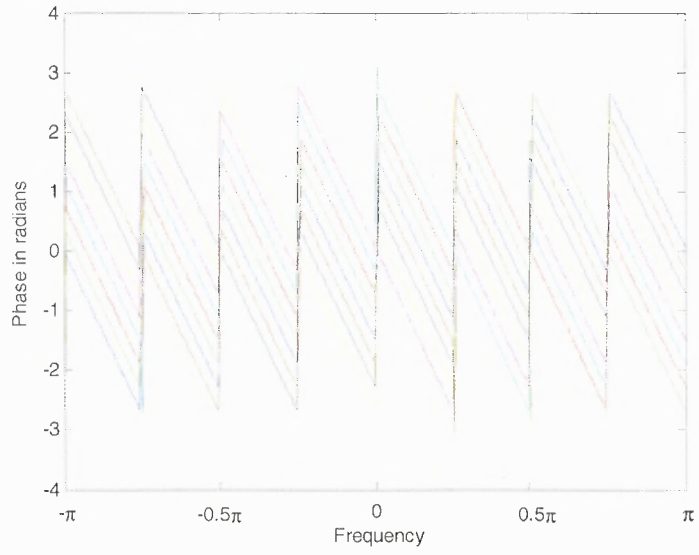

Figure 5.17 Phase spectrum of linear phase DFT bases for $N=8$.

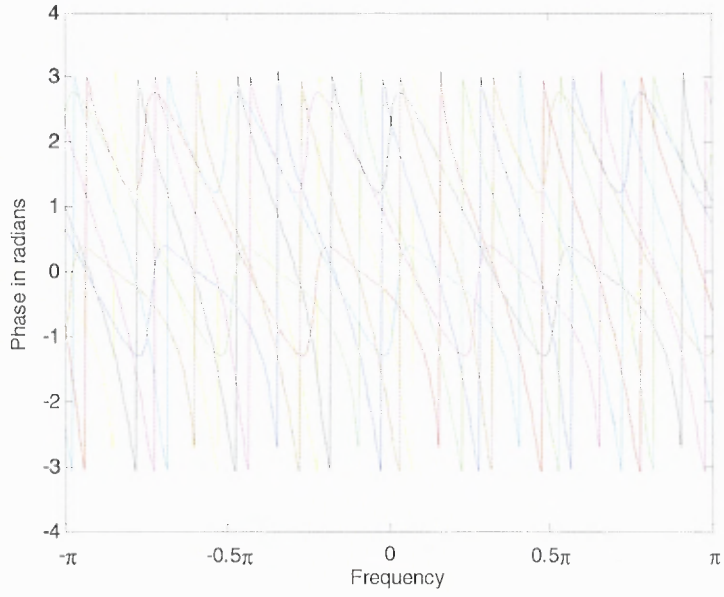

Figure 5.18 Phase Spectrum of non-linear phase GDFT bases optimized on d_{cm} for $N=8$.

5.7 Time-Frequency Localizations of GDFT Bases

Time domain center and spread values, frequency domain center and spread values $\{\bar{n}, \bar{\omega}, \sigma_n^2, \sigma_\omega^2\}$ are calculated as discussed in Section 2.2 for proposed 8-length GDFT codes optimized on d_{cm} and R_{AC}, Walsh and DFT function sets and plotted in Figure 5.17. Note that the time and frequency spreads of some basis functions of these sets may not be visible in the figure since they overlap. From the figure, it is observed that all the code families considered have constant time spreads σ_n^2's, as they have the same fixed power level. Walsh code sequences have less frequency domain spread values compared to all function sets. The largest frequency spread is achieved by GDFT set optimized on R_{AC}.

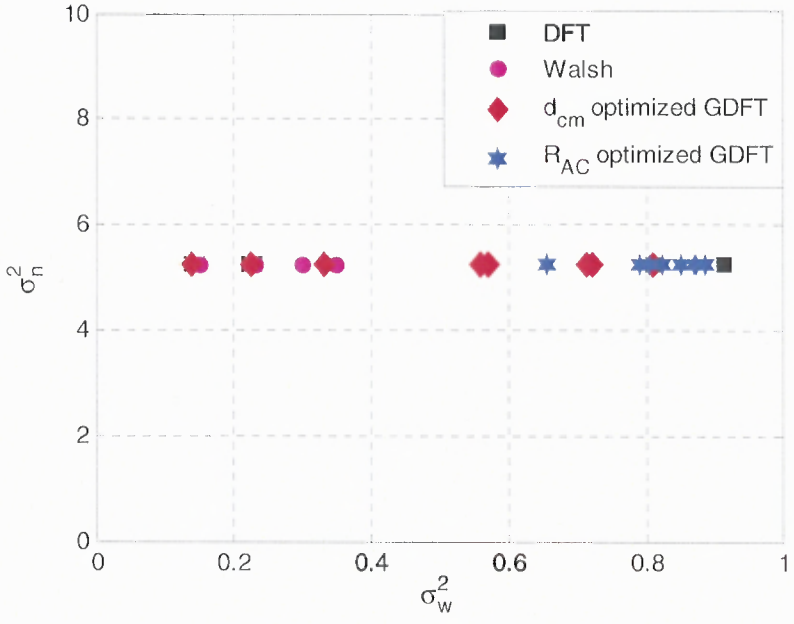

Figure 5.19 Time-frequency localizations for Walsh, DFT and, proposed 8-length GDFT function sets.

5.8 Higher Size GDFT Sets with Closed Form PSF's

In this section, the previous discussions will be extended to the higher size optimal GDFT sets based on two metrics, namely d_{cm} and R_{AC}. The goal is to define the parameters of the function defined in Equation (5.26) generating orthonormal GDFT basis yielding minimum values of d_{cm} and R_{AC} for several sizes. The importance of minimizing these two metrics will be emphasized in the following chapters through system simulations.

The numerical optimization tool, f*minsearch* of MATLAB is employed for obtaining higher size *PSF*'s of the optimum GDFT sets based on different design metrics. The phase shaping function kernel of Equation (5.26) is used in the phase function of (5.15) with different values of the parameters $\{a_1, b_1, c_1, a_2, b_2, c_2\}$. Since the phase is already constraint to the interval $[0, 2\pi]$, no additional constraint is put on the values. The algorithm is run for four different transform sizes, *N=16, 32, 64* and *128*. The performance metrics of the higher size optimum sets based on d_{cm} and R_{AC} are tabulated in Table 5.8 and Table 5.9, respectively.

Table 5.10 and Table 5.11 display the correlation performance metrics for various known codes along with the optimal A_{GDFT} sets for the length of *N=31/32* and *N=61/63/64,* respectively.

Table 5.8 Various Performance Metrics When Optimal Design is Based on the Metric d_{cm} for Code Lengths of $N = 8, 16, 32, 64$ and 128

Size (N)	Corresponding correlation metrics optimized based on d_{cm} along with DFT				
	d_{am}	d_{cm}	$d_{\max}$	R_{AC}	R_{CC}
8 GDFT 8 DFT	0.703 0.875	0.288 0.327	0.703 0.875	3.261 4.375	0.534 0.375
16 GDFT 16 DFT	0.764 0.938	0.267 0.321	0.764 0.938	6.918 9.688	0.539 0.354
32 GDFT 32 DFT	0.827 0.969	0.251 0.319	0.827 0.969	14.357 20.34	0.536 0.344
64 GDFT 64 DFT	0.894 0.984	0.243 0.318	0.894 0.984	25.61 41.67	0.593 0.339
128 GDFT 128 DFT	0.956 0.992	0.236 0.318	0.956 0.992	53.49 84.33	0.579 0.335

Table 5.9 Various Performance Metrics When Optimal Design is Based on the Metric R_{AC} for Code Lengths of $N = 8, 16, 32, 64$ and 128

Size (N)	Corresponding correlation metrics optimized based on R_{AC} along with DFT				
	d_{am}	d_{cm}	$d_{\max}$	R_{AC}	R_{CC}
8 GDFT 8 DFT	0.125 0.875	0.679 0.327	0.679 0.875	0.089 4.375	0.987 0.375
16 GDFT 16 DFT	0.137 0.938	0.935 0.321	0.935 0.938	0.136 9.688	0.991 0.354
32 GDFT 32 DFT	0.083 0.969	0.966 0.319	0.966 0.969	0.105 20.34	0.997 0.344
64 GDFT 64 DFT	0.071 0.984	0.982 0.318	0.998 0.984	0.092 41.67	0.998 0.339
128 GDFT 128 DFT	0.044 0.992	0.992 0.318	0.992 0.992	0.056 84.34	0.999 0.336

Table 5.10 Performance Metrics for Various Popular Code Families Along with Optimum GDFT Sets on d_{cm} and R_{AC} for *N=31* or *32*

Code	d_{am}	d_{cm}	$d_{\max}$	R_{AC}	R_{CC}
Walsh [32x32]	0.969	0.969	0.969	6.593	0.787
DFT [32x32]	0.969	0.319	0.969	20.34	0.344
31/32 Gold	0.387	0.387	0.387	0.968	0.961
31/30 Oppermann $\{m,n,p\}=\{1,1,1\}$ [25]	0.968	0.318	0.968	19.678	0.344
GDFT [32x32] ($opt\, d_{cm}$)	0.827	0.251	0.827	14.357	0.536
GDFT [32x32] ($opt\, R_{AC}$)	0.083	0.966	0.966	0.105	0.997

Table 5.11 Performance Metrics for Various Popular Code Families Along with Optimum GDFT Sets on d_{cm} and R_{AC} for *N=61, 63 or 64*

Code	d_{am}	d_{cm}	$d_{\max}$	R_{AC}	R_{CC}
Walsh [64x64]	0.984	0.984	0.984	10.391	0.835
DFT [64x64]	0.984	0.318	0.984	41.67	0.339
63/64 Gold	0.349	0.349	0.349	0.995	0.984
61/60 Oppermann $\{m,n,p\}=\{1,1.15,1\}$ [25]	0.984	0.371	0.984	39.24	0.346
GDFT [64x64] ($opt\, d_{cm}$)	0.894	0.243	0.894	25.61	0.593
GDFT [64x64] ($opt\, R_{AC}$)	0.071	0.982	0.998	0.092	0.998

The phase shaping functions of the higher size GDFT sets discussed above are given in Appendix B.

In Figure 5.21, 5.23, 5.25 and 5.27, the auto-correlation function of a code in size-16, 32, 64 and 128 GDFT sets optimized based on R_{AC} is displayed along with the auto-correlation function of a code in size-16, 32, 64 and 128 DFT set, respectively. Similarly, cross-correlation functions of the first and second codes of low-d_{cm} based GDFT design and the DFT set for *N=16, 32, 64* and *128* are displayed in Figure 5.22, 5.24, 5.26 and 5.28, respectively. Having zero correlation value at zero delay implies the orthogonality of the basis functions considered. In the cross-correlation figures, only the first pair is considered since this pair generates the highest cross-correlations for both GDFT and DFT sets.

The main advantage of the proposed method is its ability to design a wide selection of constant modulus orthogonal code sets based on the desired correlation performance metrics mimicking the specs of real world application at hand. Moreover, the proposed GDFT technique is an enhancement to the DFT based implementations with potential performance improvements.

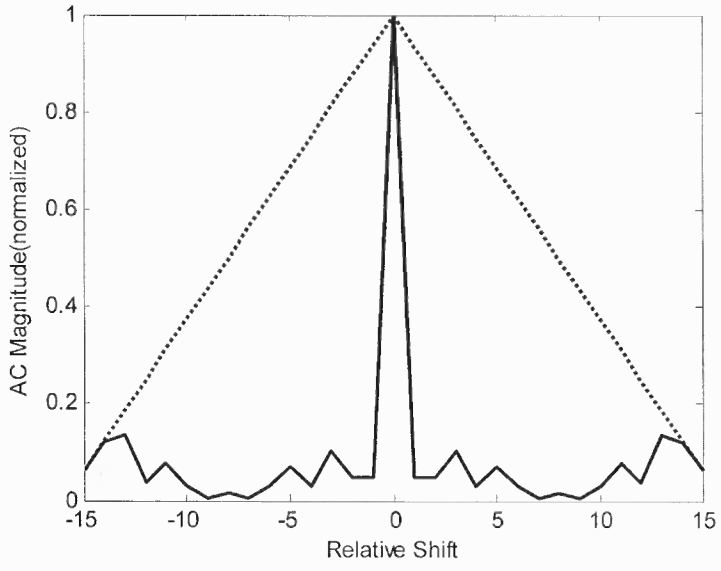

Figure 5.20 Magnitude of auto-correlation functions for R_{AC} based GDFT design (solid line) and DFT (dashed line) sets for size *N=16.*

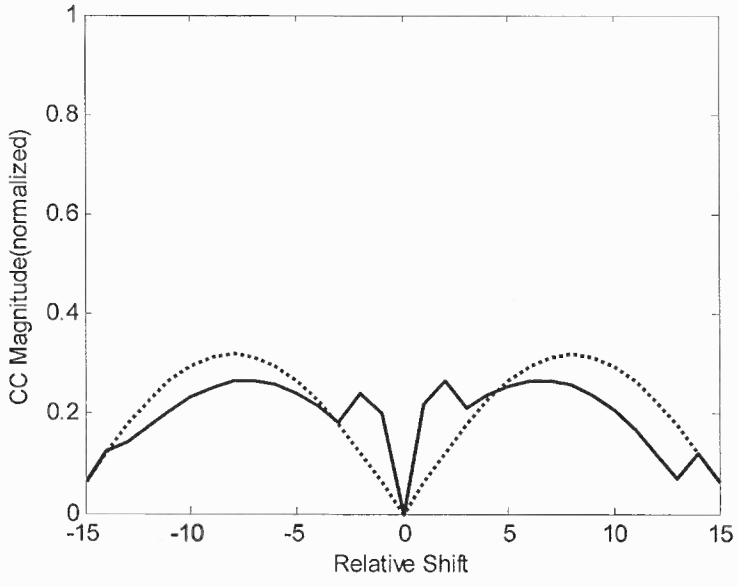

Figure 5.21 Magnitude of cross-correlation functions for d_{cm} based GDFT design (solid line) and DFT (dashed line) sets for size *N=16.*

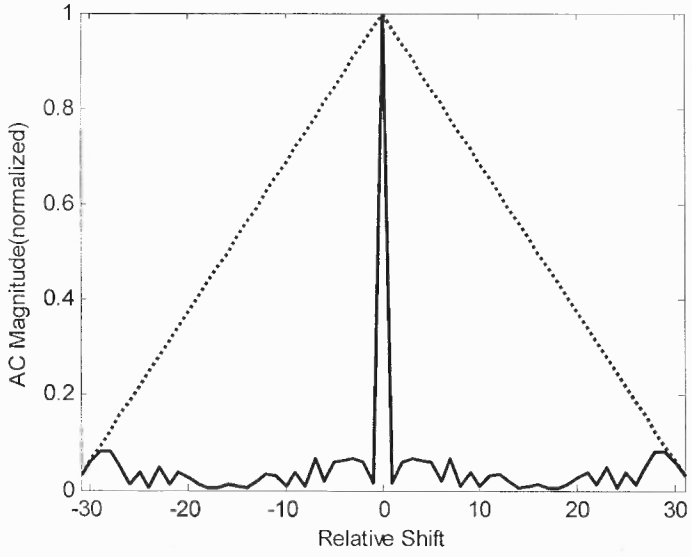

Figure 5.22 Magnitude of auto-correlation functions for R_{AC} based GDFT design (solid line) and DFT (dashed line) sets for size *N=32.*

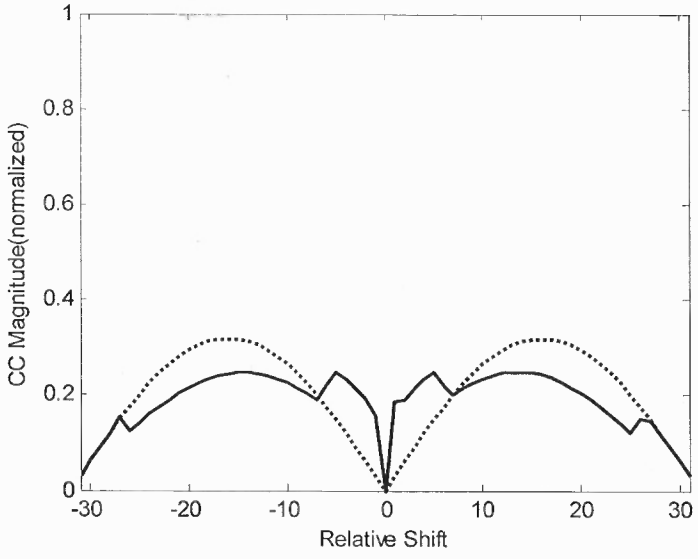

Figure 5.23 Magnitude of cross-correlation functions for d_{cm} based GDFT design (solid line) and DFT (dashed line) sets for size *N=32.*

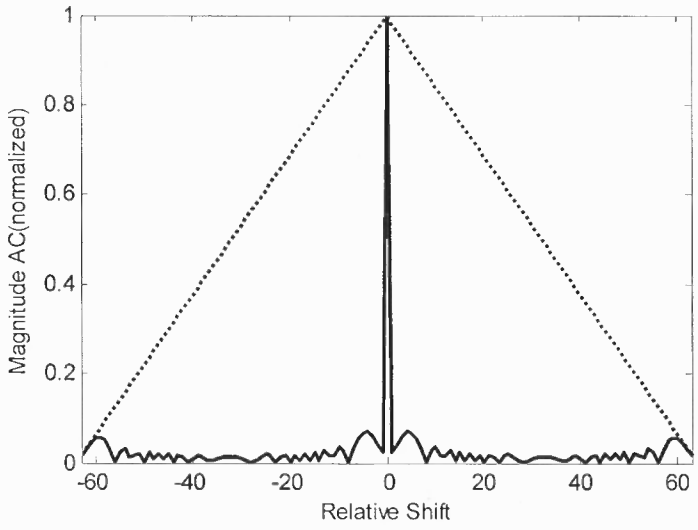

Figure 5.24 Magnitude of auto-correlation functions for R_{AC} based GDFT design (solid line) and DFT (dashed line) sets for size $N=64$.

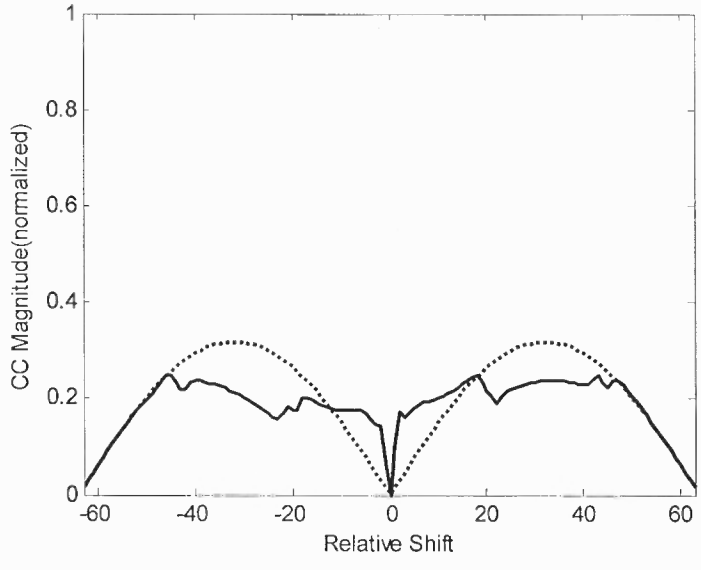

Figure 5.25 Magnitude of cross-correlation functions for d_{cm} based GDFT design (solid line) and DFT (dashed line) sets for size $N=64$.

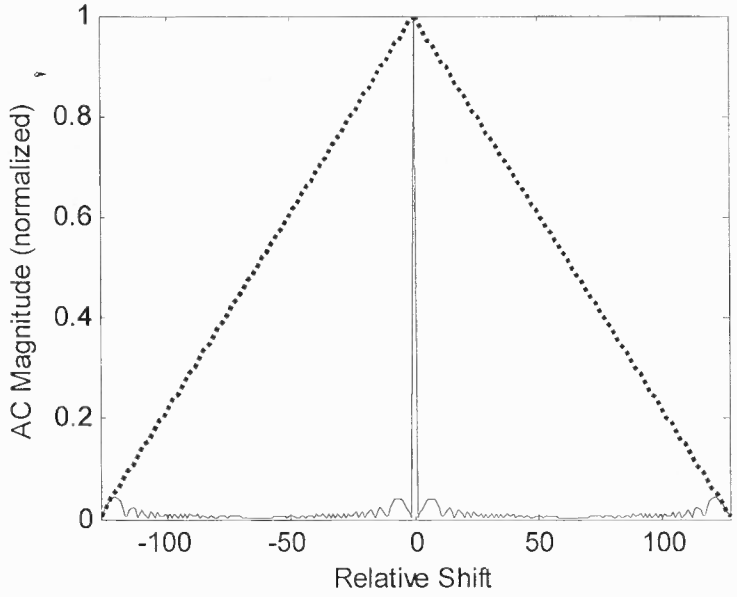

Figure 5.26 Magnitude of auto-correlation functions for R_{AC} based GDFT design (solid line) and DFT (dashed line) sets for size *N=128*.

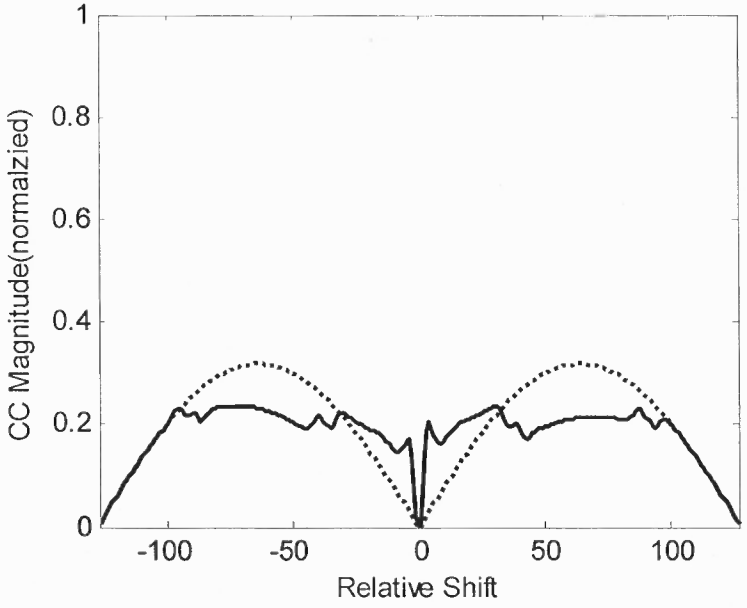

Figure 5.27 Magnitude of cross-correlation functions for d_{cm} based GDFT design (solid line) and DFT (dashed line) sets for size *N=128*.

CHAPTER 6

SPREADING CODE DESIGN WITH GDFT FOR CDMA

6.1 Introduction

In this chapter, the performances of orthogonal GDFT codes in a DS/CDMA communications system will be discussed. First the mathematical model of DS/CDMA systems considered will be given. Later, the proposed GDFT codes will be employed in synchronous and asynchronous DS/CDMA system in AWGN and Rayleigh multi-path channels.

6.2 Mathematical Model for DS/CDMA Communications

Direct Sequence Code Division Multiple Access (DS/CDMA) is one of the most popular applications among the various CDMA techniques. In DS/CDMA, each user is assigned a spreading code as the carrier to transmit its data bits through the channel. In the receiver, the received signal is despreaded by the locally generated code sequence and then demodulated. In order to successfully despread the input sequence, the receiver needs to know the code sequence of the intended user as well as to synchronize the received signal with the locally generated code. After detection, the original data bits are recovered.

Assume that k^{th} user has its data sequence $b_k(t)$ and spreading code waveform $e_k(t)$ in continuous time mathematically expressed as [50]

$$\begin{aligned} b_k(t) &= \sum_{l=-\infty}^{\infty} b_{k,l} p_T(t-lT) \\ e_k(t) &= \sum_{m=-\infty}^{\infty} e_k(m) p_{T_c}(t-mT_c) \end{aligned} \tag{6.1}$$

where $b_{k,l} \in \{+1,-1\}$, $p_\tau(t)=1$ for $0 \le t \le \tau$, otherwise $p_\tau(t)=0$. T is the symbol duration and T_c is the chip duration. The period of spreading code sequence $e_k(m)$ for k^{th} user is $N = T/T_c$ which is called the spreading or processing gain. Note that, all the analysis in this section is in base-band.

The received signal in a synchronous channel is expressed as

$$r(t) = n(t) + \sum_{k=0}^{K-1} \sqrt{2P} e_k(t) b_k(t) \tag{6.2}$$

where K is the number of active users in the system, and $n(t)$ is the channel noise and assumed to be Gaussian with spectral density of $N_0/2$. Maintaining synchronization between users is possible in the case of the forward communication. However, it is not possible to synchronize users in the case of the reverse communication. Therefore, for the reverse communication, Equation (6.2) becomes

$$r(t) = n(t) + \sum_{k=0}^{K-1} \sqrt{2P} e_k(t-\tau_k) b_k(t-\tau_k) \tag{6.3}$$

where τ_k is the channel delay for k^{th} user. If a filter matched to the reference user's transmitted signal, $s_l(t)$, is used in the receiver, the filter output is given by

$$Z_l = \int_0^T r(t) e_l(t) dt \tag{6.4}$$

The correlator output at $t = T$ simplifies to the following equation after some mathematical manipulations [50]

$$Z_l = \sqrt{P/2}\left\{ b_{l,0}T + \sum_{\substack{k=1 \\ k \neq l}}^{K-1}\left[b_{k,-1}R_{k,l}(\tau_k) + b_{k,0}\hat{R}_{k,l}(\tau_k) \right] \right\} + \int_0^T n(t)e_l(t)dt \quad (6.5)$$

where $b_{l,0}$ is l^{th} user's transmitted data sent in the first symbol interval which is to be detected in the receiver and the continuous-time partial correlation functions, $R_{k,l}(\tau)$ and $\hat{R}_{k,l}(\tau)$ are defined as [50]

$$\begin{aligned} R_{k,l}(\tau) &= \int_0^{\tau} e_k(t-\tau)e_l(t)dt \\ \hat{R}_{k,l}(\tau) &= \int_{\tau}^{T} e_k(t-\tau)e_l(t)dt \end{aligned} \quad (6.6)$$

for $0 \le \tau \le T$. Pursey showed that for $0 \le jT_c \le \tau \le (j+1)T_c$ partial correlation functions can be given as follows [50]

$$\begin{aligned} R_{k,l}(\tau) &= d_{k,i}(j-N)T_c + [d_{k,l}(j+1-N) - d_{k,l}(j-N)](\tau - jT_c) \\ \hat{R}_{k,l}(\tau) &= d_{k,l}(j)T_c + [d_{k,l}(j+1) - d_{k,l}(j)](\tau - jT_c) \end{aligned} \quad (6.7)$$

where $d_{k,l}(m)$ is the ACF between two sequences, namely $e_k(n)$ and $e_l(n)$ as defined in Equation (5.1). The second term in the parenthesis in Equation (6.5) is interference due to *K-1* users in the system and is called as multi-user interference (MUI). In order to increase detection probability of the intended users bit, this term is to be minimized. In other words, spreading codes with good cross-correlation properties must be used in the system.

In the case of fading channel, the above analysis is valid with the change in the channel characteristic function. A frequency selective or multipath channel is modeled as an *L-tap* filter for the k^{th} user active in the system and is formulized as [59]

$$h_k(t) = \sum_{m_k=0}^{L_k} \beta_{k,m_k} \delta(t - \tau_{k,m_k}) \tag{6.8}$$

where L_k is the number of multipath components for user k, β_{k,m_k}, is the amplitude of each path, which is a Rayleigh distributed random variable. Therefore, the received signal of this scenario becomes

$$r(t) = n(t) + \sum_{k=0}^{K-1} \sum_{m_k=1}^{L_k} \sqrt{2P} \beta_{k,m_k} e_k(t - \tau_{k,m_k}) b_k(t - \tau_{k,m_k}) \tag{6.9}$$

The output of the correlator at the l^{th} receiver is obtained as

$$r(t) = \sqrt{P/2} b_{l,0} \beta_{l,0} T + \int_0^T n(t) e_l(t - \tau_{l,0}) dt + \sum_{k=0}^{K-1} \sum_{m_k=1}^{L_k} \alpha_{k,m_k} \tag{6.10}$$

The third term in Equation (6.10) is the interference due to *K-1* active users and the delayed (faded) versions of these user's signals as well as the delayed versions of the user's own signal.

When the number of users is low in CDMA systems, the interested user signal coming from farther distance will be masked if the other user signals are received at higher power levels. This is called the near-far problem in CDMA systems. This problem typically arises when the signal of interest is coming from cell boundaries and can be combated in the base station providing power control. In this dissertation, it is assumed that the base station provides perfect power control which ensures that signals from all mobiles are received at the same power level P independent of their distances.

As a conclusion, the performance of DS/CDMA mainly depends on MUI and ISI which already depend on auto- and cross-correlation properties of the spreading codes used in the system. In the following section, the BER performances of the optimized GDFT codes on AWGN and Rayleigh channel along with the well-known spreading codes will be given.

6.2.1 BER Performance of DS/CDMA System with GDFT on AWGN Channel

In all BER simulations in this dissertation, perfect code synchronization is assumed. In Figure 6.1, BER performances of optimum GDFT sets based on d_{cm}, $d_{\max}$, R_{AC} and R_{CC} are compared in an AWGN channel. As can be seen from the figure, the best performance is achieved by the GDFT set optimized on d_{cm} metric. Therefore, for all the other BER performance comparisons on AWGN channel, the GDFT sets optimum on d_{cm}, will be considered.

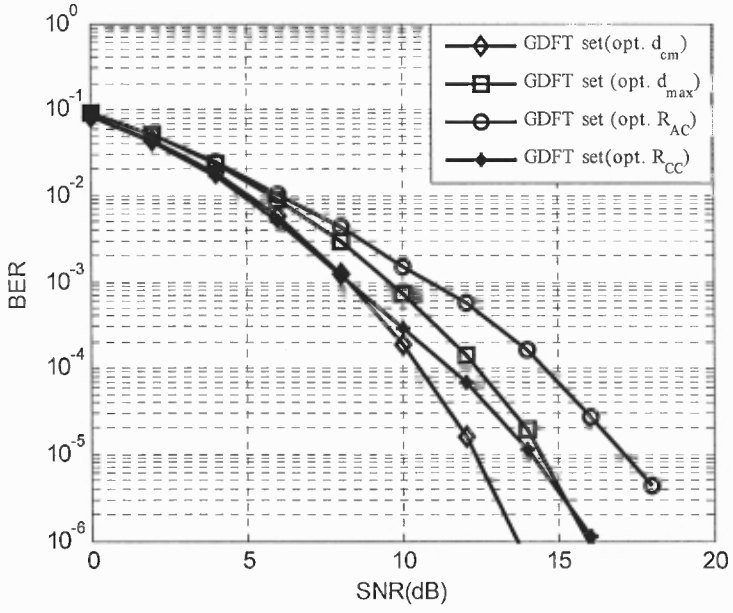

Figure 6.1 BER performance of GDFT's optimized on various metrics for 2-user in an asynchronous AWGN channel, *N=8*.

Figure 6.2 displays the BER performances of various GDFT sets designed based on minimizing the metric d_{cm} employed in an asynchronous AWGN channel for CDMA communications with two users along with DFT of size-8. The performance metrics of the compared codes were previously listed in Table 5.8. As typical in CDMA systems, the performance gets better as the code length increases.

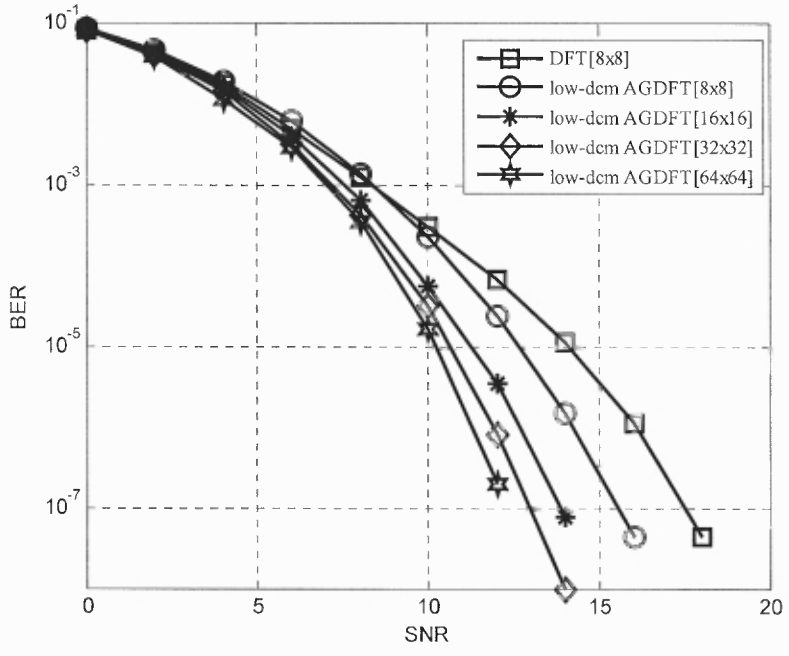

Figure 6.2 BER Performance of various lengths GDFT's along with size-8 DFT for 2-user in an asynchronous AWGN channel.

Figures 6.3 and 6.4 compares BER performance of several binary and complex code sets along with GDFT set optimized based on minimization of the d_{cm} parameter employed in a CDMA communications system in an AWGN channel for *N=8* and *N=32, r*espectively. The performance metrics of the compared codes were previously listed in Table 5.7 and 5.10 for *N=8* and *N=32*, respectively. Among the codes compared in these figures, the best performance is achieved with the GDFT code which has the minimum

d_{cm} value. The worst performance is achieved by Walsh codes which give the worst d_{cm} value. Therefore, on the AWGN channel for asynchronous 2-user, the average BER performance depends on the d_{cm} value of the set. Note that among all the sets compared, Gold codes are not orthogonal, the length of Gold and Oppermann codes is seven, and more importantly, the size of Oppermann set is only six. On the other hand, GDFT sets are orthogonal, available for all-lengths and complete in size. In general, it is observed that for $N=8$, complex spreading codes provide better performance compared to real spreading codes.

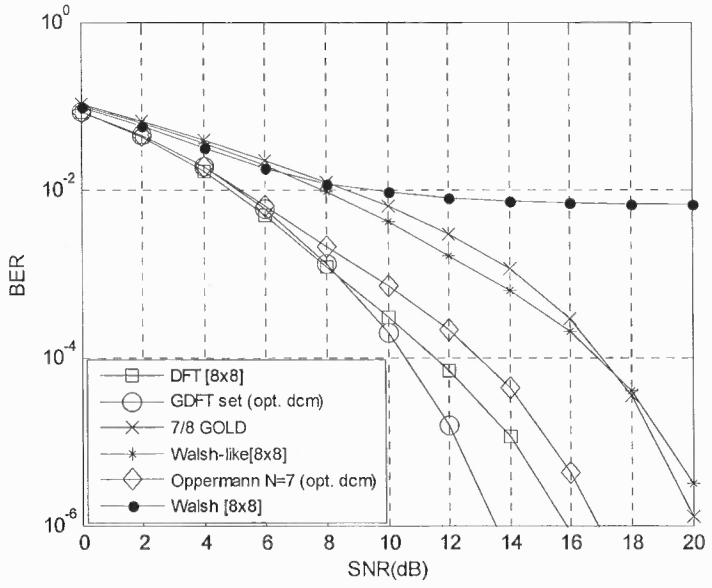

Figure 6.3 BER performance of various code sets for 2-user and an asynchronous AWGN channel with $N=8$ ($N=7$ for Gold and Oppermann).

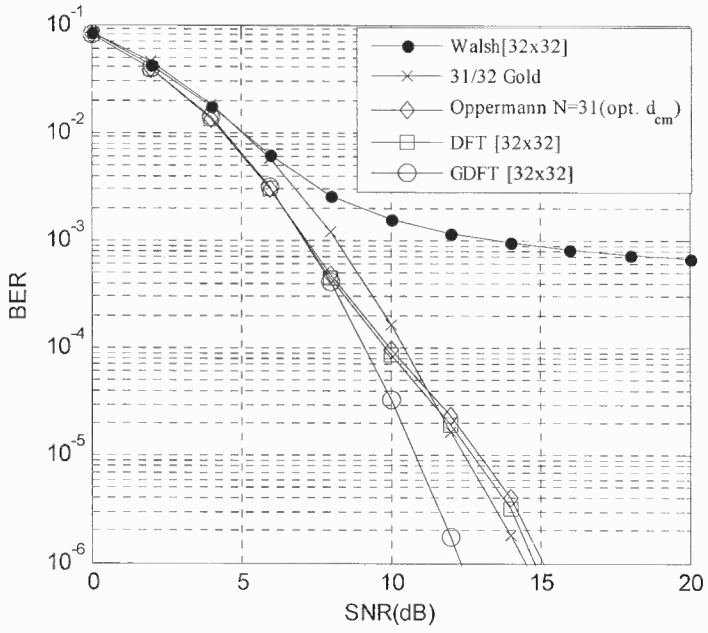

Figure 6.4 BER performance of various code sets for 2-user and an asynchronous AWGN channel with *N=32* (*N=31* for Gold and Oppermann).

6.2.2 BER Performance of DS/CDMA System with GDFT on Rayleigh Channel

BER simulations have been repeated for a Rayleigh channel. A two-ray multipath channel with the impulse response as given in Equation (6.8) with $L_k = 1$ for all users is assumed in the simulations. The parameters $\beta_{k,0}$ and $\beta_{k,1}$ are the Rayleigh distributed random variables defining power of the desired and interfering paths, respectively and the sum of $\beta_{k,0}$ and $\beta_{k,1}$ is set to be equal to one. Figure 6.5 displays BER performance of size-8 GDFT sets optimized on various metrics for single user on the Rayleigh multipath channel when the power of interfering path is *3dB* less than the power of the desired path ($D/I = 3dB$) with the corresponding delays, $\tau_{k,0} = 0$ and $\tau_{k,1} = T/8$, respectively. From the figure, it is observed that the best performance is achieved with the GDFT set

optimized on R_{AC} metric. Therefore, in the rest of the BER simulations, the GDFT sets optimized on R_{AC} will be considered.

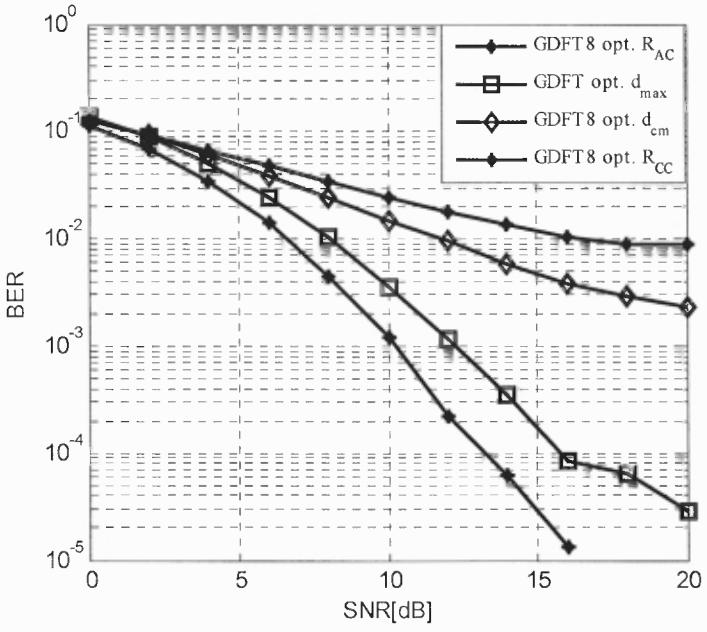

Figure 6.5 BER performance of GDFT's optimized on various metrics for single user in a Rayleigh multi-path channel.

Figure 6.6 displays BER performance of size-8 DFT and GDFT for two-user on the synchronous Rayleigh multipath channel when the power of interfering path is *3dB* and *5dB* less than the power of the desired path with the corresponding delays, $\tau_{k,0} = 0$ and $\tau_{k,1} = T/8$, respectively. The GDFT set is generated by *PSF* of Equation (5.26) optimized based on minimization of R_{AC}.

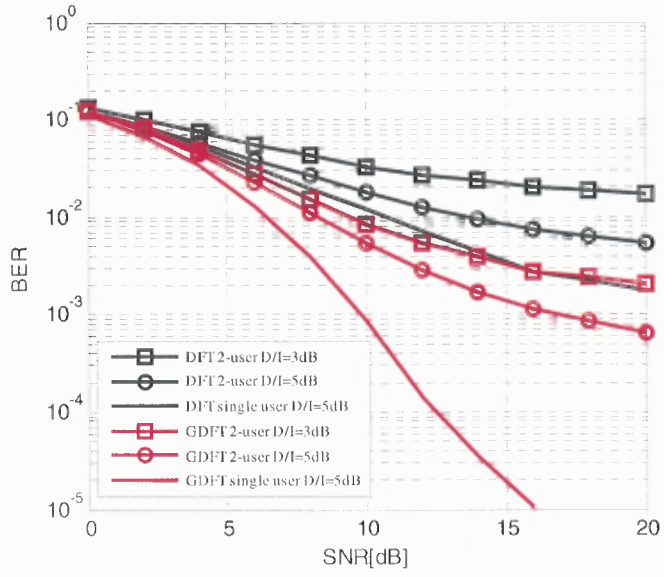

Figure 6.6 BER Performances of 8-length DFT and GDFT spreading code sets over synchronous Rayleigh fading channels for 1-user and 2-user with $D/I = 3dB$ and $D/I = 5dB$.

From the figure, one can conclude that DFT set with its highest R_{AC} gives a poor performance even for single user case. Moreover, the performance gets worse when the number of users is increased. In Figure 6.7, BER performances of 8-length Walsh and GDFT set optimized on R_{AC} are compared. The GDFT set with its low-R_{AC} outperformed the Walsh set on the channel considered. Figure 6.8 and Figure 6.9 display the BER performances of 32- and 64-length DFT and GDFT sets for 2-user in the same channel considered, respectively. The GDFT sets with their low-R_{AC} values significantly outperformed DFT sets for all the lengths compared. Moreover, the performance of GDFT sets improve as the length increased.

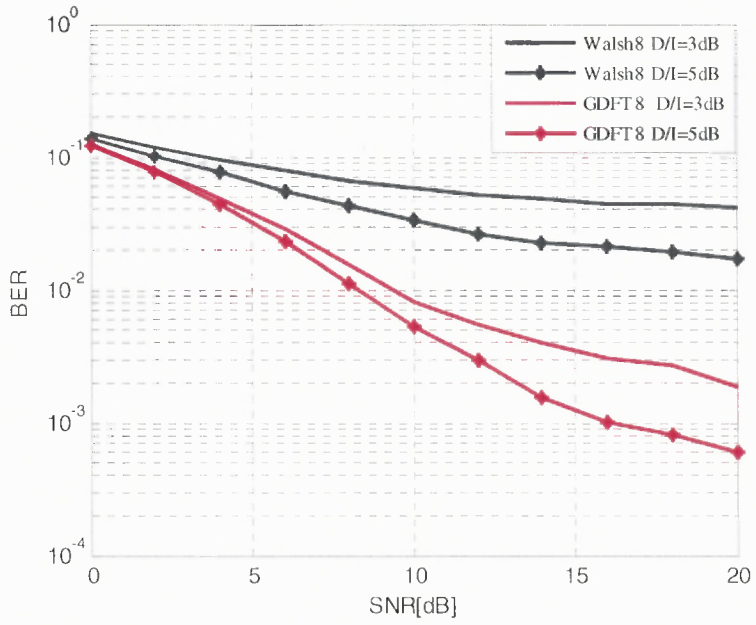

Figure 6.7 BER Performances of 8-length Walsh and GDFT spreading code sets over synchronous Rayleigh fading channels for 2-user with $D/I = 3dB$ and $D/I = 5dB$.

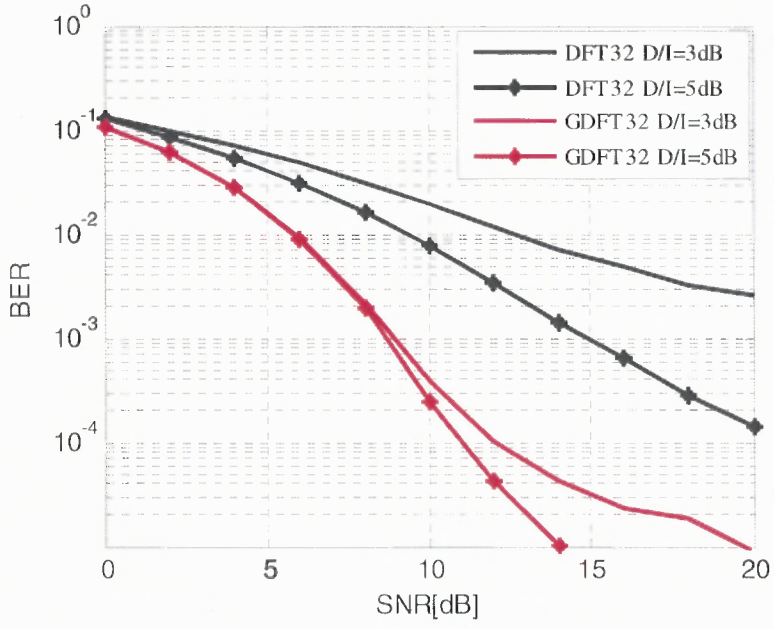

Figure 6.8 BER Performances of 32-length DFT and GDFT spreading code sets over synchronous Rayleigh fading channels for 2-user with $D/I = 3dB$ and $D/I = 5dB$.

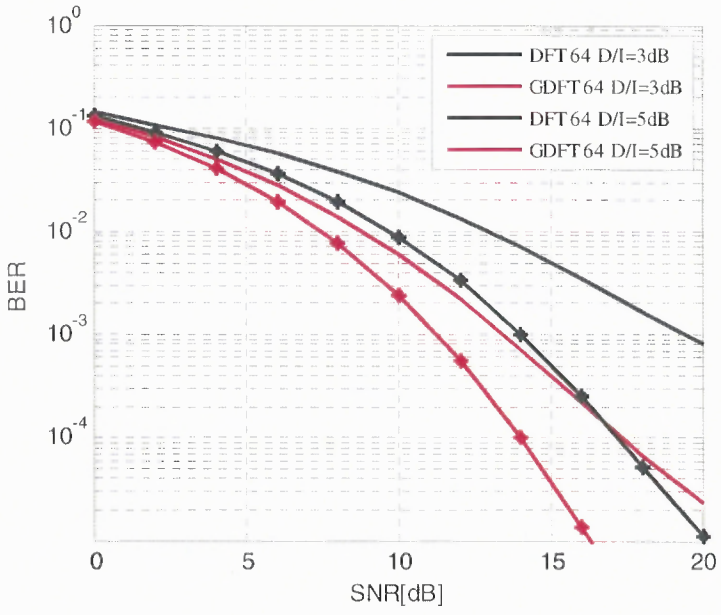

Figure 6.9 BER Performances of 64-length DFT and GDFT spreading code sets over synchronous Rayleigh fading channels for 2-user with $D/I = 3dB$ and $D/I = 5dB$.

From the BER figure, it is concluded that the average BER performance over on the multi-path channel considered depends on the metric R_{AC}. Therefore, the GDFT set with its low R_{AC} value outperforms DFT and Walsh sets for all the lengths compared on the channel model considered here.

From the simulations, one can conclude that MUI for 2-user is strongly coupled with the metric d_{cm} whereas ISI for the same number of users is coupled with the metric R_{AC}. In any communications system, depending on the dominant factor, one can employ the GDFT set optimized on either d_{cm}, R_{AC}, d_{am}, R_{CC} or F_k. Although, this dissertation has concentrated on GDFT sets optimized on only one metric at a time, one can easily design GDFT sets optimized on more than one metric using the cost function defined in Equation (5.8).

CHAPTER 7

PEAK-TO-AVERAGE POWER RATIO REDUCTION IN OFDM WITH GDFT

7.1 Introduction

OFDM, with its spectral efficiency and robustness to multipath fading, has become the most popular multiplexing method. However, the main disadvantage of an OFDM based communications technique is its high PAPR at the transmitter. PAPR dominates the power/battery efficiency of the radio transceiver. Non-linear devices in OFDM transmitters clip the peaks of the transmitted RF signal resulting in in-band and out-of-band interferences. In-band interference causes degradation in bit-error-rate (BER) performance whereas out-of-band interference leads to spectral widening and energy leakage to neighboring channels. Therefore, in the implementation of OFDM systems, a high PAPR demands large back-off, higher efficiency RF power amplifiers (PA), highly linear up-converters, large dynamic range Analog-to-Digital (A/D) converters, and low phase noise level Local Oscillators (LO).

This work utilizes the design advantages of closed form phase shaping function in the GDFT framework for generating multiple representations of the OFDM symbol/frame in SLM method. This work also introduces an efficient selection method for SLM on the autocorrelation properties of the input signal vector feeding the multiplexer. In the proposed efficient method, only one inverse GDFT operation is used in the transmitter, in contrast to the many in the conventional SLM. This efficient method can also be used in DFT-based SLM. The chapter is organized as follows. First, the OFDM system is described; the PAPR problem and the effects of RF nonlinearity on OFDM systems are explained in detail. In the following sections, the proposed GDFT based SLM PAPR

reduction methods along with their performance comparisons for various metrics are presented. Then, the performance improvements of the GDFT based SLM PAPR reduction in a general OFDM communications system compliant with the WiMAX standard is quantified.

7.2 OFDM Communications

OFDM has been widely used in communications systems for the last several decades including digital subscriber loop (DSL), digital audio broadcasting (DAB) technologies, and WiMAX. An OFDM frame is formed through an inverse DFT with the transform coefficient vector populated by the predefined signaling look up table and incoming data bit stream, $\underline{\theta} = \{\theta_k, k = 0,1,...,N-1\}$, expressed in vector notation as

$$\underline{x} = A_{DFT}^{-1}\underline{\theta} \tag{7.1}$$

where A_{DFT} is DFT matrix and $\underline{x} = [x(n)]$, $n = 0,1,...,N-1$. In the literature, it is common to use continuous time domain representation of OFDM symbol as follows,

$$x(t) = \frac{1}{\sqrt{N}} \sum_{k=0}^{N-1} \theta_k e^{i2\pi f_k t} \quad 0 \le t \le T_s \tag{7.2}$$

Note that f_k is the frequency of the subcarrier modulating data symbol θ_k with $f_k = k\Delta f$ in the spectrum. Δf is the frequency separation and defined as $\Delta f = 1/T_s$ where T_s is the OFDM symbol duration. In DFT kernel, the carrier frequencies are chosen in such a way that all subcarriers are orthogonal to each other. Before transmission, a cyclic prefix is added to OFDM frame signal in order to avoid Inter-symbol Interference (ISI) in frequency selective channels.

7.3 RF Non-linearity in OFDM Transceiver

In an OFDM communications system, nonlinearity is mostly caused by power amplifiers, A/D converters and Local Oscillators. Among these devices, power amplifiers produce a major nonlinearity due to the varying envelope of OFDM signal frames. One possible solution to this concern is to design highly linear amplifiers that have been under study for many years. Another solution is to reduce fluctuations of OFDM frame that goes through the RF power amplifier.

In a typical scenario, OFDM frames are deteriorated due to clipping effect of the power amplifier operating in the non-linear region. The level of deterioration depends on the input back off (IBO) of the amplifier. In Figure 7.1, AM/AM characteristic of a power amplifier with associated input and output backoff's along with linear and non-linear operation regions are displayed [60]. 1-dB compression point is usually given as the saturation point of the amplifier.

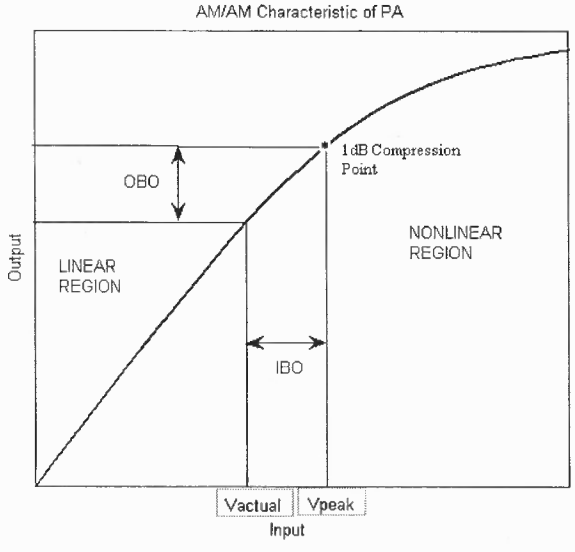

Figure 7.1 AM/AM characteristic of a typical PA.

In order to operate in the linear region, the average input power is reduced. The difference between the input saturation power and the actual/average input power is called IBO. Similarly, the difference between the corresponding output powers is defined as the output back-off (OBO) and expressed as follows,

$$IBO_{dB} = 10\log\frac{P_{in,1dB}}{P_{in,avg}} \tag{7.3}$$

$$OBO_{dB} = 10\log\frac{P_{out,1dB}}{P_{out,avg}}. \tag{7.4}$$

In this work, the high power amplifier is modeled as Rapp's solid state amplifier with AM/AM characteristic given as [60]

$$v_{out} = \frac{v_{in}}{\left(1+\left(\frac{|v_{in}|}{v_s}\right)^{2p_0}\right)^{\frac{1}{2p_0}}} \tag{7.5}$$

where v_{out} and v_{in} are the output and input voltages, respectively, and v_s is the output voltage at the saturation point. p_0 defines the smoothness of the transition from linear region to saturation region. Choosing $p_0 = 2$ is a good approximation to the commonly used power amplifiers. Figure 7.2 displays AM/AM responses of an ideal (linear) and the Rapp modeled amplifier used in the performance simulations reported in this dissertation.

Increasing input voltage level drives the amplifier into saturation. This should be avoided in order not to cause any nonlinearity in the system. Passing through this amplifier (depending on its input saturation voltage), the peaks of OFDM signal will be clipped causing in-band and out-band degradations. In-band degradation results in worse BER performance while out-band degradation widens the spectrum of OFDM frame.

The amount of clipping depends on IBO. In general, IBO is chosen to be equal or higher than PAPR of the signal in order to avoid in-band and out-band interferences. However, high backoff values decrease amplifier efficiency and therefore reduce the battery life for the mobile device.

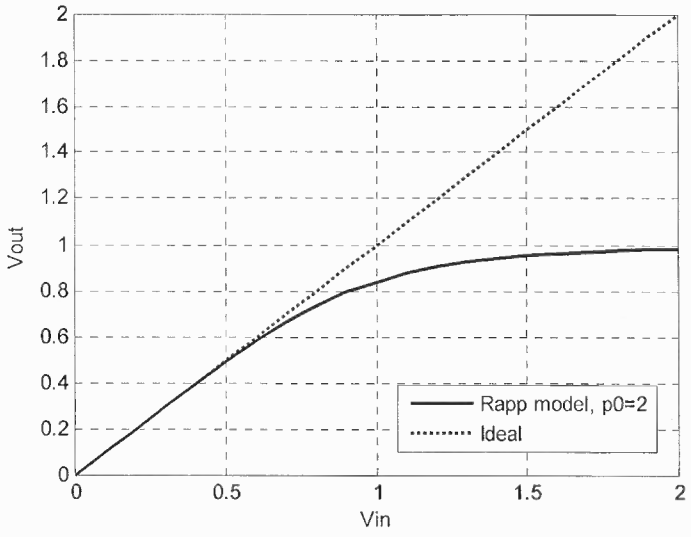

Figure 7.2 AM/AM characteristic of Rapp Amplifier simulated ($v_s = 1\,V$).

There are three popular efficiency metrics for amplifiers, which are defined as follows [61],

Drain efficiency is defined as the drain output power to dc input power,

$$\eta_{DRAIN} = \frac{P_{out}}{P_{in}} \tag{7.6}$$

Power-Added Efficiency (PAE) includes the RF drive power P_{dr} and given as

$$\eta_{PAE} = \frac{P_{out} - P_{dr}}{P_{in}} \tag{7.7}$$

However, this efficiency becomes negative for small output powers and not used in practice.

Overall Efficiency is commonly used and defined as

$$\eta = \frac{P_{out}}{P_{in} + P_{dr}} \tag{7.8}$$

The efficiency calculations are easy for constant amplitude signals. However, for varying amplitude input signals, instantaneous and average efficiencies are preferred. Instantaneous efficiency is defined as the efficiency at a specific output power and maximum at the maximum output power. Signals with amplitude variations produce varying efficiencies. Therefore, in this case, the average efficiency should be considered in the system design. Also, the average efficiency defines the battery life of the given device. It is defined as the average output power to average dc input power as follows

$$\eta_{ave} = \frac{P_{out,ave}}{P_{in,ave}} \tag{7.9}$$

In efficiency calculations, a highly linear Class-A amplifier is considered as a special case. For this type of amplifier, the dc input current (and power) is constant. The maximum value of instantaneous efficiency is 50% (η_{peak}=0.5). The average efficiency for non constant envelope signals and Class-A type amplifiers is defined as [61]

$$\eta_{ave} = \frac{\eta_{peak}}{PAPR} \tag{7.10}$$

where PAPR is commonly used to identify envelope fluctuations in the signal and defined in dB's as follows

$$PAPR_{dB} = 10\log\left[\frac{\max_{0\le t<T}|x(t)|^2}{\frac{1}{T}\int_0^T |x(t)|^2\,dt}\right] \tag{7.11}$$

Note that the value of the signaling (constellation) vector $\underline{\theta}$ in Equation (7.1) dictates the level of PAPR for the given transform, i.e. DFT. In this paper, only NL samples of the input signal $x(t)$ are considered where $L \geq 1$ integer. If the input signal is oversampled by L, then the oversampled signal samples are obtained as [62]

$$x(n) = x(n\frac{T}{L}) = \frac{1}{\sqrt{N}} \sum_{k=0}^{N-1} \theta_k e^{i2\pi k \Delta f n \frac{T}{L}} \quad n = \{0,1,...,NL-1\} \tag{7.12}$$

From Equation (7.12), $x(n)$ may be interpreted as the inverse Fourier transform of the input data symbols block, $\underline{\theta}$, with $N(L-1)$ zeros padded [62]. It is well known in the literature that the continuous time PAPR is usually higher than the discrete time PAPR. However, in [63] it was shown that $L=4$ is a sufficient approximation to obtain accurate PAPR using L-oversampled time domain signal samples. Therefore, PAPR for this case is expressed as

$$PAPR = \frac{\max_{0 \leq n < NL-1} |x(n)|^2}{E\left[|x(n)|^2\right]} \tag{7.13}$$

where $E[.]$ denotes the expectation operation. The theoretical maximum of PAPR for N subcarriers is equal to N although the maximum PAPR occurs infrequently in practice. Therefore, statistical analysis of PAPR in OFDM is found to be useful. It is known that real and imaginary parts of the OFDM signal, $x(t)$, tend to be Gaussian distributed with zero mean and variance of 0.5 for $N \geq 64$. Hence, the amplitude of OFDM symbol $\underline{x}$ in Equation (7.1) has a Rayleigh distribution. In contrast, its power distribution becomes a central Chi-square with two-degrees of freedom with the cumulative distribution as given [62, 63]

$$F(\gamma) = \int_0^{\gamma} \frac{1}{2\sigma^2} e^{-\frac{y}{2\sigma^2}} dy \tag{7.14}$$

with $\sigma = 1/2$. Assuming that the samples of an OFDM frame to be mutually uncorrelated, the probability of peak value of the continuous time signal smaller than γ is defined as [34, 62]

$$P(\max |x(t)|^2 \le \gamma) = \left(1 - \exp(-\gamma)\right)^N \tag{7.15}$$

Whenever the oversampling is introduced, the samples of the OFDM signal are not uncorrelated any more. However, distribution of PAPR of the OFDM signal oversampled by L is well approximated by PAPR distribution of OFDM signal with αN subcarriers. Then, the new distribution becomes

$$P(\max_{0 \le n \le NL-1} |x(n)|^2 \le \gamma) = \left(1 - \exp(-\gamma)\right)^{\alpha N} \tag{7.16}$$

In [63], it was shown that choosing $\alpha = 2.8$ is a good approximation in Equation (7.16) for $N \ge 64$, and $L > 4$. In this work, L is assumed to be *4* to accurately estimate PAPR of the transmitted signal.

7.4 Design and Performance of GDFT Based SLM Methods

The main advantage of using GDFT over DFT in SLM is the analytical representation of its phase shaping function structuring the phase selection of SLM method in the phase space. In this work, a GDFT based SLM PAPR reduction technique and an efficient implementation of the phase selection process for SLM are presented. Then, various performance metrics of interest in OFDM communications and the performance of the proposed techniques are introduced. Furthermore, the performance of GDFT based SLM

PAPR reduction in an OFDM communications system compliant with the popular WiMAX standard is quantified

7.4.1 Phase Optimized GDFT based SLM

The conventional SLM method generates multiple representations of the OFDM symbol obtained through multiple phase sets and picks the one with the lowest PAPR to transmit [28]. The probability of PAPR exceeding a threshold γ for OFDM symbols with the oversampling factor of L is shown as [63]

$$P\{PAPR > \gamma\} = 1 - [1 - \exp(-\gamma)]^{\alpha N} \tag{7.17}$$

Assume that M of OFDM symbols/frames corresponds to the same data sequence with different PAPR values. In this case, the probability of Equation (7.17) becomes [28]

$$P\{PAPR_{\min} > \gamma\} = [P(PAPR > \gamma)]^M = [1 - (1 - \exp(-\gamma))^{\alpha N}]^M \tag{7.18}$$

The number of multiple signals is $M = 2^m$ and PAPR decreases as m increases. A simple way to generate multiple copies of the input data sequence by choosing M different vectors with the elements of complex roots of unity for each OFDM frame is also introduced in [28]. More specifically, the phase values for the elements of inverse DFT coefficient vectors are chosen as the integer multiples of $\pi/2$ in their design. This method is extended by relaxing phase values of inverse DFT coefficient vector elements employing the GDFT framework. A special case for G matrix defined in Equation (4.12) is expressed as

$$G^i(k,n) = \left\{ \begin{array}{ll} e^{j\frac{2\pi}{N}\psi_i(n)}, & k = n \\ 0, & k \neq n \\ & k,n = 0,1,...,N-1 \end{array} \right\} \; i = 0,\ldots,M-1 \tag{7.19}$$

where a trivial parametric *PSF* may be expressed as

$$\psi^{i}(n) = a_i n^{b_i} \qquad a_i, b_i: \text{Real} \quad n = 0,1,...,N-1, \; i = 0,1,\ldots,M-1 \tag{7.20}$$

As a special case, $a_i = 1$ for $\forall i$ is picked, and the GDFT kernel is expressed as

$$A_{GDFT_i} = A_{DFT} G^{i} = [e^{j\frac{2\pi}{N}(kn+n^{b_i})}] \qquad k,n = 0,1,...,N-1, \; i = 0,1,\ldots,M-1 \tag{7.21}$$

In contrast to DFT based SLM, a set of GDFT's are generated for various values of phase parameter b_i in Equation (7.20) and used in SLM for each data symbols block (inverse DFT coefficient vector $\underline{\theta}$) to reduce PAPR. The GDFT with minimum PAPR is identified along with the corresponding value of phase shaping function parameter b_i and the resulting OFDM frame is sent through the communications channel as displayed in Figure 7.3. The value of the parameter b_i is also transmitted to the receiver as the side information. It is assumed that the receiver receives b_i error-free and proceeds accordingly. The number of GDFT processors in Figure 7.3 depends on the number of side information bits to be transmitted per OFDM frame. For the case of *m=3* bits, the number of inverse GDFT processors employed in the transmitter is $M = 8$. Selection of the phase parameters, b_i, is straightforward since the range of phase space is limited to the interval $[0, 2\pi]$,

$$\begin{aligned} &\psi_i(0) = 0, \quad \text{for } \forall i \\ &\psi_i(1) = 1, \quad \text{for } \forall i \\ &0 < \psi_i(n) = n^{b_i} \le N, \quad n = 2,3,...,N-1, \text{ for } \forall i \end{aligned} \tag{7.22}$$

In OFDM systems, N is chosen as an integer power of two due to the FFT implementation of DFT. Therefore, with $N = 2^l$, the range of phase for the selection of parameter b_i is shown to be

$$0 < b_i \leq \frac{l}{\log_2(n)} \leq l \quad n \in [2, N-1] \tag{7.23}$$

The interval $(0, l]$ is used for PAPR reduction simulations as the range of parameter b_i in Equation (7.20). The number l determines the required side information bits of this method. Assume that the number of side information bits is m. Then, there are $M = 2^m$ possible values that can be assigned to the parameter b_i from the set $\left\{\frac{l}{2^m}, \frac{2l}{2^m}, ..., l\right\}$. The number of possible b_i values is equal to M.

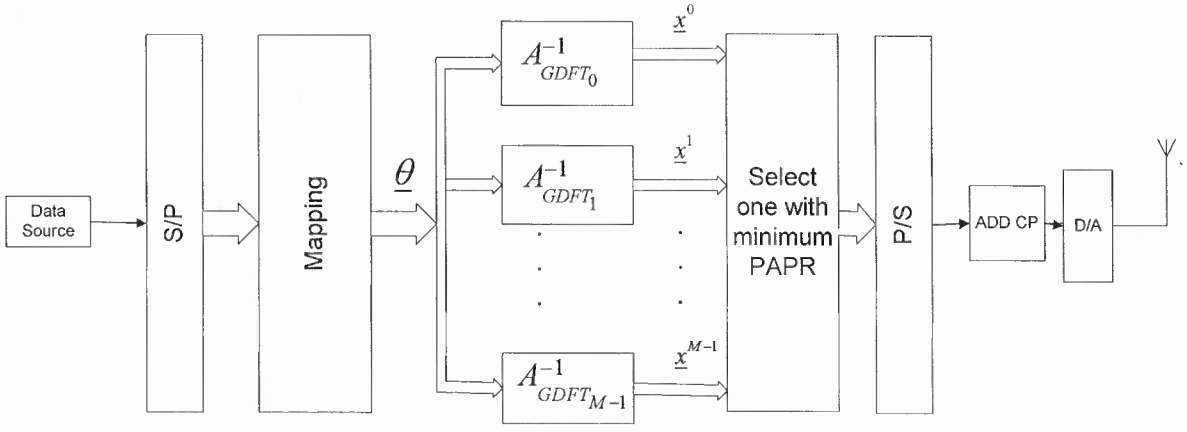

Figure 7.3 PAPR reduction with *Phase Optimized GDFT* based SLM.

7.4.2 Efficient GDFT based SLM

In the conventional SLM method, the transmitter must perform multiple inverse transform operations. Therefore, the complexity of the transmitter is increased prohibitively. Herein an efficient implementation of SLM is proposed, which makes an

estimate of the optimum GDFT by minimizing PAPR for the given signal vector $\underline{\theta}$ in advance of any inverse transform operation performed at the transmitter. Then, it generates the corresponding OFDM frame for the estimated optimum GDFT. Hence, only one inverse transform operation is required yielding significant reduction in the implementation cost.

In this method, prior to performing any inverse DFT operation, the signal vector is simply multiplied by various diagonal complex G^i matrices of Equation (7.19). The selection for G_{OPT} is made based on the autocorrelation properties of the resulting vectors, $\{\underline{y}^i\}$; $i = 0,1,...,M-1$, as displayed in Figure 7.4.

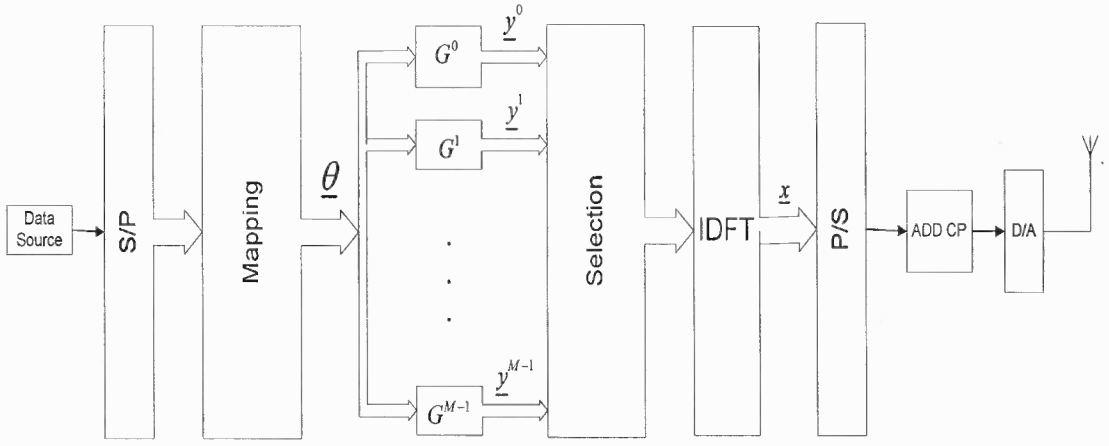

Figure 7.4 PAPR reduction by E*fficient GDFT* based SLM.

The input signal vector corresponding to a set of input bits is expressed as $\underline{\theta} = \{\theta_k, k = 0,1,...,N-1\}$ for the predefined signaling (constellation) technique. This vector is independently multiplied with a set of diagonal and constant modulus G^i matrices of GDFT as defined in Equation (7.21). The *phase modified* signal vector $\underline{y}^i$, for each G^i and given signal vector $\underline{\theta}$, might be written as

$$\underline{y}^i = G^i \underline{\theta}$$
$$[\underline{y}^i]^T = e^{j\frac{2\pi}{N}k b_i}\theta_k; \quad k \in [0, N-1], i \in [0, M-1] \tag{7.24}$$

The number of G^i phase shaping matrices depends on the number of side information bits being transmitted. There are $M = 2^m$ diagonal G^i matrices in the set for the selection of optimal GDFT minimizing PAPR. The autocorrelation functions of the resulting $\underline{y}^i = [y^i(k)]$ sequences are calculated as

$$R^i_{yy}(m) = \sum_{k=(1-N)}^{N-1} y^i(k) y^i(k+m); \quad i \in [0, M-1] \tag{7.25}$$

and compared to the uniquely ideal autocorrelation $R^{ideal}_{\theta\theta}(m)$ with zero phase.

$$R^{ideal}_{\theta\theta}(m) = \delta_m \quad \delta_m = \begin{cases} 1 \text{ for } m = 0 \\ 0 \text{ for all integers but } m \neq 0 \end{cases} \tag{7.26}$$

The mean square error is used as the metric to select the best estimate as follows

$$\varepsilon^{mse}_i = \sum_{m=(1-N)}^{N-1} \left| R^i_{yy}(m) - R^{ideal}_{\theta\theta}(m) \right|^2; \quad i \in [0, M-1] \tag{7.27}$$

$$b_{OPT} = b_i; \quad \varepsilon^{mse}_{OPT} = \min_{0<i\leq M-1} \left\{ \varepsilon^{mse}_i \right\} \tag{7.28}$$

The value of b_{OPT} is transmitted to the receiver as the side information. Assuming this information is received error-free, G^{OPT} is generated accordingly.

Note that there are infinitely many OFDM frames with constant amplitude yielding *0dB* PAPR as the optimum OFDM frames based on the PAPR metric. The unique *0dB* PAPR OFDM frame with zero phase function is assumed in this dissertation in order to keep the implementation simple.

7.5 PAPR Reduction of GDFT based SLM

PAPR reduction is evaluated in terms of cumulative complementary density function (CCDF) defined as the probability of PAPR exceeding a given threshold value. The calculated, according to Equation (7.16) and simulated CCDF's for the conventional OFDM frames employing QPSK and various numbers of carriers are displayed in Figure 7.5. It is observed from the figure that the CCDF performance gets worse as the number of carriers increases. Moreover, the theoretical and simulated CCDF functions converge as the number of the subcarriers increases.

Similarly, Figure 7.6 displays CCDF of PAPR for various numbers of side information bits and QPSK modulation for *N=256*, employing the *Phase Optimized GDFT* method. Calculated CCDF results are obtained using statistical model of Equation (7.18) with $\alpha = 2.8$. As the number of side information bits increases PAPR improves, and also theoretical and simulation performance curves start to merge.

It is observed from that PAPR decreases significantly as the number of side information bits increases. As an example for *m=14*, almost *4dB* PAPR reduction is achieved at $CCDF(PAPR) = 10^{-2}$ with the *Phase Optimized GDFT* method, and it is more than *2.5dB* with the *efficient GDFT* method. Even for *m=2*, more than *1dB* PAPR reduction is possible at $CCDF(PAPR) = 10^{-2}$ for both methods. For an OFDM frame generated from *256* subcarriers each employing QPSK without any guard interval, using *m=2* reduces the load of the system by 39% where the cost of side information bits is negligible and the implementation is simple at the transmitter.

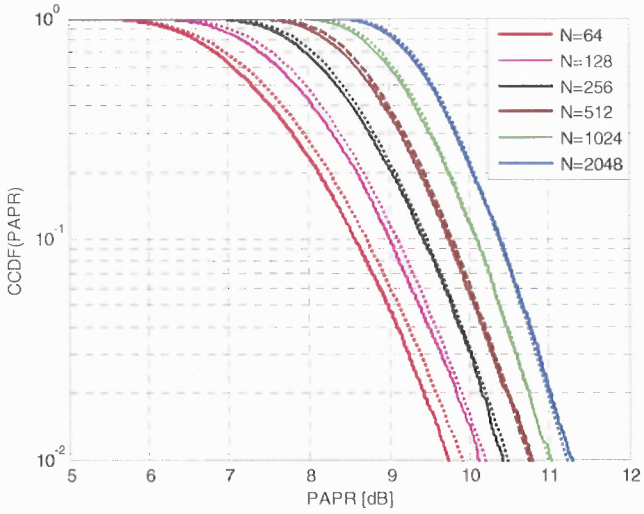

Figure 7.5 CCDF of PAPR for different numbers of subcarriers in conventional OFDM (DFT based) using QPSK; calculated with α=2.8 in Equation (7.16)(dotted), and simulated (solid).

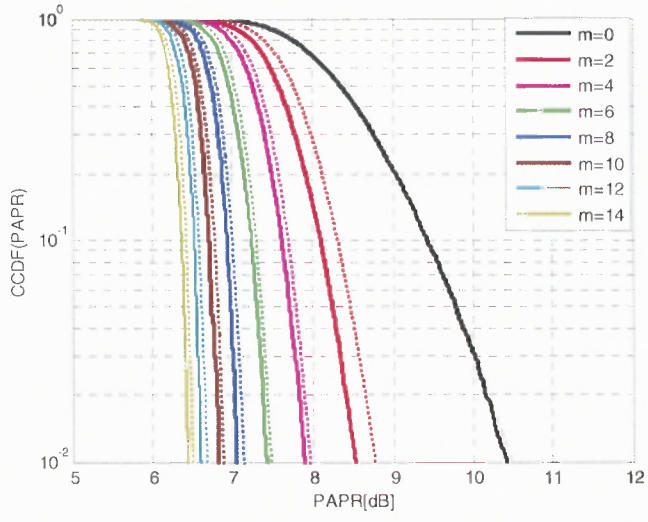

Figure 7.6 CCDF of PAPR for the *Phase Optimized GDFT* method using QPSK, various numbers of side information bits and *N=256*; calculated with α=2.8 in Equation (7.16) (dotted), and simulated (solid).

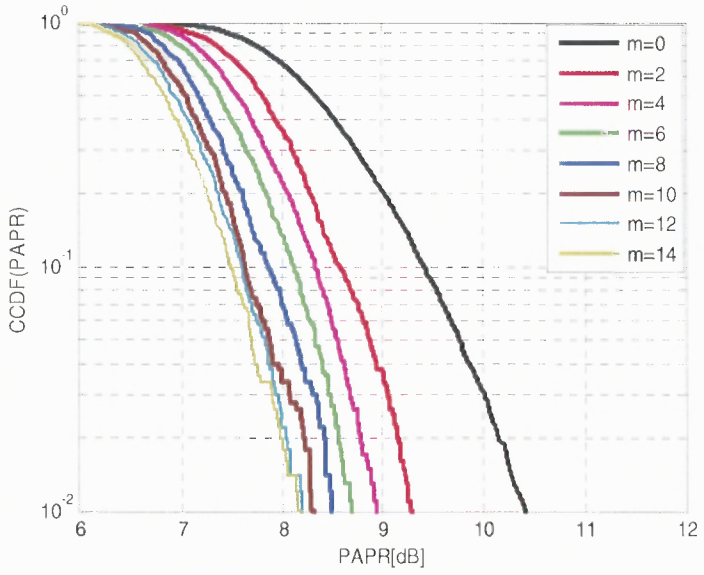

Figure 7.7 CCDF of PAPR for QPSK-OFDM with *Efficient GDFT* method using QPSK and various numbers of side information bits and *N=256*.

For comparison purposes, the achievable PAPR values of the conventional OFDM and the proposed GDFT based SLM methods for $P(PAPR > \gamma) = 10^{-1}$, are tabulated in Table 7.1 for various numbers of side information bits. From the table, one can conclude that almost *4dB* PAPR reduction is achieved by GDFT based SLM with *m=14* bits.

Although the *Efficient GDFT* method offers little less PAPR reduction than the *Phase Optimized GDFT* method, it does not require multiple inverse transforms and very efficient to implement at the transmitter without almost any additional cost. Moreover, only *0dB* PAPR OFDM frame with zero phase function is considered. Since there are many *0dB* PAPR frames with non-zero phase functions the autocorrelation based selection method presented may be upgraded. Hence, $\Delta PAPR$ in Table 7.1 may be further reduced with the increase of the computational cost in the selection process as a design trade-off.

Table 7.1 *PAPR(dB)* for Various Side Information Bits, $N=256$ and $P(PAPR>\gamma)=10^{-1}$

m	$PAPR_{DFT}$ (dB)	$PAPR_{GDFT}^{EFF}$ (dB)	$PAPR_{GDFT}^{OPT}$ (dB)	$PAPR_{SLM}$ (dB)	$\Delta PAPR$ [dB]		
					EFF-GDFT	OPT-GDFT	SLM (7.18)
2	10.4	8.6	8.1	8.3	1.8	2.3	2.1
4	10.4	8.3	7.6	7.7	2.1	2.8	2.7
6	10.4	8.1	7.2	7.3	2.3	3.2	3.1
8	10.4	7.9	7.0	7.0	2.5	3.4	3.4
10	10.4	7.7	6.7	6.8	2.6	3.7	3.6
12	10.4	7.6	6.5	6.6	2.8	3.9	3.8
14	10.4	7.5	6.4	6.4	2.9	4	4

7.6 Power Amplifier Efficiency with PAPR Reduction

Average efficiency of a Class-A amplifier was defined in Equation (7.10) and Figure 7.8 depicts its average efficiency curve as a function of PAPR. The GDFT based SLM was shown to reduce PAPR successfully, and therefore, the required IBO and corresponding OBO of the amplifier. In this section, the improvements of RF power amplifier efficiency due to the proposed PAPR reduction methods are quantified.

Figure 7.8 assumes that the input signal always has a constant PAPR. However, in an OFDM system, each frame has a different PAPR value. Therefore, the overall average efficiency should be considered. If the probability density function of PAPR is available, the overall average efficiency for a Class-A type amplifier is defined by [64, 65]

$$E[\eta_{ave}] = \int_{0}^{PAPR_{\max}} \frac{\eta_{PEAK}}{\gamma} f(\gamma) d\gamma \tag{7.29}$$

where $f(\gamma)$ is the probability density function of PAPR and $\gamma_{\max}$ is the maximum value of PAPR which is equal to the number of subcarriers used in the OFDM system.

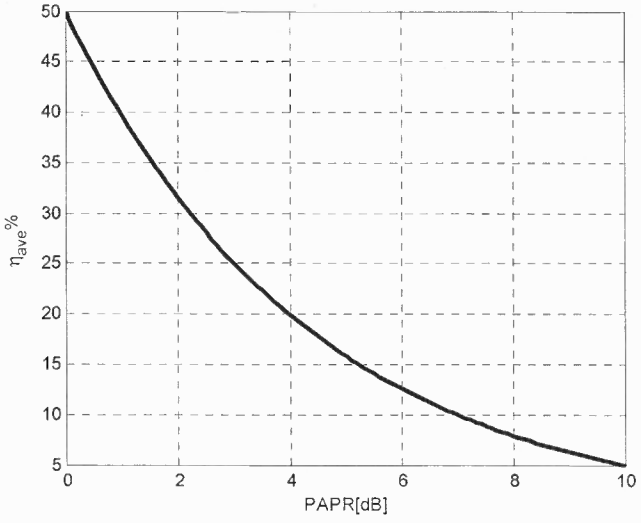

Figure 7.8 Average efficiency vs. PAPR for a Class-A type amplifier [64].

Figure 7.9 displays the average efficiencies of OFDM systems employing *Phase Optimized GDFT a*nd *Efficient GDFT* methods as PAPR reduction methods. The system becomes the conventional OFDM system for *m=0.* In this case, the amplifier efficiency is about 7.5%. It is quite low compared to 50% maximum efficiency of Class-A type power amplifier. The efficiency improves to *10.3%* when *Efficient GDFT* based SLM with m=14 bits is used, and goes up to 12% when *Phase Optimized GDFT* based SLM is employed. These PAPR improvements result in 37% and 60% longer battery life, respectively, for the scenario considered.

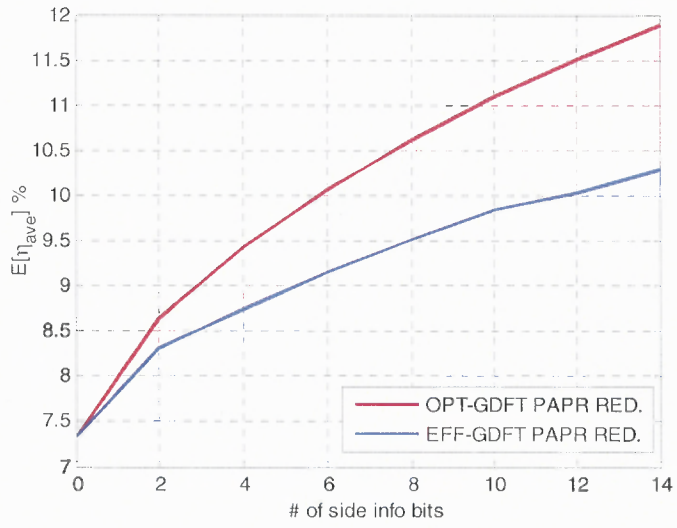

Figure 7.9 Average Efficiency as a function of side information bits, *m*.

Figure 7.10 displays the CCDF's of PAPR when *Phase Optimized GDFT based SLM* is employed for various numbers of subcarriers with zero and four bits of side information, $m=0$ and $m=4$. Similarly, Table 7.2 tabulates the PAPR reductions for various cases. Although $N=64$ provides the most PAPR reduction for $m=4$, higher values of N also benefit from sizable PAPR reductions.

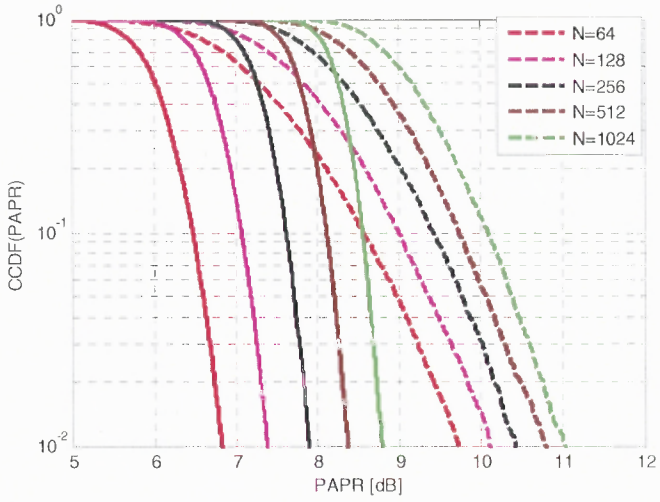

Figure 7.10 CCDF of PAPR for *the Phase Optimized GDFT* based SLM; with *m=0* (solid) and with *m=4* (dotted).

Table 7.2 PAPR(dB) for Various Transform Sizes, $P(PAPR>\gamma)=10^{-1}$, *m=4*

N	$PAPR_{DFT}$ [dB]	$PAPR_{GDFT}^{EFF}$ [dB]	$PAPR_{GDFT}^{OPT}$ [dB]	$PAPR_{SLM}$ [dB]	$\Delta PAPR$ [dB]		
					EFF-GDFT	OPT-GDFT	SLM
64	9.7	7.1	6.5	6.5	2.6	3.2	3.2
128	10.1	7.8	7.1	7.2	2.3	3.0	2.9
256	10.4	8.3	7.6	7.7	2.1	2.8	2.7
512	10.8	8.9	8.2	8.2	1.9	2.6	2.6
1024	11.0	9.4	8.6	8.6	1.6	2.4	2.4

In order to make a fair comparison, the overhead bits per OFDM frame due to *m* side information bits is fixed regardless of *N* and the resulting CCDF's of PAPR are displayed in Figure 7.11. In the simulations, *Phase Optimized GDFT based SLM* method is employed with QPSK, and the overhead is set to *0.5%* for all *N*. The results show that

if the overhead is fixed, CCDF curves get closer and *8dB* PAPR is achieved at lower probabilities regardless of *N*.

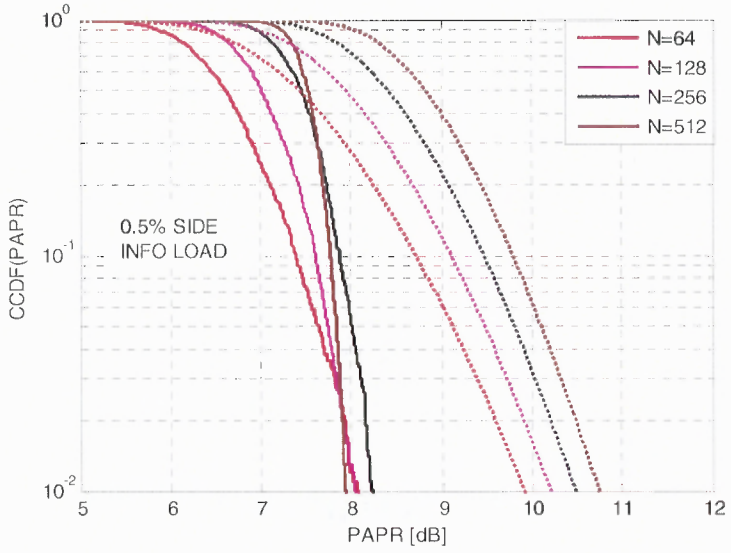

Figure 7.11 CCDF of PAPR for QPSK based OFDM frames using *Phase Optimized GDFT* based SLM method with fixed overhead of 0.5% per frame (solid), and QPSK based conventional OFDM (dotted) with zero overhead (*m=0*).

7.7 BER Performance of OFDM Using GDFT based SLM Methods

Most OFDM systems use QPSK, 16-QAM and 64-QAM depending on the channel properties. In this work, only QPSK and 16-QAM modulations are considered. BER performances of QPSK modulated OFDM and 16-QAM modulated OFDM in AWGN channel are displayed in Figure 7.12. 16-QAM performs worse due to higher number of constellation points in its signal set.

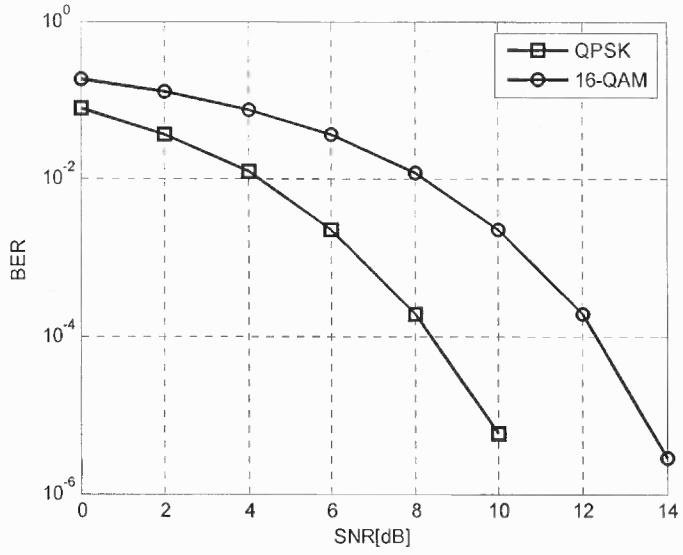

Figure 7.12 BER Performances of QPSK and 16-QAM based OFDM systems in AWGN channel with *N=256*.

BER performances of real world transceivers are strongly related to the RF power amplifier nonlinearities. Therefore, the selection of IBO based on the PAPR level of the transmitter is very important. BER performance of an OFDM system for various IBO levels and the proposed GDFT based SLM methods are simulated on AWGN channel. In BER simulations, the output saturation power is assumed to be 1V, and the IBO is chosen as the difference between the driving average power and the input power at the *1dB* compression point.

Figure 7.13 and Figure 7.14 displays BER curves of an OFDM system with *N=256* for various IBO levels, QPSK and 16-QAM signaling without using any SLM PAPR reduction, respectively. The importance of power amplifier nonlinearities is well quantified in this figure. Note that the BER curves of both signaling methods approach to the ideal case for *IBO=8dB*. In contrast, Figure 7.15 and Figure 7.16 displays BER curves of similar systems now employing the proposed GDFT based SLM PAPR

reduction methods. First of all, it is observed from the figures that both GDFT based SLM techniques perform quite similar. Naturally, one would employ the *Efficient GDFT* based SLM over *Phase Optimized GDFT* based SLM due to its implementation advantages. Moreover, if the main concern in the system is amplifier efficiency for a desired BER performance, one can improve amplifier efficiency by introducing the proposed PAPR reduction methods. As it is shown in Figure 7.9, both techniques improve the overall efficiency for a Class-A type amplifier by reducing the required backoff of the amplifier.

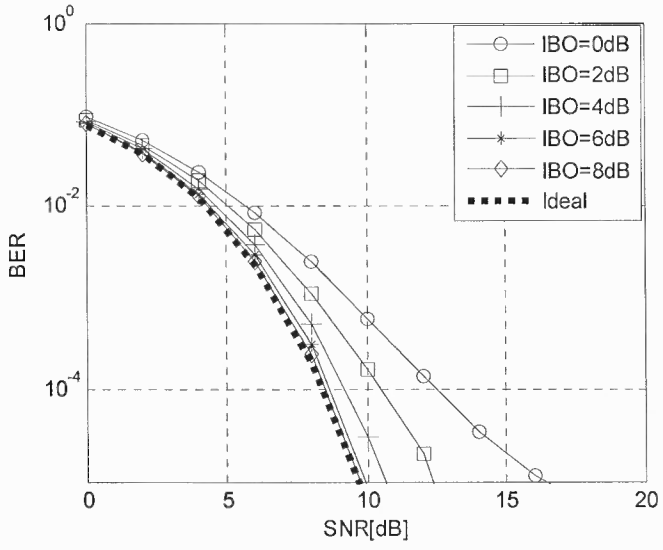

Figure 7.13 Impact of RF Power Amplifier nonlinearities on BER performance for N=*256, IBO=0, 2, 4, 6* and *8dB*, and modulation type of QPSK.

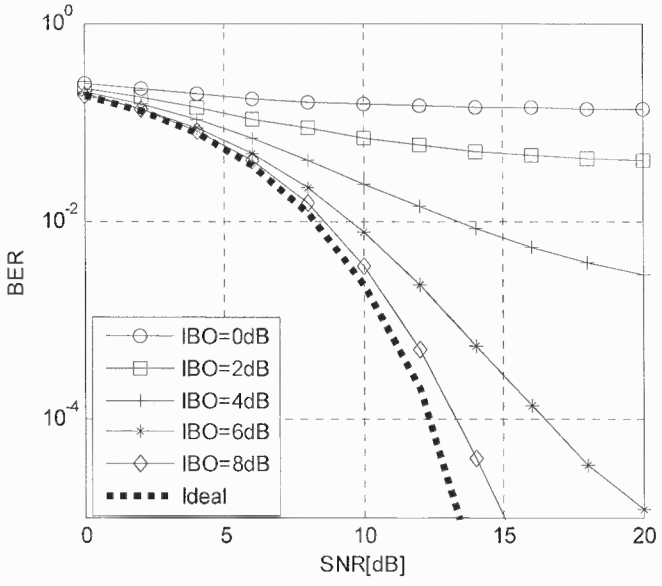

Figure 7.14 Impact of RF Power Amplifier nonlinearities on BER performance for *N=256*, *IBO=0, 2, 4, 6* and *8dB*, and modulation type of 16-QAM.

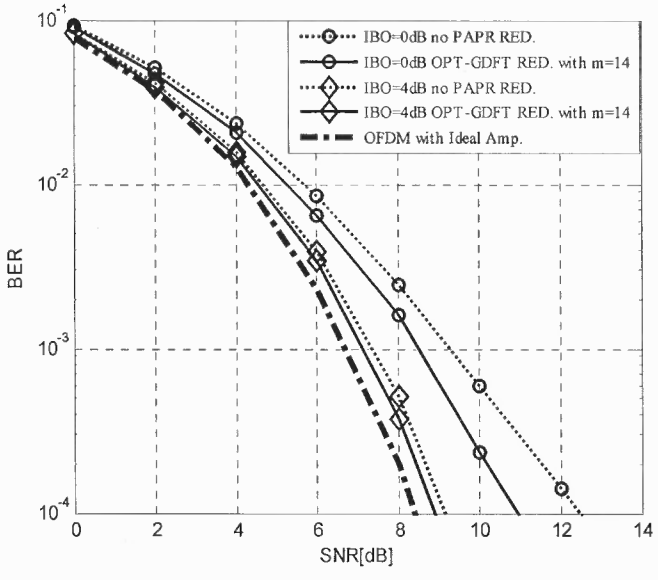

Figure 7.15 BER Performance of QPSK based OFDM with RF Power Amplifier nonlinearities for *N=256*, and employing *Phase Optimized GDFT* based method.

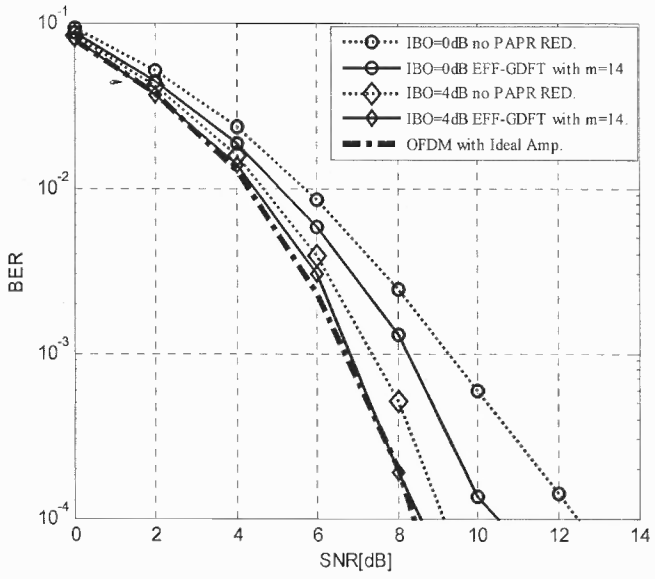

Figure 7.16 BER Performance of QPSK based OFDM with RF Power Amplifier nonlinearities for *N=256*, and employing *Efficient GDFT* based SLM method.

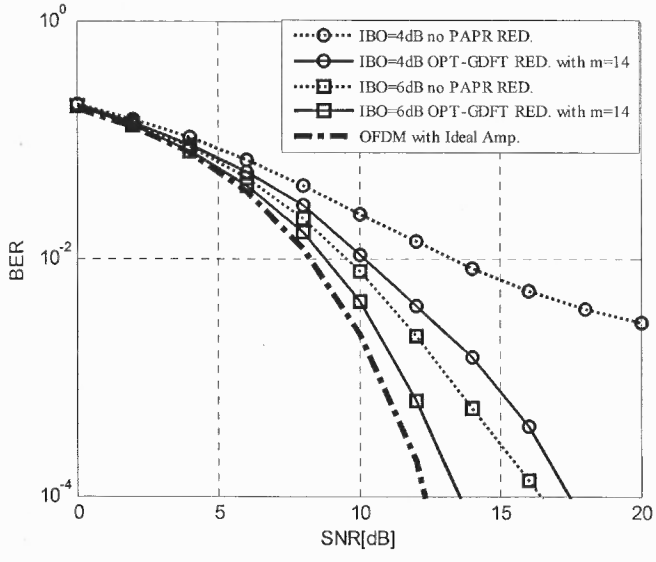

Figure 7.17 BER Performance of 16-QAM based OFDM with RF Power Amplifier nonlinearities and N=256, and employing *Phase Optimized GDFT* based SLM method.

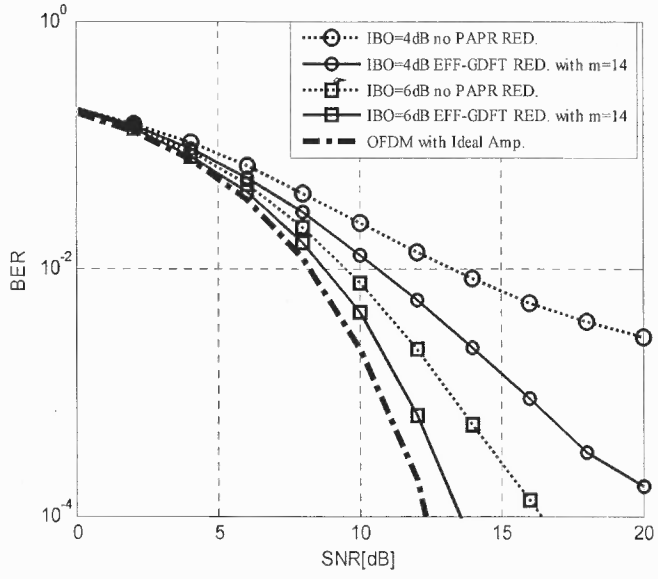

Figure 7.18 BER Performance of 16-QAM based OFDM with RF Power Amplifier nonlinearities and *N=256*, and employing *Efficient GDFT* based SLM method.

7.8 Spectral Efficiency of OFDM Using GDFT based SLM Methods

In this section, spectral improvements offered by these methods will be highlighted. Power Spectral Density (PSD) of OFDM signal with and without RF Power Amplifier nonlinearities are displayed in Figure 7.19 for various IBO's. The sampling frequency and the bandwidth of the system are chosen as 80MHz and 20MHz, respectively. Amplifier nonlinearity increases the sidelobe levels and causing out-of-band leakage in OFDM spectrum. It is observed from this figure that side lobe level increases up to -15dB when an OFDM frame passes through an amplifier operating with 0dB backoff, and it increases up to -35dB for 10dB input backoff case.

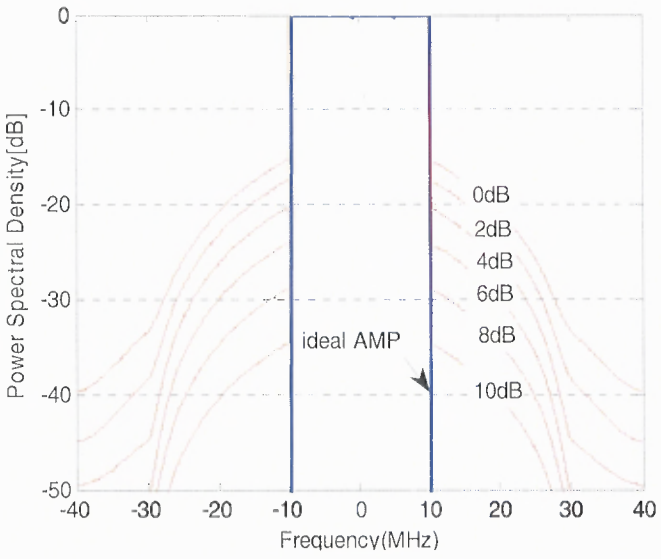

Figure 7.19 PSD of 16-QAM modulated OFDM signal with ideal and nonlinear RF Power Amplifier for *N=256* and various IBO's.

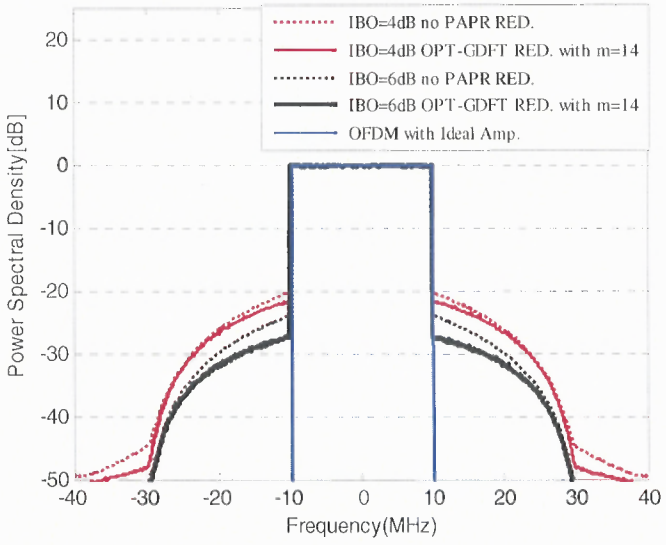

Figure 7.20 Power Spectral Density of 16-QAM modulated OFDM with RF Power Amplifier and *N=256* employing Phase Optimized GDFT based SLM PAPR reduction.

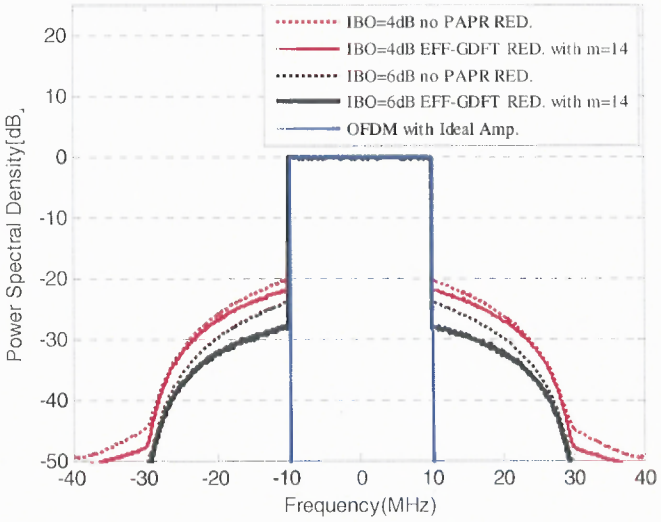

Figure 7.21 Power Spectral Density of 16-QAM modulated OFDM with RF Power Amplifier and *N=256* employing *Efficient GDFT* based SLM PAPR reduction.

The side lobe levels decrease when the proposed PAPR reduction methods are used as displayed in Figure 7.20 and Figure 7.21. The spectral efficiencies provided by the proposed PAPR reduction techniques in OFDM communications are highlighted in these figures for *IBO=4dB* and *IBO=6dB*, and *m=14* and the benefits of GDFT based SLM PAPR reduction are quantified.

7.9 Performance of GDFT Based SLM in WiMAX Standard

The first version of WiMAX, *World Wide Interoperability for Microwave Access*, was standardized as IEEE 802.16. Later, IEEE.802.16.2004 was introduced and the available frequencies are specified from 2GHz up to 11GHz. Then, it was upgraded to 802.16.2005 with Scalable OFDM property [66, 67]. IEEE 802.16.2004 has been the most popular one implemented in WiMAX applications. The specs of IEEE 802.16 standards are

given in [66, 67]. Similarly, the specs of fixed and Mobile WiMAX applications can be found in [67].

MATLAB was used to simulate the performance of a Mobile WiMAX system based on IEEE 802.16e (2005) standard. Specifications of the considered system are summarized in Table 7.3. In the performance simulations, guard interval is not employed since multipath channel is not considered in this study.

Table 7.3 Specs of Wimax System Simulated [67]

FFT size	1024
Number of data subcarriers	720
Number of pilot subcarriers	120
Number of null-Guard subcarriers	184
Channel bandwidth	10MHz

7.9.1 PAPR Performance

CCDF of PAPR's in the simulated WiMAX system employing the proposed PAPR reduction methods are displayed in Figure 7.22 and Figure 7.23. The *Phase Optimized GDFT* based SLM method achieves almost *3.5dB* PAPR reduction while the Efficient GDFT based SLM method achieves almost *2dB* PAPR reduction with $m=14$.

7.9.2 BER Performance

BER performances of WiMAX systems employing the proposed PAPR reduction methods are given in Figure 7.24 and Figure 7.25 for different values of IBO's and 14 number of side information bits. It is observed that both methods improved the BER

performance. With 14 number of side information bits, the performance gets closer to ideal performance.

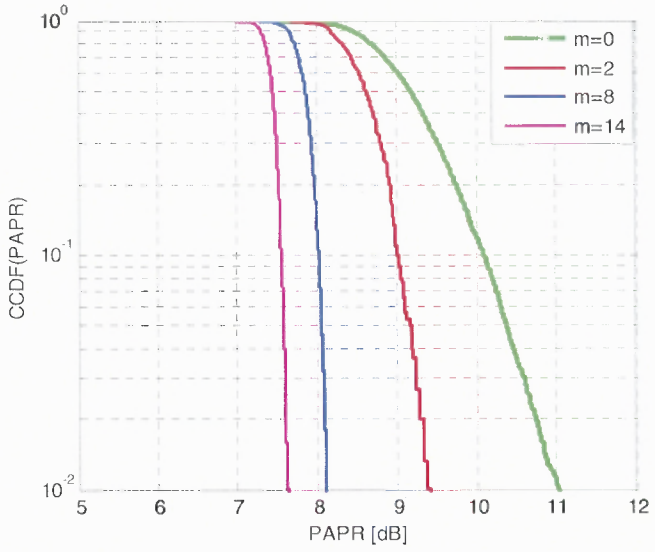

Figure 7.22 CCDF of PAPR for WiMAX (IEEE 802.16e) and various values of *m* employing *Phase Optimized* GDFT based SLM method for *FFT size=1024*.

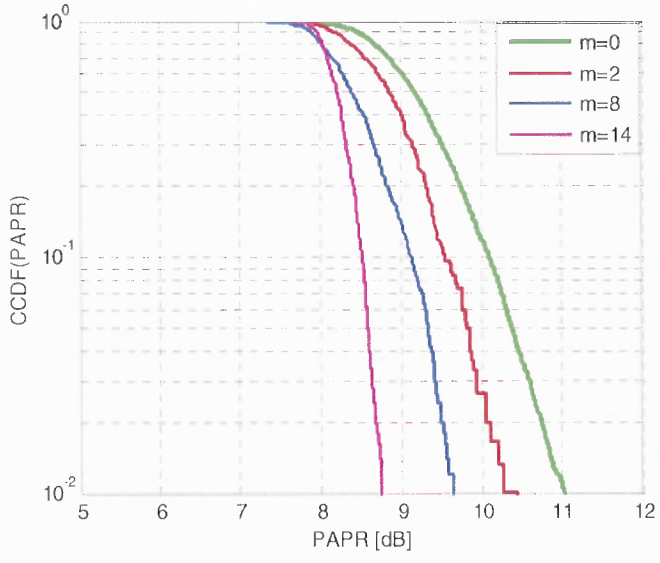

Figure 7.23 CCDF of PAPR for WiMAX (IEEE 802.16e) and various values of *m* employing *Efficient GDFT* based SLM method for *FFT size=1024*.

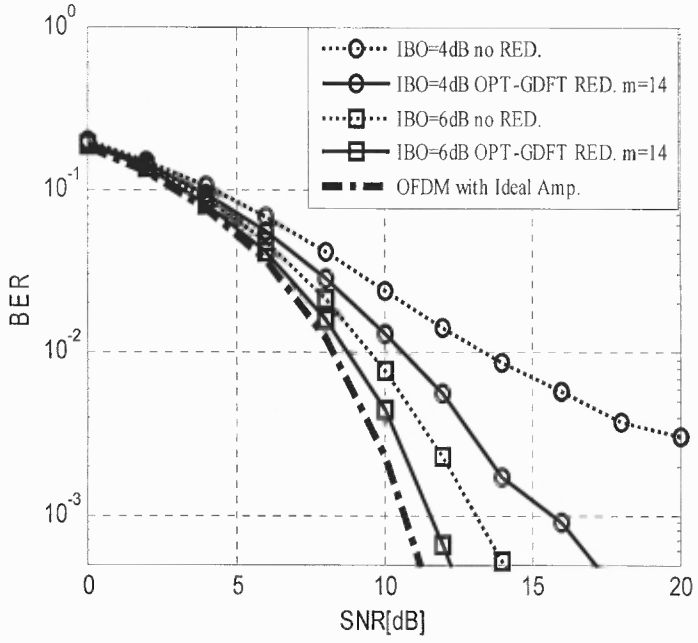

Figure 7.24 BER performance of Mobile Wimax with RF Power Amplifier nonlinearities employing (a) *Phase Optimized* GDFT based SLM with *m=14*, *IBO=4dB* and *IBO=6dB, FFT size=1024*.

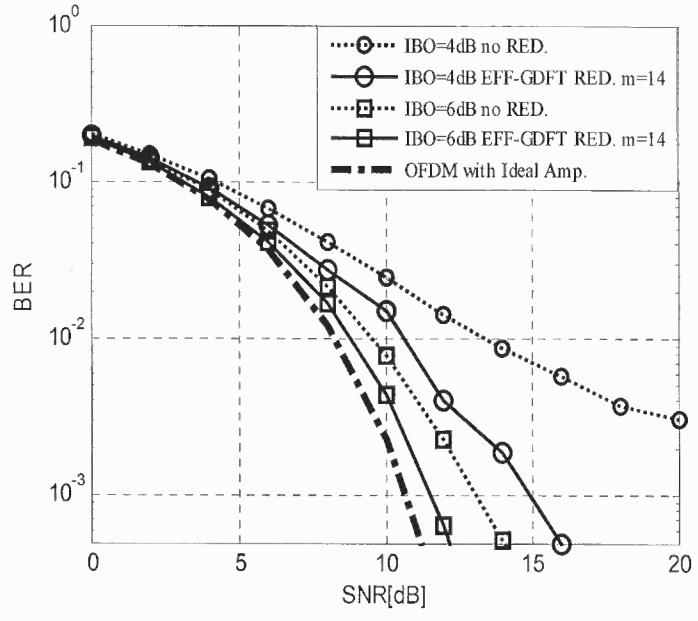

Figure 7.25 BER performance of Mobile Wimax with RF Power Amplifier nonlinearities employing *Efficient* GDFT based SLM based SLM with *m=14*, *IBO=4dB* and *IBO=6dB, FFT size=1024*.

CHAPTER 8

CONCLUSIONS AND FUTURE WORK

In this dissertation, Generalized Discrete Fourier Transform with Non-linear Phase is introduced, where the linear-phase DFT is extended to non-linear phase DFT. The proposed framework made it possible to define infinitely many orthogonal functions sets. Depending on the application, the GDFT basis with desirable properties can be formed using the proposed framework. As a result of this study, the following conclusions have come forth.

- Theoretical analysis of the proposed Non-linear GDFT framework was given in the context of roots of unity.
- Efficient design methods of GDFT sets, derived from the DFT matrix, are presented. Each GDFT matrix is written as a product of a unitary DFT matrix and a generalization matrix G. Since DFT has its own efficient algorithm, FFT, the complexity of the G matrix defines the complexity of the system.
- It was shown that various popular orthogonal function sets including Walsh, DFT, and Walsh-like sets, can be written in the framework of GDFT, with their unique generalization matrix.
- The proposed GDFT framework is employed in the generation of orthogonal GDFT function sets with various correlation performances. It was shown that with the proposed framework, an infinite number of function sets with various correlation properties can be created. Optimum function sets with respect to the defined correlation metrics have been investigated through generic search algorithms. Optimized GDFT sets have been compared with industry-standard DFT, and other code families, with respect to their correlation features. It was shown that GDFT sets yield superior correlation properties over the known code families listed in the literature. Moreover, the minimum value of the performance metric d_{max}, defined as the maximum of the peaks of the all possible auto- and cross-correlation sequences, obtained by GDFT framework, has a value 1.6 times the best achievable lower bound (Welch).
- A closed form *Phase Shaping Function (PSF)*, which generates orthogonal GDFT sets, has been defined by curve-fitting the search results found by brute force. This closed form *PSF* is a second degree Gaussian function with six defining parameters. Changing these six parameters allows the generation of a wide variety of orthogonal

sets, on one end, from very frequency-localized sets to widely spread sets, and on the other end, from sets with very good cross-correlation properties to ones with very good auto-correlation properties.

- The parameters of the proposed *PSF* for optimal GDFT sets based on peak cross-correlation, d_{cm}, and mean squared auto-correlation, R_{AC}, have been presented.

- It was also proved theoretically that all sequences of any GDFT set generated using a *PSF* have the same auto-correlation magnitudes. Auto-correlation sequences change only in phase.

- The proposed closed form *PSF* for length-8 has been shown to generate polyphase Barker codes with lowest possible auto-correlation peaks.

- The correlation improvements of GDFT codes inspired the idea of designing complex spreading codes for DS/CDMA communications systems. BER performances of the proposed GDFT codes have been compared with popular real-valued spreading codes listed in the literature as well as with complex-valued DFT codes in AWGN and Rayleigh channel conditions. In all channel conditions, GDFT codes outperformed competing real-valued and complex-valued codes. It is concluded that the BER performance on AWGN channel with two users in the system is closely coupled with the metric d_{cm}. In contrast, for two users, the BER performance on multipath fading channel conditions is correlated to the metric R_{AC}.

- The traditional SLM method with its limited phase set has been expanded to *Phase Optimized GDFT based SLM* and *Efficient GDFT based SLM* methods, with relaxed phase space. The performance improvements of the proposed PAPR reduction techniques in OFDM communications have been presented with respect to BER, power amplifier metrics, and spectral efficiency metrics. It was shown that significant BER, efficiency and spectral improvements have been achieved by the use of both of the proposed PAPR reduction methods for all communications scenarios considered.

- Although PAPR reduction with *Efficient GDFT based SLM* is less than *Phase optimized GDFT based SLM* method, the efficient method requires only one inverse transform operation in the transmitter and moderately decreases the complexity of system. Therefore, *Efficient GDFT based SLM* is a promising PAPR reduction method for future OFDM based communications systems, with no additional complexity in the transmitter.

Recently, MIMO radar concept has been introduced to increase the detection capability of extended targets or multiple numbers of point targets. In this application, each antenna transmits a waveform which is orthogonal to all the other waveforms

transmitted. In addition to orthogonality, these waveforms are required to have good auto- and cross-correlation properties for identifying extended targets or accurately detecting multiple targets. The GDFT framework with its potential in correlation improvements can be employed in MIMO radar in the future.

APPENDIX A

MINIMUM VALUE OF MEAN SQUARED CROSS-CORRELATION FOR CONSTANT AMPLITUDE CODE SETS

Consider a constant amplitude function set defined as $\left\{ e_k(n)=e^{j\phi_k(n)} \right\}$; $k=0,1,2,...,M\text{-}1, n=0,1,\ldots N-1$ where N is the length of each function or basis and M defines the set size. The aperiodic correlation function for this set is given as

$$d_{k,l}(m)=\begin{Bmatrix} \frac{1}{N}\sum_{n=0}^{N-1-m} e_k(n)e_l^*(n+m), & 0<m\le N-1 \\ \frac{1}{N}\sum_{n=0}^{N-1+m} e_k(n-m)e_l^*(n), & 1-N<m\le 0 \\ 0 \quad , \quad |m|\ge N \end{Bmatrix} \tag{A.1}$$

The mean squared auto-correlation metric for this set is

$$R_{AC}=\frac{1}{M}\sum_{k=0}^{M-1}\sum_{\substack{m=1-N \\ m\neq 0}}^{N-1}\left|d_{k,k}(m)\right|^2 \tag{A.2}$$

In order to define a bound for the complete set, first a simple function from the set is considered. Let the corresponding squared auto-correlation is given as

$$r_{AC,k}=\sum_{\substack{m=1-N \\ m\neq 0}}^{N-1}\left|d_{k,k}(m)\right|^2 \tag{A.3}$$

If the symmetry properties of the auto-correlation functions are used, Equation (A.3) becomes,

$$\begin{aligned} r_{AC,k} &= 2\sum_{m=1}^{N-1}\left|d_{k,k}(m)\right|^2 \\ &= 2\sum_{m=1}^{N-1}\left|\sum_{n=0}^{N-1-m} e_k(n)e_l^*(n+m)\right|^2 = 2\sum_{m=1}^{N-1}\left|\sum_{n=0}^{N-1-m} e^{j(\phi_k(n)-\phi_k(n+m))}\right|^2 \\ &\le 2\sum_{m=1}^{N-1}(N-m)^2 \end{aligned} \tag{A.4}$$

Generalizing (A.4) for the complete set, the bound for R_{AC} becomes,

$$R_{AC} = \frac{1}{M}\sum_{k=0}^{M-1}\sum_{\substack{m=1-N \\ m\neq 0}}^{N-1}\left|d_{k,k}(m)\right|^2 \le 2\sum_{m=1}^{N-1}(N-m)^2 \tag{A.5}$$

The maximum value of R_{AC} is therefore,

$$R_{AC,\max} = 2\sum_{m=1}^{N-1}(N-m)^2 \tag{A.6}$$

Using the mathematical formulas for the summation in (A.6), $R_{AC,\max}$ becomes

$$R_{AC,\max} = \frac{(N-1)(2N-1)}{3N} \tag{A.7}$$

APPENDIX B

PHASE SHAPING FUNCTIONS OF HIGHER SIZE GDFT SETS

Table B.1 Phase Shaping Functions, $2\pi / N[a_1 \exp(-\left[\frac{n-b_1}{c_1}\right]^2) + a_2 \exp(-\left[\frac{n-b_2}{c_2}\right]^2)]$'s, for Higher Size GDFT Sets

Size	d_{cm}	R_{AC}
16	{4.214 4.263 6.258 4.327 4.348 4.362 4.368 4.366 4.356 4.338 4.313 4.279 4.239 4.191 4.136 4.074}	{4.463 1.454 4.309 0.435 2.400 3.938 5.075 5.833 6.225 6.250 5.895 5.138 3.955 2.331 0.263 4.049}
32	{0.346 0.345 0.343 0.340 0.336 0.330 0.324 0.316 0.307 0.298 0.287 0.276 0.265 0.253 0.240 0.228 0.215 0.202 0.189 0.177 0.164 0.152 0.141 0.129 0.133 1.829 4.249 0.292 0.081 0.073 0.065 0.058}	{ 6.255 3.342 0.260 3.291 0.167 2.801 5.029 1.051 3.167 5.091 0.536 2.068 3.400 4.531 5.459 6.184 0.420 0.734 0.842 0.743 0.439 6.212 5.497 4.578 3.456 2.133 0.611 5.174 3.260 1.152 5.139 2.655 }
64	{0.173 0.173 0.172 0.170 0.168 0.165 0.162 0.158 0.154 0.149 0.144 0.138 0.132 0.126 0.120 0.114 0.107 0.101 0.095 0.088 0.082 0.076 0.070 0.065 0.067 0.914 2.124 0.146 0.040 0.036 0.032 0.029 0.026 0.023 0.020 0.018 0.016 0.014 0.012 0.010 0.009 0.008 0.007 0.006 0.005 0.004 0.003 0.003 0.002 0.002 0.002 0.001 0.001 0.001 0.001 0.001 0.001 0 0 0 0 0 0 0}	{ 5.839 2.93 6.229 3.167 0.028 3.264 6.074 2.690 5.505 1.952 4.596 0.868 3.334 5.71 1.71 3.902 5.999 1.719 3.626 5.436 0.866 2.480 3.995 5.41 0.441 1.654 2.765 3.774 4.679 5.481 6.18 0.49 0.98 1.365 1.644 1.819 1.889 1.853 1.712 1.466 1.115 0.659 0.099 5.717 4.949 4.077 3.101 2.023 0.843 5.844 4.462 2.979 1.396 5.998 4.219 2.343 0.371 4.587 2.426 0.172 4.109 1.671 5.428 2.813 }
128	{0.046 0.047 0.050 0.060 0.089 0.165 0.336 0.677 1.269 2.155 3.281 4.461 5.407 5.838 5.614 4.808 3.669 2.499 1.524 0.838 0.424 0.206 0.106 0.066 0.052 0.047 0.046 0.046 0.046 0.046 0.046 0.046 0.046 0.046 0.046 0.046 0.046 0.046 0.045 0.044 0.043 0.043 0.043 0.043 0.043 0.043 0.043 0.043 0.043 0.043 0.043 0.043 0.043 0.043 0.043 0.043 0.043}	{ 4.472 1.757 5.277 2.464 5.886 2.975 0.016 3.290 0.233 3.41 0.254 3.333 0.079 3.059 5.991 2.59 5.423 1.924 4.658 1.061 3.697 0.001 2.540 5.029 1.185 3.576 5.917 1.926 4.169 0.079 2.223 4.318 0.081 2.078 4.025 5.923 1.488 3.287 5.037 0.455 2.106 3.708 5.261 0.481 1.935 3.339 4.695 6.001 0.974 2.181 3.339 4.447 5.506 0.233 1.193 2.104 2.966 3.778 4.54 5.254 5.918 0.249 0.815 1.330 1.797 2.214 2.582 2.9 3.169 3.389 3.559 3.68 3.751 3.773 3.746 3.670 3.544 3.369 3.144 2.87 2.547 2.174 1.753 1.281 0.761 0.191 5.855 5.187 4.469 3.703 2.887 2.021 1.107 0.143 5.413 4.351 3.239 2.079 0.869 5.893 4.585 3.228 1.821 0.366 5.144 3.591 1.988 0.336 4.918 3.168 1.369 5.804 3.907 1.961 6.25 4.206 2.113 6.254 4.064 1.824 5.819 3.481 1.095 4.943 2.459 6.210 3.629 0.999 }

REFERENCES

[1] N. Ahmed, T. Natarajan, and K. Rao, "Discrete Cosine Transform," IEEE Transactions on Computers, vol. C-32, pp. 90-93, 1974.

[2] N. Ahmed, and K. Rao, *Orthogonal Transforms for Digital Signal Processing.* Springer-Verlag, 1975.

[3] V. Britanak, "A Unified Discrete Cosine and Discrete Sine Transform Computation," Signal Processing, EURASIP, vol. 43, no. 3, pp. 333-339, 1995.

[4] C. Burrus, and T. Parks, *DFT/FFT and Convolution Algorithms: Theory and Implementation.* John Wiley & Sons Inc., 1991.

[5] R. J. Clarke, "Relation Between the Karhunen Loeve and Cosine Transforms," IEE Proceedings of Communications, Radar and Signal Processing, vol. 128, no. 6, pp. 359-360, 1981.

[6] B. Dickinson, and K. Steiglitz, "Eigenvectors and Functions of the Discrete Fourier Transform," IEEE Transactions on Acoustics, Speech, and Signal Processing, vol. 30, pp. 25-31, 1982.

[7] P. Duhamel, and M. Vetterli, "Fast Fourier Transforms: A Tutorial Review and a State of the Art," Signal Processing, EURASIP, vol. 19, no. 4, pp. 259-299, 1990.

[8] E. Feig, and S. Winograd, "Fast Algorithms for the Discrete Cosine Transform," IEEE Transactions on Signal Processing, vol. 40, no. 9, pp. 2174-2193, 1992.

[9] K. Rao, *Discrete Transforms and Their Applications.* Van Nostrand Reinhold Company, 1985.

[10] G. Strang, "The Discrete Cosine Transform," SIAM review, vol. 41, no. 1, pp. 135-147, 1999.

[11] J. Walsh, "A Closed Set of Normal Orthogonal Functions," American Journal of Mathematics, vol. 45, no. 1, pp. 5-24, 1923.

[12] P. Yip, and K. Rao, "A Fast Computational Algorithm for the Discrete Sine Transform," IEEE Transactions on Communications, vol. COM-28, pp. 304-307, 1980.

[13] R. Gold, "Optimal Binary Sequences for Spread Spectrum Multiplexing (Corresp.)," IEEE Transactions on Information Theory, vol. 13, no. 4, pp. 619-621, 1967.

[14] S. Boztas, and P. Kumar, "Binary Sequences with Gold-like Correlation but Larger Linear Span," IEEE Transactions on Information Theory, vol. 40, no. 2, pp. 532-537, 1994.

[15] T. Kasami, "Weight Distribution Formula for Some Class of Cyclic Codes," Storming Media, 1966.

[16] R. Gold, "Maximal Recursive Sequences with 3-valued Recursive Cross-correlation Functions (Corresp.)," IEEE Transactions on Information Theory, vol. 14, no. 1, pp. 154-156, 1968.

[17] J. Chang, "Generation of 5-level Maximal-length Sequences," Electronics Letters, vol. 2, no. 7, 1966.

[18] K. Godfrey, "Three-level m Sequences," Electronics Letters, vol. 2, no. 7, pp. 241-243, 1966.

[19] V. Ipatov, "Ternary Sequences with Ideal Periodic Autocorrelation Properties," Radio Engineering and Electronic Physics, vol. 24, pp. 75–79, 1979.

[20] R. Poluri, and A. N. Akansu, "Varying Power Integer Codes for CDMA Communications," in Forty-First Asilomar Conference on Signals, Systems and Computers, 2007.

[21] D. Chu, "Polyphase Codes with Good Periodic Correlation Properties (Corresp.)," IEEE Transactions on Information Theory, vol. 18, no. 4, pp. 531-532, 1972.

[22] R. Frank, "Polyphase Codes with Good Nonperiodic Correlation Properties," IEEE Transactions on Information Theory, vol. 9, no. 1, pp. 43-45, 1963.

[23] I. Oppermann, and B. Vucetic, "Complex Spreading Sequences with a Wide Range of Correlation Properties," IEEE Transactions on Communications, vol. 45, no. 3, pp. 365-375, 1997.

[24] I. Oppermann, P. Van Rooyen, and B. Vucetic, "Effect of Sequence Selection on MAI Suppression in Limited CDMA Systems," Wireless Networks, vol. 4, no. 6, pp. 471-478, 1998.

[25] I. Oppermann, "Orthogonal Complex-valued Spreading Sequences with a Wide Range of Correlation properties," IEEE Transactions on Communications, vol. 45, no. 11, pp. 1379-1380, 1997.

[26] L. J. Cimini Jr, and N. Sollenberger, "Peak-to-average Power Ratio Reduction of an OFDM Signal Using Partial Transmit Sequences," IEEE Communications Letters, vol. 4, no. 3, pp. 86-88, 2000.

[27] A. D. S. Jayalath, and C. Tellambura, "Adaptive PTS Approach for Reduction of Peak-to-average Power Ratio of OFDM Signal," Electronics Letters, vol. 36, no. 14, pp. 1226-1228, 2000.

[28] R. Bauml, R. Fischer, and J. Huber, "Reducing the Peak-to-average Power Ratio of Multicarrier Modulation by Selected Mapping," Electronics Letters, vol. 32, pp. 2056, 1996.

[29] H. Breiling, S. Muller-Weinfurtner, and J. Huber, "SLM Peak-power Reduction without Explicit Side Information," IEEE Communications Letters, vol. 5, no. 6, pp. 239-241, 2001.

[30] J. Davis, and J. Jedwab, "Peak-to-mean Power Control in OFDM, Golay Complementary Sequences, and Reed-Muller Codes," IEEE Transactions on Information Theory, vol. 45, no. 7, pp. 2397-2417, 1999.

[31] B. Krongold, and D. Jones, "PAR reduction in OFDM via Active Constellation Extension," IEEE Transactions on Broadcasting, vol. 49, no. 3, pp. 258-268, 2003.

[32] X. Li, and L. J. Cimini Jr, "Effects of Clipping and Filtering on the Performance of OFDM," IEEE Communications Letters, vol. 2, no. 5, pp. 131-133, 1998.

[33] R. O'neill, and L. B. Lopes, "Envelope Variations and Spectral Splatter in Clipped Multicarrier Signals," Sixth IEEE International Symposium on Personal, Indoor and Mobile Radio Communications, vol. 1, pp. 71-75, 1995.

[34] J. Tellado, "Peak to Average Power Reduction for Multicarrier Modulation," PhD. Thesis, Stanford University, 2000.

[35] D. Jayalath, and C. Tellambura, "The Use of Interleaving to Reduce the Peak-to-average Power Ratio of an OFDM Signal," IEEE Global Telecommunications Conference, vol. 1, pp. 82-86, 2000.

[36] R. Baxley, and G. Zhou, "Comparison of Selected Mapping and Partial Transmit Sequence for Crest Factor Reduction in OFDM," Proceedings of Military Communications Conference, pp. 1- 4, 2006.

[37] S. Mitra, *Digital Signal Processing: A Computer-Based Approach.* McGraw-Hill, 2005.

[38] A. Oppenheim, R. Schafer, and J. Buck, *Discrete-time Signal Processing.* Prentice Hall, 1989.

[39] A. Akansu, and R. Haddad, *Multiresolution Signal Decomposition: Transforms, Subbands, and Wavelets.* Academic Press, 2001.

[40] A. Jain, "A Sinusoidal Family of Unitary Transforms," IEEE Transactions on Pattern Analysis and Machine Intelligence, vol. PAMI-1, no. 4, pp. 356-365, 1979.

[41] A. Akansu, and R. Poluri, "Walsh-Like Nonlinear Phase Orthogonal Codes for Direct Sequence CDMA Communications," IEEE Transactions on Signal Processing, vol. 55, no. 7, pp. 3800-3806, 2007.

[42] R. Poluri, "Design and Performance of CDMA Codes for Multiuser Communications," PhD. Thesis, New Jersey Institute of Technology, May 2007.

[43] R. Gray, *Toeplitz and Circulant Matrices: A review.* Now Publishers, 2006.

[44] K. Ireland, and M. Rosen, *A Classical Introduction to Modern Number Theory.* Springer Science & Business, 1990.

[45] W. Narkiewicz, *Elementary and Analytic Theory of Algebraic Numbers.* Springer Verlag, 2004.

[46] G. Bongiovanni, P. Corsini, and G. Frosini, "One-dimensional and Two-dimensional Generalised Discrete Fourier Transforms," IEEE Transactions on Acoustics, Speech and Signal Processing, vol. 24, no. 1, pp. 97-99, 1976.

[47] P. Corsini, and G. Frosini, "Properties of the Multidimensional Generalized Discrete Fourier Transform," IEEE Transactions on Computers, vol. C-28, no. 11, pp. 819-830, 1979.

[48] L. Rinaldi, and P. Ricci, "Complex Symmetric Functions and Generalized Discrete Fourier Transform," Rendiconti del Circolo Matematico di Palermo, vol. 45, no. 1, pp. 57-74, 1996.

[49] E. Stade, and E. Layton, "Generalized Discrete Fourier Transforms: The Discrete Fourier-Riccati-Bessel Transform," Computer Physics Communications, vol. 85, no. 3, pp. 336-370, 1995.

[50] M. Pursley, D. Sarwate, and W. Stark, "Error Probability for Direct-Sequence Spread-Spectrum Multiple-Access Communications-Part I: Upper and Lower Bounds," IEEE Transactions on Communications, vol. 30, no. 5, pp. 975-984, 1982.

[51] M. Golay, "The Merit Factor of Long Low Autocorrelation Binary Sequences (Corresp.)," IEEE Transactions on Information Theory, vol. 28, no. 3, pp. 543-549, 1982.

[52] D. Sarwate, "Bounds on Crosscorrelation and Autocorrelation of Sequences (Corresp.)," IEEE Transactions on Information Theory, vol. 25, no. 6, pp. 720-724, 1979.

[53] L. Welch, "Lower Bounds on the Maximum Cross Correlation of Signals (Corresp.)," IEEE Transactions on Information Theory, vol. 20, no. 3, pp. 397-399, 1974.

[54] M. Friese, "Polyphase Barker Sequences up to Length 36," IEEE Transactions on Information Theory, vol. 42, no. 4, pp. 1248-1250, 1996.

[55] S. Golomb, and R. Scholtz, "Generalized Barker Sequences," IEEE Transactions on Information Theory, vol. 11, no. 4, pp. 533-537, 1965.

[56] N. Levanon, and E. Mozeson, *Radar Signals*. Wiley, 2004.

[57] M. Wai Ho, and S. Y. R. Li, "Aperiodic Autocorrelation and Crosscorrelation of Polyphase Sequences," IEEE Transactions on Information Theory, vol. 43, no. 3, pp. 1000-1007, 1997.

[58] D. Goldberg, *Genetic Algorithms in Search and Optimization*. Addison-Wesley, 1989.

[59] J. Cheng, and N. Beaulieu, "Accurate DS-CDMA Bit-error Probability Calculation in Rayleigh Fading," IEEE Transactions on Wireless Communications, vol. 1, no. 1, pp. 3-15, 2002.

[60] C. Rapp, "Effects of HPA-nonlinearity on a 4-DPSK/OFDM-signal for a Digital Sound Broadcasting System," Proceedings of the 2nd European Conference on Satellite Communications, pp. 179-184, 1991.

[61] F. Raab, P. Asbeck, S. Cripps *et al.*, "RF and Microwave Power Amplifier and Transmitter Technologies-Part 1," High Frequency Electronics, vol. 2, no. 2, pp. 22–36, May 2003.

[62] H. Seung Hee, and L. Jae Hong, "An Overview of Peak-to-average Power Ratio Reduction Techniques for Multicarrier Transmission," IEEE Wireless Communications, vol. 12, no. 2, pp. 56-65, 2005.

[63] R. Van Nee, and A. De Wild, "Reducing the Peak-to-average Power Ratio of OFDM," Proceedings of 48th IEEE Vehicular Technology Conference, vol.3. pp. 2072-2076, 1998.

[64] Z. Chunming, R. J. Baxley, and G. T. Zhou, "Peak-to-average Power Ratio and Power Efficiency Considerations in MIMO-OFDM Systems," IEEE Communications Letters, vol. 12, no. 4, pp. 268-270, 2008.

[65] H. Ochiai, "Power efficiency Comparison of OFDM and Single-carrier Signals," Proceedings of 48th IEEE Vehicular Technology Conference, vol. 2, pp. 899-903, 2002.

[66] S. Ahson, and M. Ilyas, *WiMAX: Standards and Security.* CRC, 2007.

[67] J. Andrews, A. Ghosh, and R. Muhamed, *Fundamentals of WiMAX: Understanding Broadband Wireless Networking.* Prentice Hall, 2007.

[68] J. Nelder, and R. Mead, "A simplex Method for Function Minimization," The Computer Journal, vol. 7, no. 4, pp. 308, 1965.

[69] M. Wolfe, *Numerical Methods for Unconstraint Optimization: An Introduction.* Van Nostrand Reinhold, 1978.

[70] J. Dennis, and R. Schnabel, *Numerical Methods for Unconstrained Optimization and Non-linear Equations.* Society for Industrial Mathematics, 1996.

[71] B. Natarajan, S. Das, D. Stevens, "Design of Optimal Complex Spreading Codes for DS-CDMA Using Evolutionary Approach," IEEE Global Telecommunications Conference, vol. 6, pp. 3882-2886, 2004.